Radioactive contamination in sediments near the sunken nuclear submarine *Komsomolets*, SW of Bear Island in the Norwegian Sea

by

Janita Katrine Flo

Master of Science Thesis in Environmental Chemistry

Department of Chemistry

University of Bergen

Bergen, May 2014

Abstract

The Soviet nuclear submarine *Komsomolets* sank on the 7th of April 1989, 185 km southwest of the Bear Island in the Norwegian Sea to a depth of about 1655 m. The submarine contains one nuclear reactor, containing long-lived radionuclides such as caesium-137 (^{137}Cs) along with other fission and activation products, in addition to two mixed uranium (U)/plutonium (Pu) nuclear warheads containing weapons grade plutonium.

The Institute of Marine Research (IMR) has, in cooperation with the Norwegian Radiation Protection Authority (NRPA), monitored the areas adjacent to *Komsomolets* since 1993, where bottom water and sediment samples have been analysed for ^{137}Cs and plutonium-239, 240 ($^{239+240}$Pu). Because of the large depth and strong currents in the area, it has not been possible to determine how close to the wreck the samples were taken.

The present study has been carried out at the IMR. During sampling from R/V *G. O. Sars* in April 2013, *Komsomolets* was precisely located using a Kongsberg EM302 multibeam echosounder, a Simrad EK60 single beam echosounder and an Olex 3D bottom-mapping system. To ensure precise positioning of the sampling equipment, a Simrad MST342 wireless acoustic transponder was attached to the box-corer. The transponder communicated with R/V *G. O. Sars'* dynamic positioning system, the Kongsberg HiPAP (High Precision Acoustic Positioning), while collecting the sediment samples. An attempt to use the acoustic transponder was also performed in 2012, but due to weather conditions and lack of time, the attempt did not succeed.

1 cm thick slices from fifteen sediment cores collected adjacent to *Komsomolets* in 2012 and 2013 have been analysed for ^{137}Cs. A selection of the 0-1 and 1-2 cm layers from the 2013 sampling were analysed for $^{239+240}$Pu, ^{238}Pu, americium (^{241}Am) and uranium-238 (^{238}U). Further, isotope ratios were determined. Grain size analyses on the 0-1 cm layers of the selected cores were also performed, as well as dating of two cores from the 2012 sampling. No ^{137}Cs peaks was found in any of the cores, neither no elevated activity concentrations of Pu-isotopes, ^{241}Am and ^{238}U. The activity concentrations of ^{137}Cs in the 0-1 cm layers were comparable to ^{137}Cs activity concentrations in surface sediments found in the area adjacent to *Komsomolets* in previous years. This was also the case for the ^{137}Cs activity concentrations in surface sediments found elsewhere in the Barents Sea and deep areas of the Norwegian and Greenland Seas.

Abstract

Although several model studies have shown that a radioactive leakage from *Komsomolets* will have insignificant impact on fish and other marine organisms, there are still public concerns about the condition of the submarine and the potential for radioactive leakage.

Acknowledgments

This master thesis has been carried out as a collaboration between the University of Bergen (UIB) and the Institute of Marine Research (IMR). During this work, I have been given exciting opportunities like participating on the cruise with R/V *G. O. Sars* in April 2013, taking courses at the Norwegian University of Life Science (NMBU) during the autumn 2013, and to work with an interesting project. It has been valuable experiences!

I would like to thank my supervisors during this project; Dr. Hilde Elise Heldal at IMR and Professor Leif Sæthre at the department of Chemistry, UIB. Thank you for giving me an interesting project and for excellent supervision throughout the master thesis! Thank you, Hilde Elise for always having time for me, your good advices and comments!

I would also like to thank:

- Staff at the Chemistry laboratory at IMR for collecting samples in 2012
- Staff at the Chemistry laboratory at IMR, especially Penny Lee Liebig, for helping out with sample preparations
- Ingrid Sværen (IMR) for dating two sediment cores, and for always having time for answering questions
- Justin Gwynn (NRPA), Torbjørn Gäfvert (NRPA) and Anne Marie Aarøen Vangsnes for comments on the manuscript
- Parvine Naghchbandi (NRPA) for analyses of certain transuranic elements by alpha spectrometry
- Per Roos at DTU NUTECH in Denmark for analysing sediment samples for uranium-238 (^{238}U), and determining activity ratios of uranium and plutonium-isotopes by mass spectroscopy
- Ole Tumyr, Jordan Holl and Kristian Vasskog at the Institute of Geology at UIB for helping me perform the grain size analysis on sediment samples

I am also grateful to my family and friends for always supporting me. An especially thanks goes to Åsmund; these years would not have been the same without you!

Bergen, May 2014

Janita Katrine Flo

Content

List of abbreviations

ADC	Analogue to Digital Converter
^{241}Am	Americium-241
^{137}Ba	Barium-137
^{137m}Ba	Barium-137 (meta-stable)
Bq	Becquerel
$Ca(COO)_2$	Calcium oxalate
^{60}Co	Cobolt-60
Cps	Counts per second
CRS	Constant Rate of Supply
^{137}Cs	Caesium-137
CTD	Conductivity, Temperature, Depth
DTU	The Technical University of Denmark
d.w	Dry weight
EGC	East Greenland Current
$Fe(OH)_3$	Iron (III) hydroxide
FSU	Former Soviet Union
FWHM	Full Width Half Maximum
Ge	Germanium
HCl	Hydrogen chloride
HNO	Nitroxyl
HNO_3	Nitric acid
HPGe	High Purity Germanium

IAEA	International Atomic Energy Agency
IMR	Institute of Marine Research
K	Potassium
K_d	Distribution coefficient
LORAKON	LOkal RAdioaktivitets KONtroll
MCA	Multi Channel Analyser
NH_3	Ammonia
NH_4I	Ammonium iodide
NPL	National Physical Laboratory
NRPA	Norwegian Radiation Protection Authority
NWCC	Norwegian Coastal Current
^{210}Pb	Lead-210
^{210}Po	Polonium-210
^{238}Pu	Plutonium-238
$^{239+240}Pu$	Plutonium-239,240
^{241}Pu	Plutonium-241
^{226}Ra	Radium-226
Rb	Rubidium
^{222}Rn	Radon-222
RIO	Region Of Interest
ROV	Remotely Operated underwater Vehicle
R/V	Research Vessel
SNF	Spent Nuclear Fuel

^{90}Sr	Strontium-90
Stdv	Standard deviation
$t_{½}$	Half-life
^{99}Tc	Techentium-99
TF	Transfer factor
^{235}U	Uranium-235
^{238}U	Uranium-238
USSR	Union of Soviet Socialist republic
w.w	Wet weight
XRD	X-ray diffraction

SI prefixes

Factor	***Prefix***	***Symbol***
10^{-6}	Micro	µ
10^{-3}	Milli	m
10^{3}	Kilo	k
10^{6}	Mega	M
10^{9}	Giga	G
10^{12}	Tera	T
10^{15}	Peta	P

1. Introduction

1.1. Background and objectives of the thesis

In 1989, the Soviet nuclear attack submarine *Komsomolets* sank in the Norwegian Sea about 185 km southwest of the Bear Island (Kolstad, 1995). The submarine represents a potential threat to the environment as it contains a nuclear reactor and two nuclear warheads. The concern arouse particularly in Norway, where the resting place of the wreck is located close to the Norwegian fishing grounds (Sagalevitch, 1995).

Since 1993, the Institute of Marine Research (IMR) has yearly monitored the levels of radioactive contaminations in sediments and seawater in the area close to *Komsomolets*. Here, the extent of gamma-emitters are measured (Figure 1.1), while the Norwegian Radiation Protection Authority (NRPA) measures for alpha emitters (plutonium-239 (^{239}Pu), plutonium-240 (^{240}Pu) and americium-241(^{241}Am)) (Figure 1.2). So far, the detected levels are low and comparable with the general levels of the Norwegian and Barents Seas (Heldal et al., 2002).

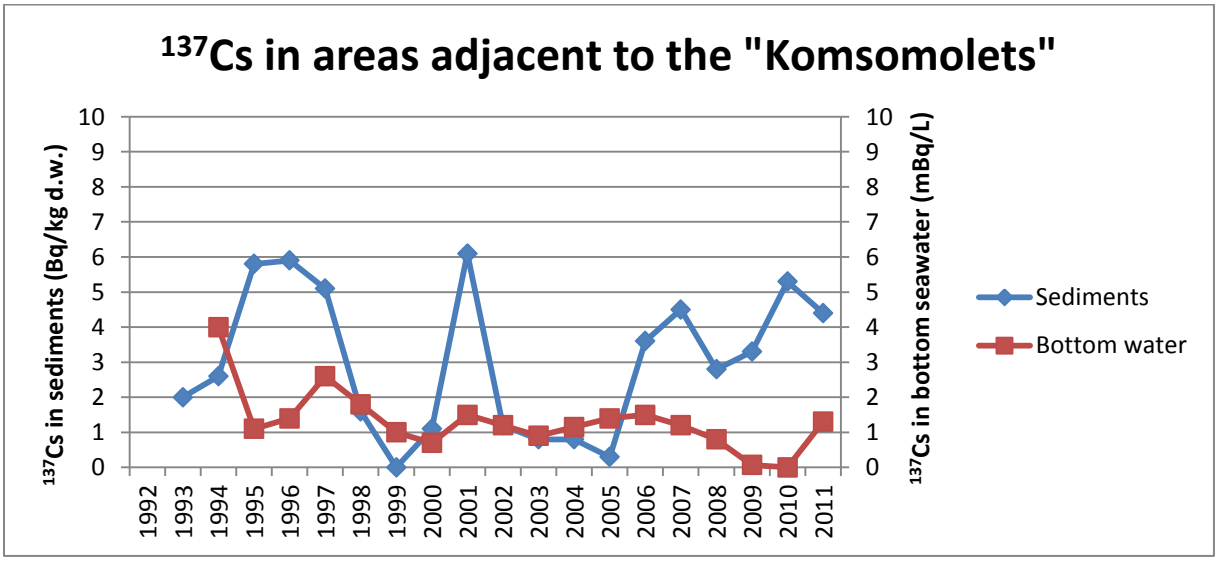

Figure 1.1. Caesium-137 (^{137}Cs) in surface sediments and bottom water samples collected in areas adjacent to the sunken nuclear submarine Komsomolets *(IMR).*

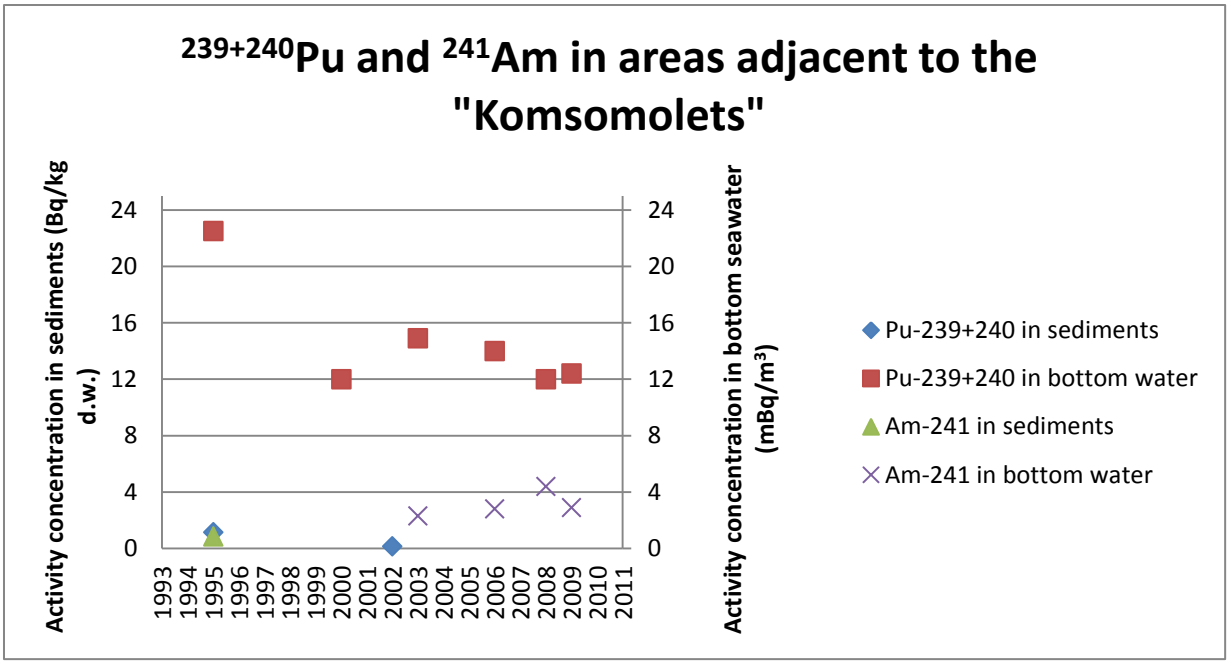

Figure 1.2. Plutonium-239,240 ($^{239+240}$Pu) and americium-241 (^{241}Am) in surface sediments and bottom water samples collected in areas adjacent to Komsomolets *(NRPA 200; 2003; 2004; 2005; 2008; 2011).*

During previous monitoring, uncertainties arose as to how close to the wreck the sediment and water samples were collected. The fact that the wreck rests as deep as approximately 1700 m, makes it difficult to know whether the monitoring can capture a potential leakage from the submarine.

During the yearly sampling at the resting place of *Komsomolets* in 2012, a transponder was attached to the sampling equipment on board the R/V *G. O. Sars* to get an exact position of the sampling. The transponder communicated with the research vessel so that the sampling equipment could be positioned relative to the wreck on the seabed. For the very first time this system was used under the yearly sampling at areas adjacent to the submarine. It had previously been tested in *Bjørnefjorden* and *Byfjorden* by Leinebø (2011), with an accuracy of about ± 1 m at a depth of 600 m. Unfortunately, there were some problems with the sampling equipment, where the box-corer would not close its grab-arms when the transponder was attached to it. After a series of unsuccessful sampling attempts, the transponder was removed, and the sediment sampling was performed as usual (Appendix F).

It was decided that the transponder was to be used on the 2013 monitoring of the resting place of *Komsomolets*. The author of this thesis was attending this cruise in the period of 01-09.04.13 on the research vessel R/V *G. O. Sars*.

The objectives for this thesis are to:

- Collect sediment cores in the immediate vicinity of the wreck of *Komsomolets* using R/V G. O. Sars wireless acoustic positioning system
- Determine the levels of gamma-emitters in the sediment cores
- Determine the levels of alpha-emitters (Pu-isotopes, U-isotopes and ^{241}Am) in selected layers of the sediment cores
- Determine geochemical parameters such as age of the sediment layers and grain size distributions
- Compare the results with levels of radionuclides in sediments elsewhere in the Barents and Norwegian Seas
- Consider if there is any sign of leakage from *Komsomolets*

1.2. The *Komsomolets*

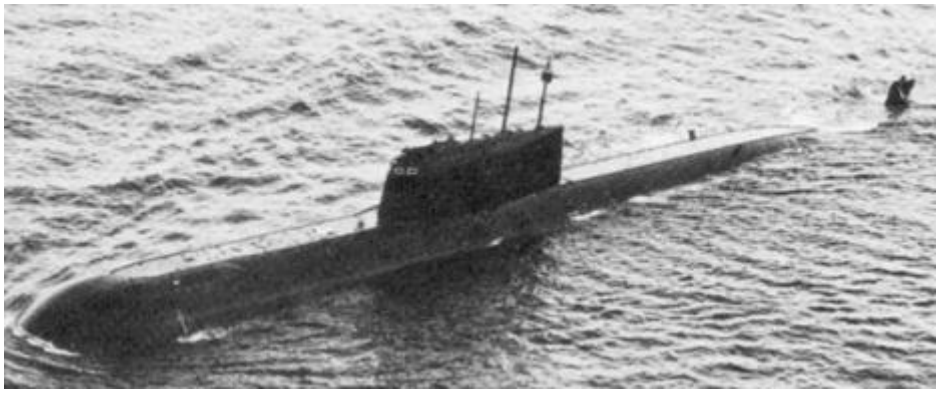

Figure 1.3. The Komsomolets *(Montgomery, 1995).*

On the 7th of April 1989, the Soviet nuclear submarine *Komsomolets* sank in the Norwegian Sea about 185 km southwest of the Bear Island (Kolstad, 1995). The tragedy started at 11.00 a.m. with a fire in the back section of the submarine (compartment 7, Figure 1.4). The back section contained reduction gear and/or diesel engines (Montgomery, 1995). According to press reports based on interviews with crew members, a liquid had been observed leaking from a hydraulic system (Eriksen, 1990). It took less than fifteen minutes for the submarine to reach the surface (Olgaard, 1994), and the reactor was switched to a stable cool-down mode, to ensure nuclear safety (Føyn, 1994a). The fire spread forwards reaching the compartment containing the pumps of the primary circuit and the nuclear reactor (compartment 5 and 4, Figure 1.4), and another fire also started at a control desk (compartment 3, Figure 1.4). Several explosions were heard, and after approximately five hours later the submarine began to sink (Olgaard, 1994).

There are probably several causes for this accident. Besides some technical defects on the submarine, the crew also had inadequate training while the officers showed poor decision-making skills (Kolstad, 1995). Of the 69 crew members on board, 42 were killed in the accident. Five crew members tried to survive in a recue capsule built into the submarine (inside the V-shaped structure in the conning tower, Figure 1.4), but only one of them survived as it was shot to the surface. The Norwegian Defence Research Establishment stated that *Komsomolets* rests at a depth of 1655 m at the location 73˚43'16" N and 13˚16'52" E (Høibråten et al., 2003). The wreck is thought to rest in an almost upright position, where it is lodged 2.5-3 m in muddy sediments (Høibråten et al., 1997).

1.2.1. The submarine

Komsomolets (or "K-278") means "member of the Young Communist League", and is classified as a "Mike" in NATOs classification system for submarines (Montgomery, 1995). It was launched in May 1983 in Severodvinsk, and has a length of approximately 120 m.

Komsomolets is the only submarine ever built in the "Mike" class, and is very special in that both its inner pressure hull and outer hull is made of titanium (Kolstad, 1995). The outer hull has a thickness of 9.8 mm and the pressure hull, which is approximately 10 cm thick, consists of seven compartments, which is shown in Figure 1.4 (Høibråten et al., 2003). Titanium is highly resistant as well as being lighter than both iron and steel, and by using this as a construction material; it was possible for *Komsomolets* to work at depths of 1000 m.

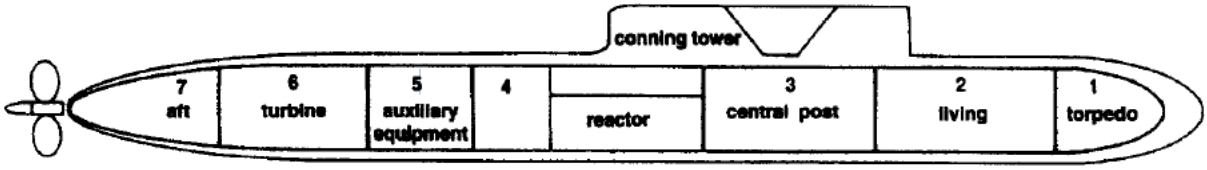

Figure 1.4. Layout of the nuclear submarine Komsomolets *showing the locations and use of various compartments (Høibråten et al., 1997).*

1.2.2. Radionuclide inventory

The reactor is a 190 megawatts (MW) OK-650 b-3 pressurised-water reactor (PWR) (Nilsen et al., 1996), and is made of low-alloy steel with corrosion protection on the inside. Its installation includes a gas system to compensate for volume changes (Høibråten et al., 2003). The reactor is located in compartment four (Figure 1.4), which is separated from the central post by an especially thick bulkhead, and the fuel consists of metal alloys of uranium and

aluminium canned in stainless steel (Kolstad, 1995). There is no direct contact between the low-alloy steel and the titanium alloys, and lead is widely used for shielding in the reactor compartment.

Soviet and Russian authorities have released very little information about the reactor construction and the reactor core, but the fuel is said to have an enrichment of 30% uranium-235 (Kolstad, 1995). It is uncertain how many working hours it had before the tragedy, but it is estimated that 20-25 kg was used at the time of the accident, resulting in a produced quantity of approximately 2 kg plutonium-239 (^{239}Pu) in the reactor core (Føyn, 1994a). This assumption is made based on the knowledge that this type of reactor will have an original content of about 200 kg uranium-235 (^{235}U). In 1991, the amount of isotopes in the reactor was given by the Russian authorities (marked in Table 1.1) (Høibråten et al., 1997).

Both the contents of transuranic radionuclides and the activities for the most important activation products (iron-55 (^{55}Fe), cobolt-60 (^{60}Co) and nickel-63 (^{63}Ni)) are calculated by the Kurchatov Institute (Gladkov et al., 1994). The alpha emitters' ^{239}Pu, plutonium-240 (^{240}Pu) and Curium-242 (^{242}Cm) are listed in Table 1.1, along with the short lived beta emitter plutonium-241 (^{241}Pu) and its daughter nuclide Americium-241 (^{241}Am). Table 1.1 also shows the activation products, which are produced by interaction between neutrons from the nuclear reactor and materials in the reactor itself and its shielding (Gladkov et al., 1994).

The submarine contains two nuclear torpedoes with nuclear warheads, which is located in compartment one (Figure 1.4) in the bow. These torpedoes were designed for use in great depths, but the exact construction of the weapons is unknown (Høibråten et al., 2003).

Estimates of the contents of radioactive material have been made, where contemporary nuclear warheads would be expected to contain about 10 kg of ^{235}U or about 4 kg ^{239}Pu (Høibråten et al., 2003). Assuming that the Soviet/Russian weapons-grade plutonium contains 94% of ^{239}Pu and 6% of ^{240}Pu, this activity corresponds to a total of about 6,0 kg Pu in the two weapons altogether (Cochran and Norris, 1993). The activity is shown in Table 1.1 and the development over time for some of the most important radionuclides is listed in Figure 1.5.

Table 1.1. Komsomolets *radionuclide inventory. The half-lives and the given and calculated activities (year 1989 and year 2089) are shown. This information is calculated by Gladkov et al. (1994) and summarized by Høibråten et al. (1997).*

Isotope	***Half-life***	***Activity (Bq)***	
		1989	***2089***
Reactor:			
Iron-55	2.73 y	$1.3 \cdot 10^{14}$	$1.2 \cdot 10^{3}$
Cobalt-60	5.272 y	$5.9 \cdot 10^{13}$	$1.1 \cdot 10^{8}$
Nickel-63	99.6 y	$4.4 \cdot 10^{12}$	$2.2 \cdot 10^{12}$
Krypton-85	10.72 y	$4.8 \cdot 10^{14}$	$7.5 \cdot 10^{11}$
Strontium-90	28.78 y	$\mathbf{2.8 \cdot 10^{15}}$	$2.5 \cdot 10^{14}$
Ruthenium-106	1.020 y	$8.9 \cdot 10^{14}$	-
Caesium-134	2.062 y	$3.5 \cdot 10^{15}$	$8.6 \cdot 10^{0}$
Caesium-137	30.254 y	$\mathbf{3.1 \cdot 10^{15}}$	$3.1 \cdot 10^{14}$
Cerium-144	284.893 d	$9.8 \cdot 10^{15}$	-
Promethium-147	2.6234 y	$7.5 \cdot 10^{15}$	$2.5 \cdot 10^{4}$
Plutonium-239	24204 y	$\mathbf{4.4 \cdot 10^{12}}$	$4.4 \cdot 10^{12}$
Plutonium-240	6555 y	$1.7 \cdot 10^{12}$	$1.7 \cdot 10^{12}$
Plutonium-241	14.353 y	$3.1 \cdot 10^{14}$	$2.5 \cdot 10^{12}$
Plutonium-242	373000 y	$1.0 \cdot 10^{9}$	$1.0 \cdot 10^{9}$
Americium-241	432.1 y	$4.4 \cdot 10^{10}$	$3.8 \cdot 10^{10}$
Americium-242m	142 y	$1.5 \cdot 10^{9}$	$9.2 \cdot 10^{8}$
Americium-243	7362 y	$1.7 \cdot 10^{9}$	$1.7 \cdot 10^{9}$
Curium-242	162.8 d	$5.6 \cdot 10^{12}$	-
Curium-234	28.5 y	$4.8 \cdot 10^{8}$	$4.2 \cdot 10^{7}$
Curium-244	18.077 y	$3.1 \cdot 10^{10}$	$6.7 \cdot 10^{8}$
Weapons:			
Plutonium-239	24204 y	$1.3 \cdot 10^{13}$	$1.3 \cdot 10^{13}$
Plutonium-240	6555 y	$3.0 \cdot 10^{12}$	$3.0 \cdot 10^{12}$
Long-lived decay products:			
Neptunium-237	2140000 y	-	$2.5 \cdot 10^{8}$
Americium-241	432.1 y	-	$9.0 \cdot 10^{12}$

y = years, d = days

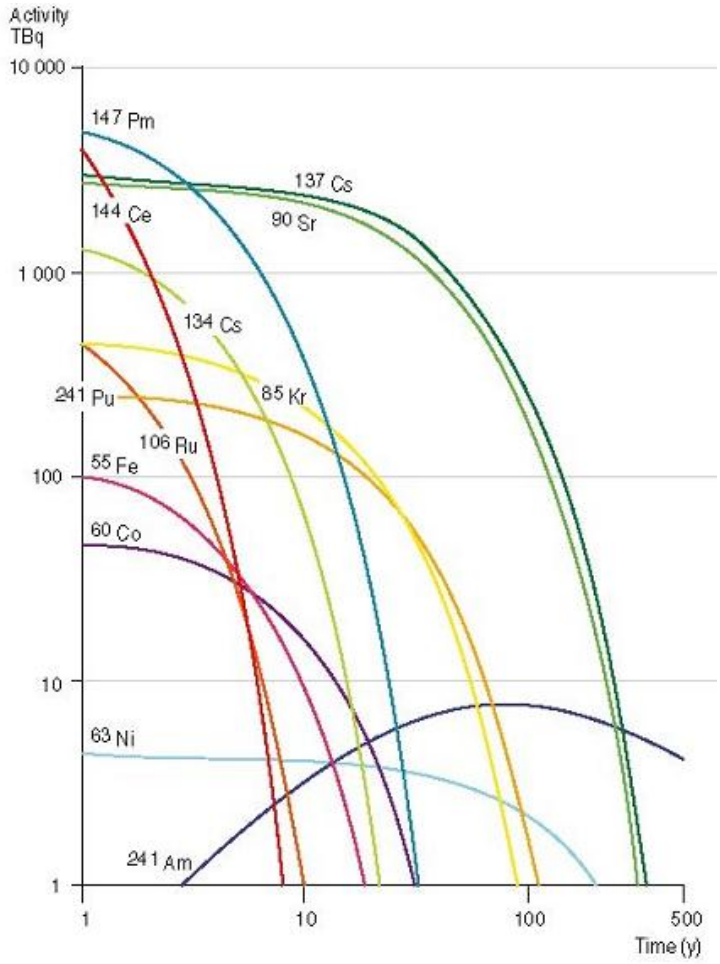

Figure 1.5. Contents of the most important radionuclides (besides ^{239}Pu and ^{240}Pu) in the reactor of the submarine Komsomolets *as a function of time (AMAP, 1998).*

1.2.3. Damages due to the accident

The front part of the submarine is most seriously damaged with holes in both the inner pressure hull and the outer hull. Videotapes taken during Russian expeditions in the summers 1991-1993, show a large hole (approx. 20 m^2) on the top of the front part of the pressure hull, situated just above the torpedoes in the first compartment (Høibråten et al., 1997). There are also several small cracks, and a large crack, approximately 2-3 cm wide on the port side of the submarine.

The Yablakov report (1993) stated that the hatches in the torpedo section were open, and the nuclear materials in the warheads were in contact with seawater. Russian authorities pointed to an extensive corrosion due to a galvanic corrosion process accelerated by the titanium hull (Føyn, 1994a). However, since we lack detailed information about the material used, the protective coating of the warheads or the titanium hull of the submarine, it is impossible to

predict the exact time of when the corrosion will take place. Holes in the torpedo section were sealed by nine titanium plugs during the expedition to *Komsomolets* in 1994 (Høibråten et al., 2003). This was done in order to prevent seawater from flowing through, and to minimise the immediate corrosion of the warheads.

1.2.4. Observed releases of radionuclides

Reports based on Russian measurements and the measurements taken by the IMR and the NRPA, state that there has been no observation of release of plutonium (Figure 1.2) (Føyn, 1994b) (NRPA, 2012). Of fission products from the reactor, only a slight elevation of caesium-137 (^{137}Cs) is recorded. These observations were made under the Russian cruises from 1991-1994, where the deep submersible manned vehicles MIR (one and two) were used. They were equipped to provide the radiation monitoring specially (Sagalevitch, 1995). The releases of the radionuclide were observed near the ventilation pipe, which went from the reactor to the top of the conning tower (Høibråten et al., 1997). In 1994, measurements were also taken inside the reactor-compartment ventilation tube, where the peak of the spectra revealed ^{137}Cs activity concentrations between 0.4 MBq/m^3 and 4 MBq/m^3 (Høibråten et al., 2003). The values decreased rapidly outside the pipe, where no ^{137}Cs was detected in any spectra that were collected on the upper deck of the reactor compartment.

1.3. Sources of caesium-137 (^{137}Cs)

The most important sources of caesium-137 (^{137}Cs) in the Norwegian and Barents Seas are global fallout from nuclear weapon tests in the 1950s and 1960s, fallout from nuclear weapons testing near Novaya Zemlya, discharges from the nuclear reprocessing plants at Seallfield (UK) and Cap de la Hague (France) and the Chernobyl accident in 1986 (e.g. Aarkrog, 1994, Strand et al., 1994, Kershaw and Baxter, 1995, Salbu et al., 1997, Smith et al., 2000). An overview of these sources and other actual and potential sources of ^{137}Cs in these waters are listed below.

1.3.1. Nuclear weapon tests

Nuclear weapons explosions have provided the largest inventory of both fission and neutron activation products in the global environment (AMAP, 1998). The first fission weapon test was performed in New Mexico, USA in July in 1945. This test, and the other fission weapon tests detonated in the years 1945-1952, resulted in depositions locally and did not influence the Polar Regions (Aarkrog, 1994). Thermonuclear bombs (H-bomb) on the other hand, first

tested at Eniwetok Island in the Pacific Ocean on 1 November 1952, led to global fallout. The major sites for such atmospheric releases beside the Bikini Island and the Eniwetok Island (USA), were the Nevanda test site (USA), and Semipalatinsk (Kazakstan, Former Soviet Union (FSU)).

In total, 522 atmospheric nuclear tests have taken place, where most of the atmospheric release occurred in the two periods 1952-1958 and 1961-1962 (UNSCEAR, 1993). They were separated by a temporary test ban treaty in 1959-1960. A treaty banning all atmospheric tests was sign in 1963 by USA, the Union of Soviet Socialist republics (USSR) and Great Britain. This led to a decrease in total global fallout, and since 1980, no atmospheric tests have been carried out by any country. Table 1.2 shows an overview of the total production of selected radionuclides by atmospheric nuclear tests.

Table 1.2. Total releases of selected radionuclides by atmospheric nuclear tests (UNSCEAR, 1993)

Radionuclides	***Total productions (PBq)***
Strontium-90 (^{90}Sr)	604
Caesium-137 (^{137}Cs)	912
Plutonium-239 (^{239}Pu)	6.5
Plutonium-240(^{240}Pu)	4.3
Plutonium-239 (^{241}Pu)	142

80 of the atmospheric nuclear tests took place at Novaya Zemlya (Figure 1.8), as well as 42 underground weapon tests (last one performed in 1990) (JNRE, 1996). Underwater nuclear weapon tests took also place at this archipelago in 1955, 1957 and 1961 (AMAP, 1998), where the detonations are assumed to have a short-term impact on the seawaters and a long-term impact on the sediments.

1.3.2. The Chernobyl accident

The Chernobyl nuclear power plant accident is probably the most well-known accidental explosion, releasing about 100 PBq ^{137}Cs (JNRE, 1996). The accident took place in Ukraine on April 26 1986, and affected the Northern Hemisphere, manly Europe and former USSR (Egorov et al., 1999). Due to run-off from contaminated areas on land and the marine transport from the Baltic, the North and the Norwegian Seas, contamination to the Arctic

Region still occur (Aarkrog, 1994). Figure 1.6 shows a map with sources of radioactivity in Europe, where the location of the Chernobyl accident are marked.

Figure 1.6. Sources of radionuclides in the northern environment: The sunken nuclear submarines K-159 *and* Komsomolets *(potential threat), the reprocessing plants Sellafield and Cap de la Hague, nuclear installations in Russia (Mayak, Tomsk and Krasnoyarsk), Chernobyl in Ukraine and nuclear weapons test site Novaya Zemlya (the archipelago located on the border between the Kara Sea and the Barents Sea) (NRPA, 2011).*

1.3.3. European reprocessing industry

Discharges from the European reprocessing plants Sellafield (formerly Windscale), UK, and Cap de La Hague, France, are the main sources for radioactive contamination to marine areas along the Norwegian coast and to the Arctic Region (Figure 1.7) (JNRE, 1996). The principle radionuclides released are the beta/gamma emitters ^{137}Cs, plutonium-241(^{241}Pu), strontium-90 (^{90}Sr), and ruthenium-106 (^{106}Ru), and the alpha emitters dominated by plutonium-238 (^{238}Pu), plutonium-239 (^{239}Pu) and americium-241 (^{241}Am) (Gray et al., 1995). Sellafield, the principle source with respect to quantities discharged, has discharged radioactive waste into the Irish Sea since 1951. A total release of ^{137}Cs from this power plant have been estimated to be 10^{15} PBq (Aarkrog, 1994), with a maximum release in the period 1974-1978 (JNRE, 1996).

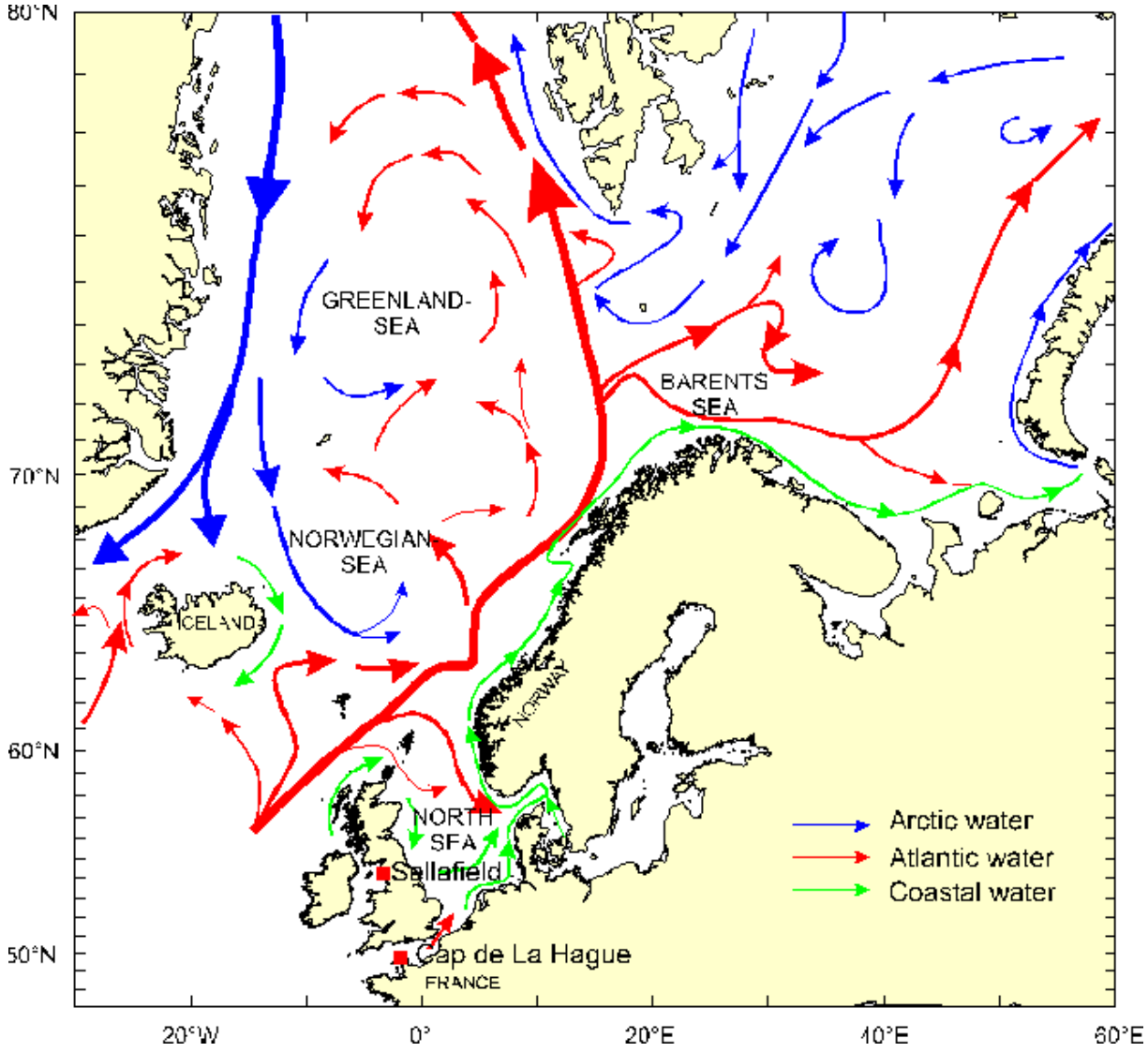

Figure 1.7. Circulation of surface waters of the North, Norwegian, Greenland and Barents Sea, where Sellafield and Cap de La Hague are marked (IMR).

1.3.4. Russian nuclear installations

Mayak (Chelabinsk), Krasnoyarsk and Tomsk are the three reprocessing plants for spent nuclear fuel in Russia (Figure 1.6). Mayak started operating in 1948, and was the first plant established in the USSR for production of nuclear weapons material (JNRE, 1996). Radioactive wastes from Mayak and Tomsk are discharged into the drainage area of the Ob River, while waste from Krasnoyarsk are discharged directly into the Yenisy River. These rivers are major contributors of freshwater to the Kara Sea, which can contain large amounts of dissolved and particulate material (Standring et al., 2008). This material can contain radionuclides, which can be spread further into the Barents Sea after entering the Kara Sea.

1.3.5. Dumped radioactive materials

FSU has dumped large amount of radioactive waste disposal in shallow seawaters of the Arctic Seas from 1959 - 1991, where they are present as actual and potential sources. In 1993, the Russian Federation published the so-called "White book", which reported that the total amount were approximately 90 PBq at the time of dumping, where 89 PBq of the total inventory was high-level radioactive waste (Yablakov et al., 1993). According to the last edition of the White Book in 2000, this is to be found on the seabed in the Arctic (Sivintsev et al., 2005):

- Three nuclear powered submarines with fuel
- nuclear submarine (NS) *K-27* dumped in the Stepovogo Fjord in the Kara Sea
- NS *Komsomolets* accidentally sunk in the Norwegian Sea in 1989
- NS *K-159* accidentally sunk in the Barents Sea near the Kola Bay entrance in 2003
- A submarine reactor with spent nuclear fuel (SNF) in the Novaya Zemlya trough
- Shielding assembly with parts of SNF from the nuclear icebreaker *Lenin* in the Tsivolki Fjord
- Five reactor compartments with and without SNF, from nuclear submarines and from the nuclear icebreaker *Lenin*
- 18 ships loaded with solid radioactive waste
- More than 900 other radioactive items (unpacked radioactive waste)
- More than 17000 containers with solid radioactive waste

The main dumping area was situated in the eastern part of the Novaya Zemlya shelf (Figure 1.8), where eight disposal areas hosted 70% of the FSUs total sea-disposal of radioactive waste products (Stepanets et al., 2007).

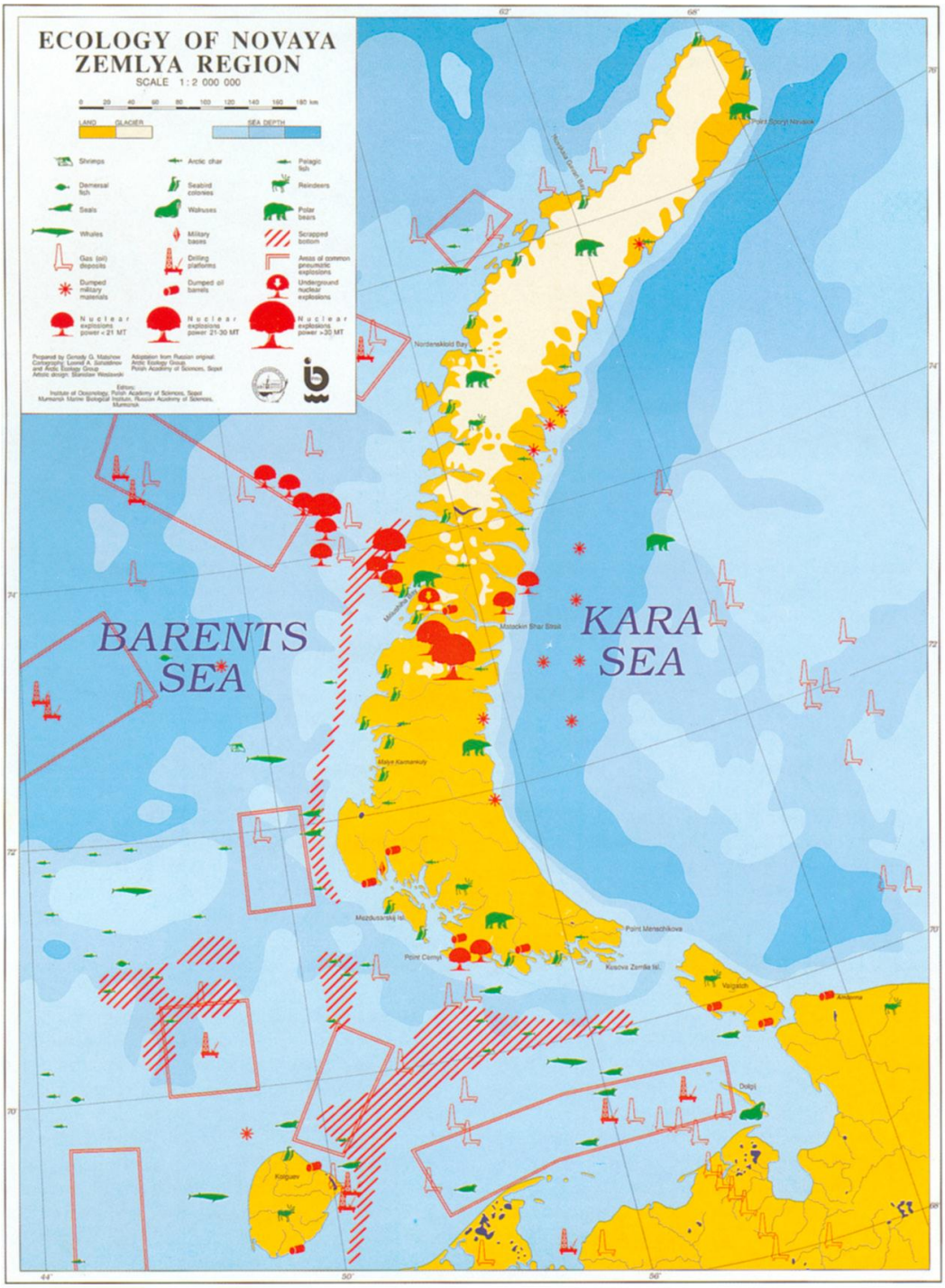

Figure 1.8. Ocean dumping sites and sites of nuclear weapon tests of FSU at the Novaya Zemlya. This map also shows an overview of gas deposits and the animal life at and around Novaya Zemlya (Champ et al., 1997).

1.4. Caesium-137 (^{137}Cs)

1.4.1. Chemical and physical properties of Caesium-137 (^{137}Cs)

Caesium-137(^{137}Cs) is a radioactive isotope of the alkali metal caesium (Cs) with atomic number 55 in group 1 in the periodic table. It is a chemical analog to potassium (K) and rubidium (Rb), and is formed anthropogenically as a fission product by nuclear fission. In the fission process a heavy nucleus, often uranium or plutonium, is bombarded with neutrons, which results in splitting of the original nucleus and formation of new elements (Choppin, 2013).

Caesium-137 (^{137}Cs) did not exist prior to discovery of nuclear fission, but after years of nuclear industry and nuclear weapons, it is present almost everywhere on earth. It is the largest contributor to dose among anthropogenic radionuclide, and has often been chosen as the most significant representative of the anthropogenic radionuclides found in the marine environment (Povinec et al., 2003).

Caesium-137(^{137}Cs) has a half-life ($t_{½}$) of 30.07 years (Schøtzig and Schraeder, 1993), and decays by beta emission (95%), where an electron is emitted. The beta decay leads to a change in elemental composition where a new element is formed. When ^{137}Cs decays, meta-stable barium-137 (^{137}mBa) are formed, which further decays by gamma emission to stable barium-137 (^{137}Ba) (Figure 1.9) (Choppin, 2013).

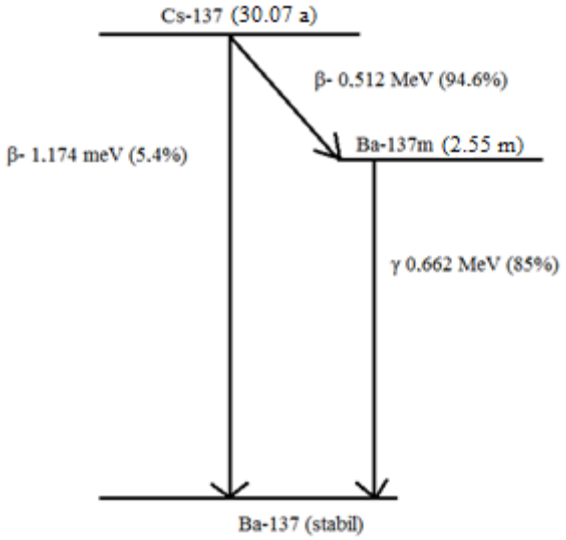

Figure 1.9. Caesium-137(^{137}Cs) decay scheme. The nuclide with half-life of 30.07 years, decays mainly (94.6%) by beta emission with an energy of 0.512 MeV to the meta-stable barium-137m (^{137}mBa), which further decays by gamma emission of 0.6617 MeV to the stable isotope barium-137 (^{137}Ba) (Choppin, 2013).

The ^{137}mBa isotope goes through a change in energy state by emitting a photon, without changing the elemental composition, which results in the stable form of barium. This process happens rapidly, where the half-life of ^{137}mBa is only 2.55 minutes (Choppin, 2013). The gamma emission from the meta-stable barium has a characteristic energy of 661.7 keV, which easily can be measured by a gamma detector (Schøtzig and Schraeder, 1993).

In this case, the half-life of the mother nuclide is much larger than the half-life of the daughter nuclide, where the amount of daughter atoms becomes constant after some time. At that time the rate of decay of the daughter becomes equal to the rate of decay of the parent. This forms a steady state condition commonly known as the "secular equilibrium" (Choppin, 2013). In this condition, the activities of the different nuclides will be equal, meaning that it is irrelevant which one of the nuclides are measured. Due to more complicated sample preparation involving radiochemical separation of the beta measurements, it is more convenient to measure the activity from the gamma emitting ^{137}mBa, whose energy is entitled the "caesium-energy".

1.4.2. Caesium-137 (^{137}Cs) in the marine environment

The distribution of radionuclides depends of their origin, nature and transport route. Caesium-137 (^{137}Cs) behaviour in the marine water column is very similar to that of conservative radionuclides (Povinec et al., 2003), where it will be in solution in seawater, which make its water transport easily to trace (Livingston, 2004). Caesium-137 (^{137}Cs) was therefor often used as an oceanographic tracer (England and Maier-Reimer, 2001), which is extremely valuable for the transport and dispersion of costal pollution from Europe to the Artic. That is because the sources are few and relatively well defined, and the ^{137}Cs-nuclide can be quantified accurately at extremely low activity concentrations (Chen et al., 1994). But due to the diffuse input following the Chernobyl accident, the use of ^{137}Cs as an oceanographic tracer, has been somewhat diminished. However, ^{137}Cs can be used in modelling experiments to study releases from point sources such as sunken nuclear submarines.

1.4.3. Caesium-137 (^{137}Cs) in sediments

Sediments are the final sink for most particles and organic materials present in seawater (SFT, 2007). Caesium-137 (^{137}Cs) is, as mentioned, not very easily scavenged by particulate matter and is therefore found in the water column, but it is also found in sediments. The percentage of sedimentation of this radionuclide is rather small, where only 2% of all the ^{137}Cs transported through the North Sea is stored in the North Sea sediments, where the rest passes through (Beks, 2000). Sediments consist mostly of clay, silica, calcium carbonate and organic matter (Sarmiento and Gruber, 2006), where this radionuclide binds irreversible to the clay mineral illite (Coughtrey, 1983). This means that higher levels of ^{137}Cs activity concentrations may be expected in sediment cores with high clay content. The sedimentation rate also influences the activity concentration of ^{137}Cs on the seabed, where this process can be quite complicated. It depends on numerous factors such as gravity force and counter currents (Lukashin and Shcherbinin, 2007).

The relationship between radionuclides in bottom sediments and seawater can be described by the distribution coefficient, K_d (formula 1.1) (IAEA, 2004).

(1.1) $$K_d = \frac{Concentration\ per\ unit\ mass\ of\ sediment\ (kg/kg\ or\ Bq/kg\ d.w.)}{Concentration\ per\ unit\ mass\ of\ water\ (kg/kg\ or\ Bq/kg)}$$

IAEA presented in 2004 a list of the recommended K_d for open ocean environment for different radionuclides, where the K_d of ^{137}Cs was set to 2×10^3. This value can easily be compared to other K_ds, where the recommended K_d of plutonium (Pu) for instance is 1×10^5.

Pu has a much higher K_d then ^{137}Cs, therefore making it an unconservative radionuclide, where it is easily scavenged and is to be fined in the sediments (Hunt et al., 2013). The process, however, is not that simple. The distribution of Pu between seawater and sediments greatly depends on its oxidation state (Ikäheimonen, 2003), where it may remobilize to the marine environment under the right conditions (Lindahl et al., 2010).

1.5. Dispersion of caesium-137 (^{137}Cs) from *Komsomolets*

Several scientists have modelled the spread of caesium-137 (^{137}Cs) from *Komsomolets*. Heldal et al. (2013) assessed the effect of a potential long term leakage and a pulse release of ^{137}Cs from the wreck. The dispersal patterns of the two scenarios were quite similar, where the result of the pulse release is shown in Figure 1.10.

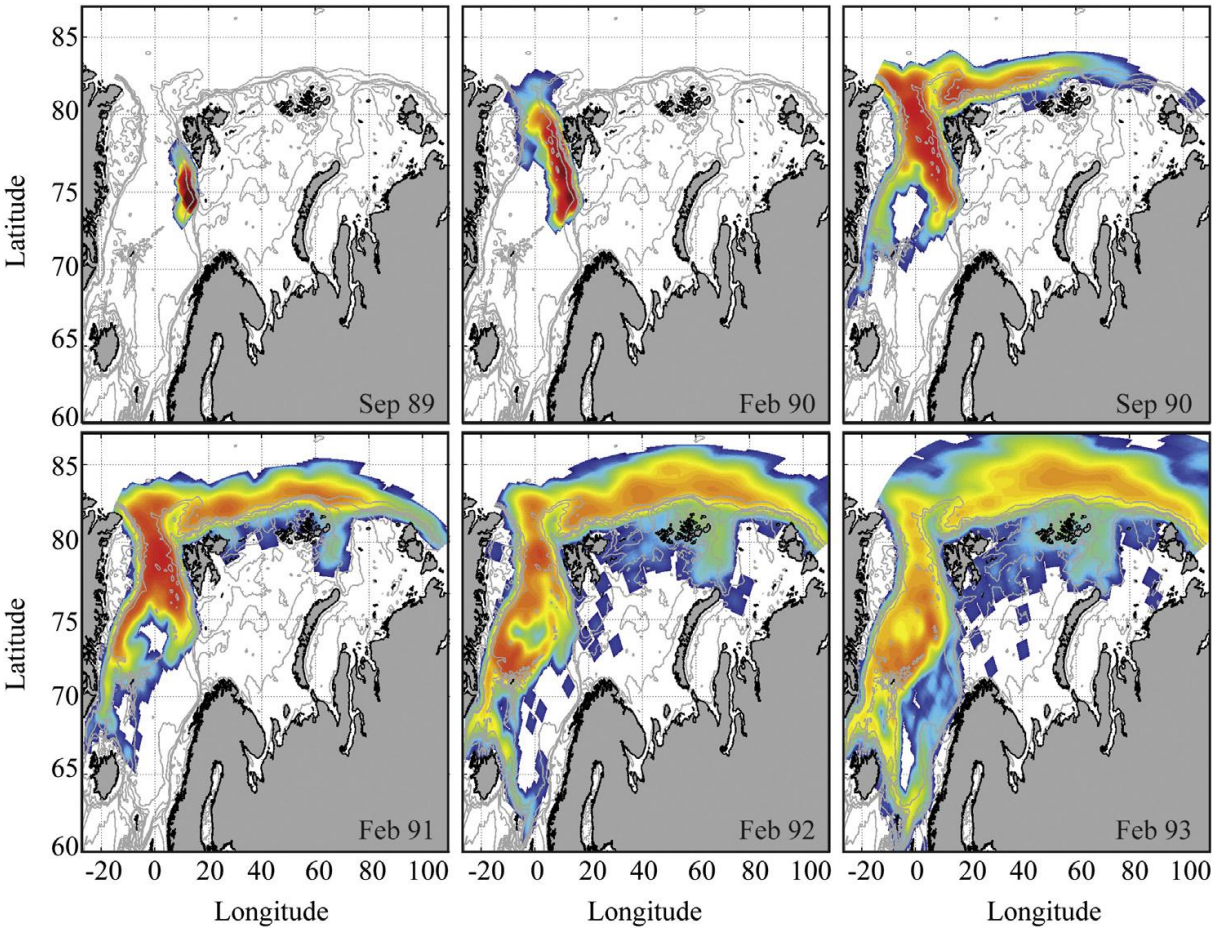

Figure 1.10. Bq/m^2 surface at different times after a pulse discharge of 100% of the total inventory of caesium-137 (^{137}Cs) from the Komsomolets *on April 26th, 1989. The colour scale is logarithmic and indicates levels from 0 (blue) to 5 (red) (Heldal et al., 2013).*

Figure 1.10 shows how the discharges from *Komsomolets* are either transported into the Arctic Ocean and eastwards along the shelf edge or re-circulated in the Fram Strait and

transported southwards in the East Greenland Current (EGC). A minor part flows into the Barents Sea, where it only flows southward on the eastern side of Spitsbergen. The part flowing south along East Greenland is recirculated in the Greenland Sea, recirculated in the Norwegian Sea, or advected out of the Norwegian Sea through the Denmark Strait.

The results indicate that both continuous leakages and pulse discharges of ^{137}Cs from *Komsomolets* induce negligible activity concentrations of ^{137}Cs in cod and capelin (Heldal et al., 2013).

1.6. Other sunken nuclear submarines in the North Atlantic

Despite from *Komsomolets* there are six other sunken nuclear submarines in the North Atlantic (Eriksen, 1990). Table 1.3 show an overview of these submarines including the seventh submarine *Kursk*, which was raised 14 months after its sinking in year 2000 (Hayrynen, 2003).

Table 1.3. Sunken nuclear submarines in the North Atlantic (except the Komsomolets*).*

Name /class	***Nationality***	***Year of sinking***	***Depth (m) of resting place***	***Resting place***
Thresher (Eriksen, 1990)	American	1963	2500	350 km off Capa Cod, Newfoundland
Scorpion (Eriksen, 1990)	American	1968	3100	650 km souoth-west of Azores
k-27 /November class *(Gwynn et al., 2013)*	Soviet	1968	33	Dumped in the Stepovogo Bay at Novaya Zemlya in 1982
k-8 /November class *(Eriksen, 1990)*	Soviet	1970	4680	300 nautical miles north-west of Spain
k-219 /Yankee class (Eriksen, 1990)	Soviet	1986	1000	North-east of Bermuda
K-159/ November class (Eriksen, 1990)	Russian	2003	238	Outside the Murmansk fjord
K-141 (*Kursk*)/ Oscar II class *(Hayrynen, 2003)*	Russian	2000	(108 m)	150 km north of the naval base of Sveromorsk (raised)

Despite *kursk*, which is raised, the other submarines rests as potential sources of radioactive contamination on the seabed, where the magnitude of the threat will depend on the resting place of the submarine and on the extent of leakage (Eriksen, 1990). Radiological surveys on samples of sediments and seawater collected near the various sits of these submarines have been carried out, where no elevated levels of ^{137}Cs have been detected (IAEA, 2001). However, some levels of ^{60}Co have been detected in sediment samples collected close to the submarines *Scorpion* and *Thresher* (KAPL, 2000).

2. Materials and methods

2.1. Sample collection

The samples were collected during two cruises with R/V *G. O. Sars*; 18-19.09.2012 (2012111) and 1-9.04.2013 (2013105). The author of this thesis attended the latter cruise. The 2012-samples were collected by the staff from IMR's Chemistry laboratory.

In connection with previous monitoring of the resting place of *Komsomolets*, it has not been possible to determine how close to the wreck the samples were taken. In 2012, an attempt was made to collect samples close to the wreck, where the box-corer was equipped with a wireless acoustic transponder which communicated with R/V *G. O. Sars* dynamic positioning system (see Appendix F). Due to weather conditions and lack of time, the attempt did not succeed. The attempt was repeated with success in 2013. Therefore, the description of the sample collection is based on the collection of the 2013 samples.

2.1.1. *Search for the* Komsomolets

In earlier years, *Komsomolets* has been observed on echo sounding systems on board both R/V *Johan Hjort* and R/V *G. O. Sars*. In 2012, the submarine was located with the aid of the multibeam, the Olex system and the EK60 (Table 2.1). However, since the EK60 has a 7° detection radius from the vessel and the depth is approximately 1700 m, the actual area becomes quite large (Figure 2.1).

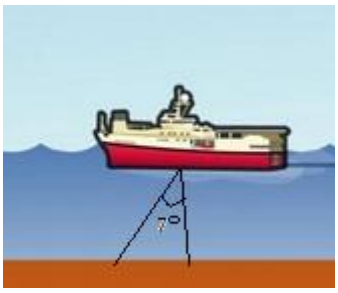

Figure 2.1. Illustration of the detection radius of Simrad EK60 system.

Despite not optimal weather conditions, we started (at the 7th of April 2013 at approximately 12.00 am) by mapping the seabed (1km^2 around the vessel) by using the multibeam and the Olex-bottom mapping system. These and other equipment used on the 2013 cruise with R/V *G. O. Sars* are listed Table 2.1. The vessel passed slowly over the area where we knew the wreck was resting (from scientific reports and the 2012 monitoring, see Appendix F). When

we received a signal from the wreck, we marked it on a map, and established a route that the vessel should follow (Figure 2.2 a). This was a crisscrossing route (Figure 2.2 a and b), where we continued to mark the map every time that the Olex system or the Simrad EK60 received a signal from what was assumed to be the *Komsomolets*. The detected signals would eventually overlap each other, where this overlap-point would indicate the exact location of the submarine. An example of such signals is shown in Figure 2.3, which is result from the vertical sonar, Simrad EK60.

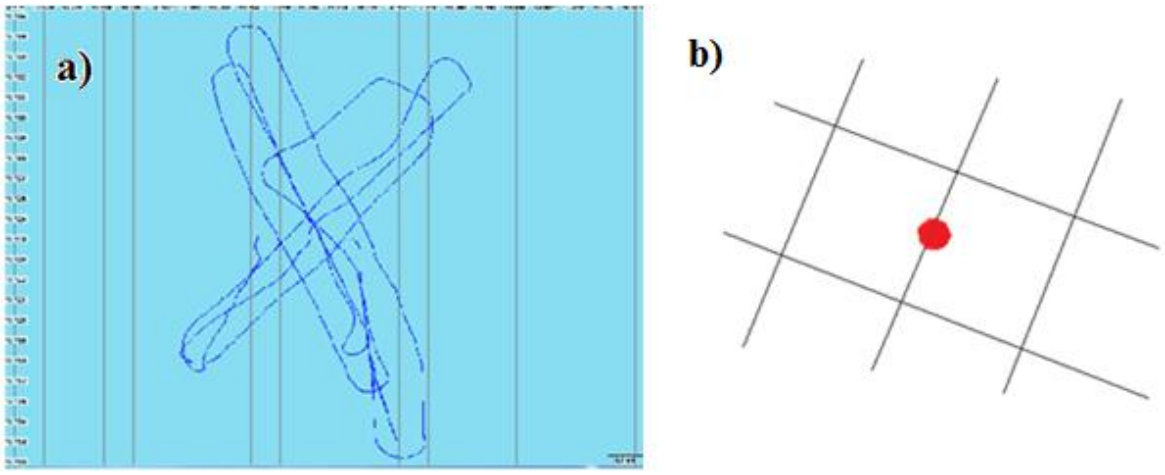

Figure 2.2. (a) The route of the vessel tracked on the computer. (b) An illustration of how the route was established (the black lines) and where the signal was marked (the red spot).

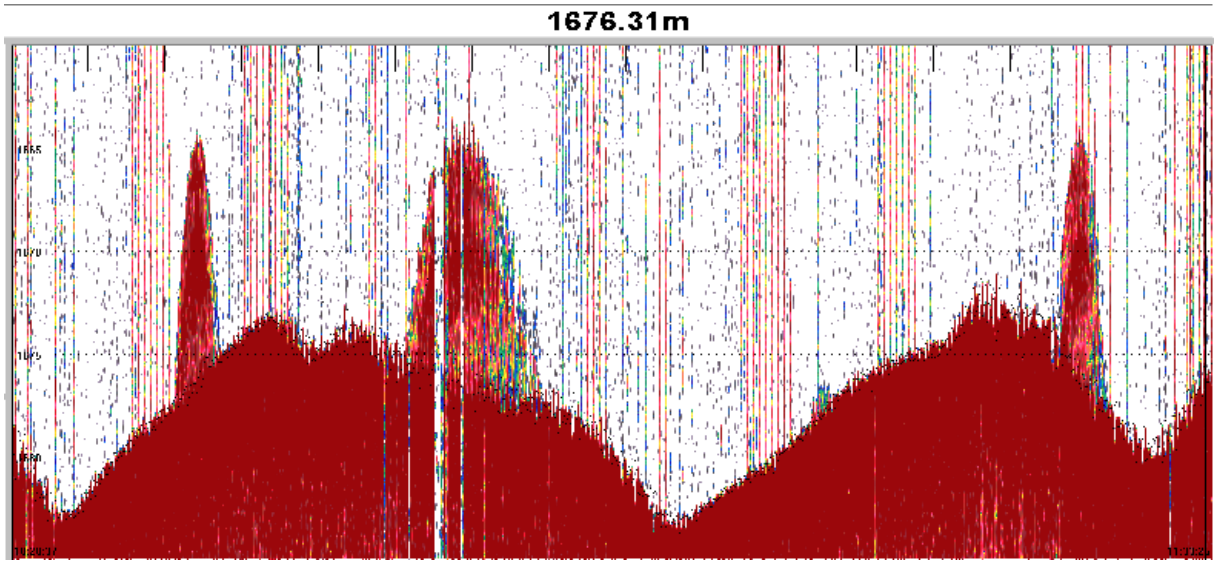

Figure 2.3. Result from Simrad EK60. The pointy signals are from Komsomolets, *and the softer, rounded signals are from the seabed.*

After approximately six hours of searching, we were satisfied with the determination of the location of the wreck (Figure 2.4), which respectively had the latitude and longitude of 73°43'45" N and 13°16'00" E.

Table 2.1. Equipment list for the 2012 and 2013 cruises with R/V G. O. Sars.

Instrument	***Application***
OLEX program	A program that can plot a real-time digital 3D picture of the seabed, aided by data from the vessels GPS and multibeam echo sounders. The program saves bottom data like depth, latitude, and longitude, which is constantly calculated and adapted to previous measurements.
Multibeam Kongsberg EM302	An echo sounder, which was used to map the seabed and to find the sunken submarine.
Simrad EK60	Fisheries vertical sonar, which was used to see the prevalence of the submarine.
Kongsberg DPS	A computer controlled system that automatically maintain the vessel's position and heading by using its own propellers and thrusters. This is used so that the vessel is placed at the exact same location during the sediment samples collection.
Kongsberg HiPAP 500: "High precision acoustic positioning"	An acoustic underwater positioning system consisting of both a transponder (receiver) and a transmitter (transducer). The transmitter, placed inside the vessel, sends a signal against the seabed transponder, and the transponder responds to this and gives a replay. The transducer then calculates the accurate position of the transponder relative to the vessel.
Simrad MST342	A transponder that was attached to the box-corer, and connected to the HiPAP 500 system of the boat. The transponder sends the necessary information about the position of the box-corer at the seabed, so that the position can be determined with high accuracy.
SBE911 Plus	A CTD that measure Conductivity, temperature and depth vertically from the sea surface to the seabed. With the help of these parameters we can calculate depth, salinity, density and the waters sound velocity.
Smøgen box-corer	Used to collect sediment samples.
Sediment cutter	Used to cut the sediment cores into 1 cm layers.

2.1.2. Determining sample locations, and positioning the box-corer

After locating *Komsomolets*, we determined 5 sample locations around the wreck (Figure 2.4). Location 1 (or "Grabb 1" as the yellow cross is named in Figure 2.4, represents station 194), was near the (assumed) front of the wreck. Location 2 (station 195) and 4 (station 197) were at the west and east side of the wreck, respectively, and location 3 (station 196) near the stern. In addition, location 5 (station 199) was 100 m upstream of the wreck (reference station). At this location, we had one unsuccessful sample collection (station 198, reference station), where the box-corer arms did not close up before entering the surface. The procedure was performed again at the same location, this time with a successful result.

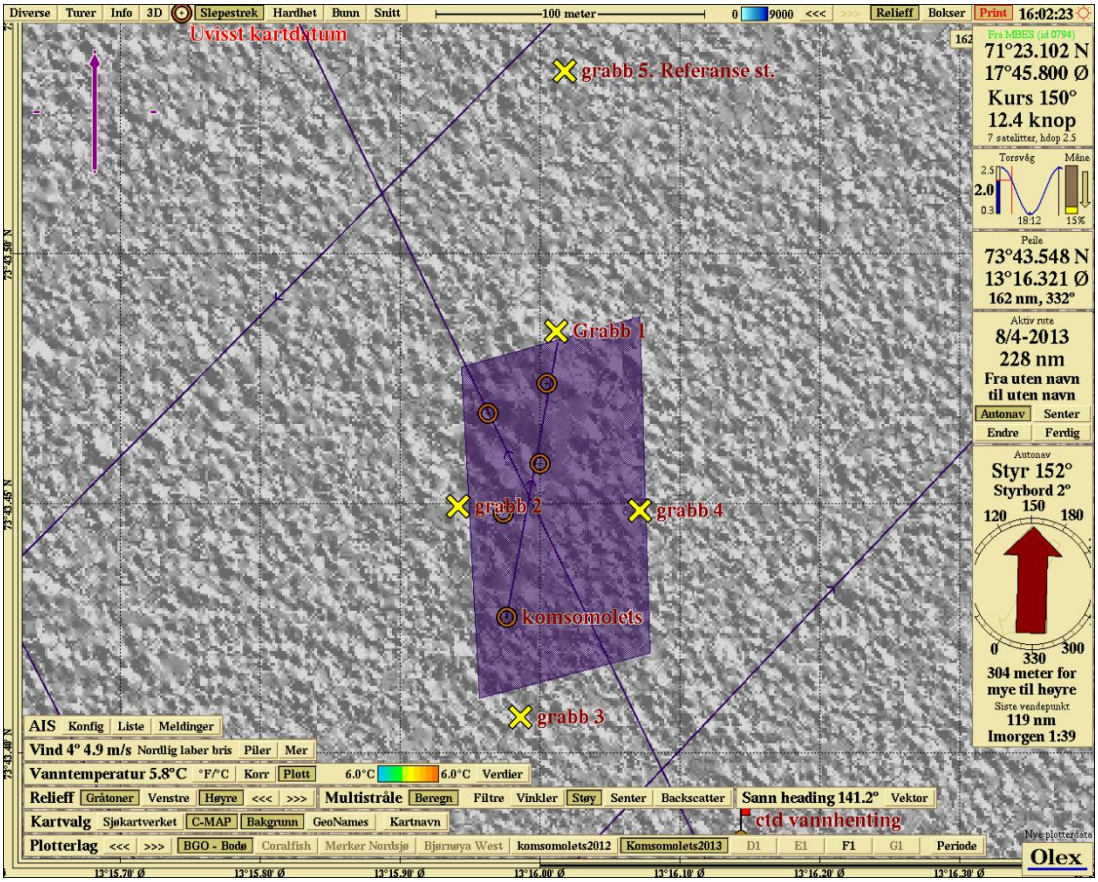

Figure 2.4. Olex picture from 2013. The wreck of Komsomolets *is located within the dark square. The red circles indicate points where we received signals from the submarine, and the yellow crosses indicate sample locations ("Grabb 1" = station 194, "grabb 2" = station 195, etc.).*

The transponder, Simrad MST342, concealed by a protecting metal tube, was attached to the box-corer as shown in Figure 2.5.The vessel, and hence the box-corer was exactly positioned using Kongsberg DPS. The box-corer was then lowered, and when the position device was

close (within 1 m) to one of the pre-determined sample locations (location 1-5 in Figure 2.4), the last 20 m of wire was released. Thereby, the box-corer hit the seabed. The actual position of where the box-corer hit the seabed was determined by the HIPAP-system of the boat, and transferred to the Olex-program.

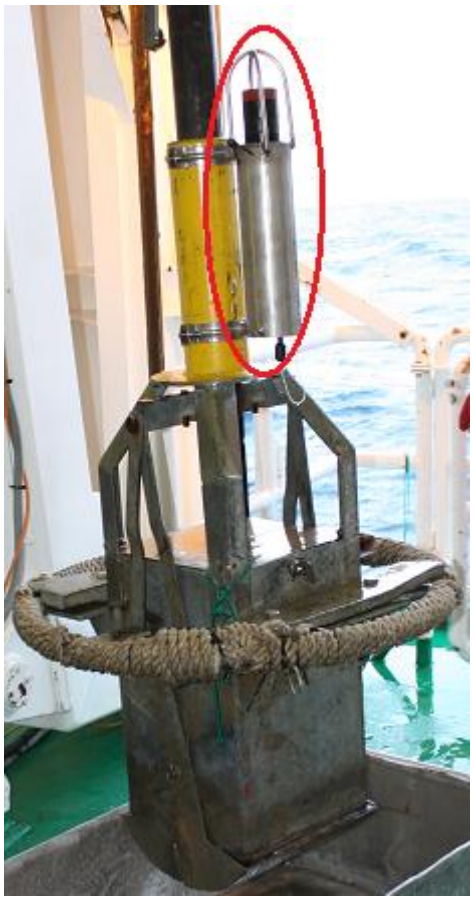

Figure 2.5. The box-corer and the transponder (marked with a red circle). Photo: Janita Flo.

2.1.3. Sediment sample collection

The samples were collected with a Smøgen box-corer (Figure 2.5). It is equipped with an inner box of stainless steel with an area of 30 x 30 cm and a height of 40 cm (Sværen, 2010a). The device takes an undisturbed portion of the seabed. The box-corer is supported with lead weights on a supporting frame, and is forced into the seabed by its weight. How far into the sediments it penetrates, depends on the composition of the seabed. When the box-corer hit the seabed, the "pin lock" holding the box-corers arms is removed. As the box-corer is slowly pulled out of the sediment, a mechanism allows the box-corer arms to swing below the sample box sealing in the sediment. Simultaneously, flaps above the sample box are closed to prevent the sample of being disturbed during recovery (Sværen, 2010a).

When the box-corer returned to the vessel, the radiation levels were checked with an Automess dose rate meter (Figure 2.6). This was done to ensure that the samples were safe to work with. Radiation levels did not exceed 0.2 µSv/h. The radiation levels were checked several times during the work.

Figure 2.6. The radiation level was checked with an Automess dose rate meter (marked with a red circle). Photo: Janita Flo.

Some of the samples had water on top of the sediments, which was removed using a hose. From the box-corer, sediment cores were collected using PVC tubes with an inner diameter of 10 cm and a length of 40 cm (Sværen, 2010a). These tubes have a sharp lower edge, and were manually pressed into the box-corer (Figure 2.7). Excess material was removed, and the cores were transferred from the box by placing a thin metal plate underneath the core and seal them with plastic lids on the top and bottom. The maximum number of cores to be taken from one box is 4.

Figure 2.7. Taking sediment core samples. Photo: Janita Flo.

Table 2.2 and 2.3 show an overview of the sediment samples collected in 2012 and 2013. Information like station number, location, date, number of cores and their length are listed, in addition to information about which of the samples were measured for caesium-137 (^{137}Cs), lead-210 (^{210}Pb) and radium-226 (^{226}Ra), and which of the samples were sent to NRPA for further measurements.

Table 2.2. 2012 samples.

Station	Date	Number of cores	Length (cm)	Latitude (N)	Longitude (E)	Analysed for ^{137}Cs	Analysed for ^{210}Pb and ^{226}Ra	Analysed for Pu and ^{241}Am	Particle size analysed
122	06.09.12	2	122-1: 12 122-2: 13	73°43'547"	13°15'621"	All cores	Core 1.2	-	-
123	06.09.12	2	123-1: 3 123-2: 7	73°43'482"	13°16'318"	All cores	Core 2.2	-	-
124	06.09.12	4	124-1: 5 124-2: 7 124-3: 7 124-4: 6	73°43'398"	13°16'088"	All cores	-	-	-
125	06.09.12	2	125-1: 7 125-2: 8	73°43'418"	13°15'784"	All cores	-	-	-

Table 2.3. 2013 samples.

Station	*Date*	*Number of cores*	*Length (cm)*	*Latitude (N)*	*Longitude (E)*	*Analysed for ^{137}Cs*	*Analysed for ^{210}Pb and ^{226}Ra*	*Analysed for Pu and ^{241}Am*	*Particle size analysed*
194	07.04.13	4	194-1: 16 194-2: 17 194-3: 17 194-4: 15	73° 43'487"	13° 16'002"	First ten cm of core 194-2	-	First two cm of core 194-2	First cm of core 194-2
195	07.04.13	2	195-1: 19 195-2: 15	73° 43'447"	13° 16'052"	First ten cm of core 195-1	-	First two cm of core 195-1	First cm of core 195-1
196	07.04.13	2	196-1: 10 196-2: 10	73° 43'446"	13° 15'938"	First ten cm of core 196-1	-	First two cm of core 196-1	First cm of core 196-1
197	07.04.13	2	197-1: 11 197-2: 12	73° 43'407"	13° 15'985"	First ten cm of core 197-2	-	First two cm of core 197-2	First cm of core 197-2
199 (ref)	08.04.13	2	199-1: 9 199-2: 8	-	-	First ten cm of core 191-1	-	First two cm of core 199-1	First cm of core 199-1

2.2. Sample preparation

The sample preparation of the 2012 samples took place during autumn 2012 and spring 2013, at IMR's Chemistry laboratory by the author of this thesis. This is the same procedure as for the 2013 samples, prepared in the spring and summer of 2013. For these samples, slicing the cores and determination of wet weights of the samples were performed by the author of this thesis, and the rest were performed by the staff from IMR's Chemistry laboratory (see Appendix A). The equipment used is listed in Table 2.4.

Table 2.4. Equipment used in sample preparation.

Instrument	***Remark***	***Application***
Mettler-Toleodo PG5001-S	Max 5100 g d = 0.1g	Weight measurements
Mettler-Toleodo PG503-S	Max 510 g d = 0.001g	Weight measurements
CHRIST ALPHA 1-4 freeze dryer with Edwards PV3 vacuum pump		Dry freezing of samples
Porcelain mortar and pestle		homogenization
Lorakon (LOkal RAdioaktivitets KONtroll) polyethylene boxes (60 mL) with lid counting container	Nolato AB art.no.110170 (box) and 112040 (lid)	Hold sample material and ensure an appropriate sample geometry
Piston		Pressing the sediment core upwards for cutting sediment samples

2.2.1. Slicing the cores

The sediment cores were cut in standing position using a piston (Table 2.4) pressing the core carefully upwards. The cores were cut in 1 cm slices (Figure 2.8) and transferred to pre-weighed aluminum cups. The wet weights were determined using Mettler-Toleodo PG503-S (Table 2.4). The length of the sediment cores collected in 2012 varied between 3 cm to 13 cm (Table 2.2) where the slicing of the cores were performed at IMR's Chemistry laboratory.

They were sliced into a total of 76 samples. The 2013 cores were longer, varying from 8 cm to 19 cm (Table 2.3). They were sliced into a total of 159 samples, and the process was performed on board R/V *G. O. Sars*. The samples, either in form of whole cores (2012) or 1 cm slices (2013), were frozen on board the vessel at a temperature of -20 °C.

Figure 2.8. Cutting the core in 1 cm layers. Photo: Janita Flo.

2.2.2. Homogenizing the samples

The frozen samples were freeze-dried using CHRIST ALPHA 1-4 freeze dryer (Table 2.4, Figure 2.9 (a)) with Edwards RW3 vacuum pump until completely dryness. The dry weight of each sample was determined using Mettler-Toleodo PG503-S (Table 2.4). After drying, the samples were crushed and homogenized using a mortar (Table 2.4, Figure 2.9 (b)). Since *Komsomolets* resting place is on a muddy ground located at a great depth, the sediment samples did not contain any stones or shells with diameter >1 cm.

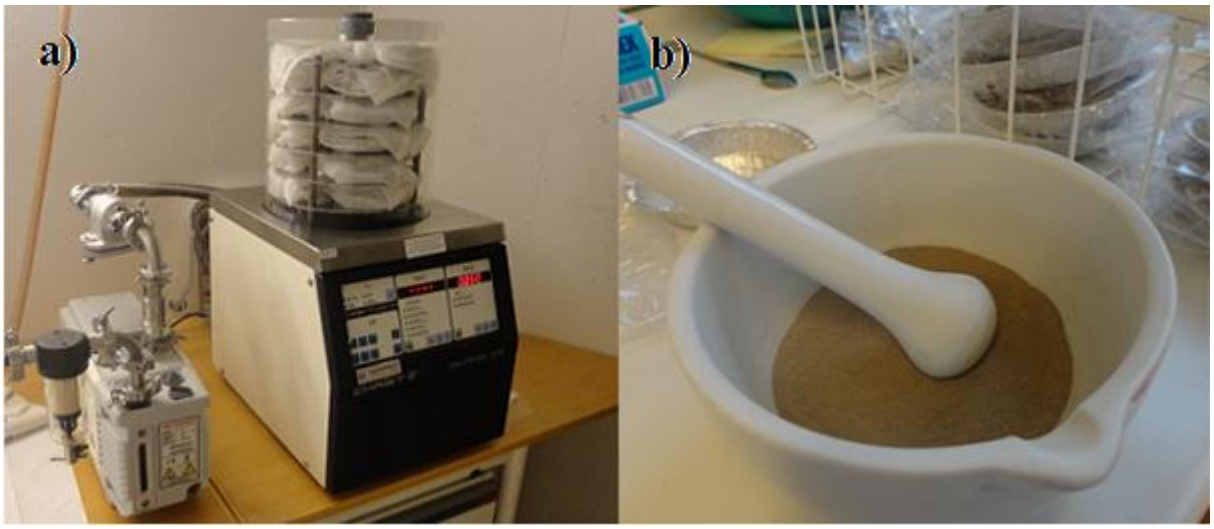

Figure 2.9. (a) Samples getting freeze-dried in the CHRIST ALPHA 1-4 freeze dryer with Edwards RW3 vacuum pump, and (b) a sample getting homogenized using a mortar. Photo: Janita Flo.

Known amounts of the sample material were put in 60 mL Lorakon polyethylene boxes (Table 2.4), up to 5 mm from the top. This ensured that all of the samples were measured with the same geometry as the calibration standard (described in section 2.4.3). The sample mass was determined using Mettler-Toleodo PG5001-S (Table 2.4), and the box was marked with name, station number and cm layer, sampling date, journal number and sample mass.

2.2.3. Lead 210 (^{210}Pb) dating

Uranium-238 (^{238}U) has a nearly infinite half-life ($t_{½}$), where its activity concentration on earth can be regarded as constant with respect to decay. However, depending on the earth crust, the actual activity concentration will vary from location to location (Goldberg, 1963). The decay-series of ^{238}U is one of the naturally existing radioactive decay-series, which is shown in Figure 2.10.

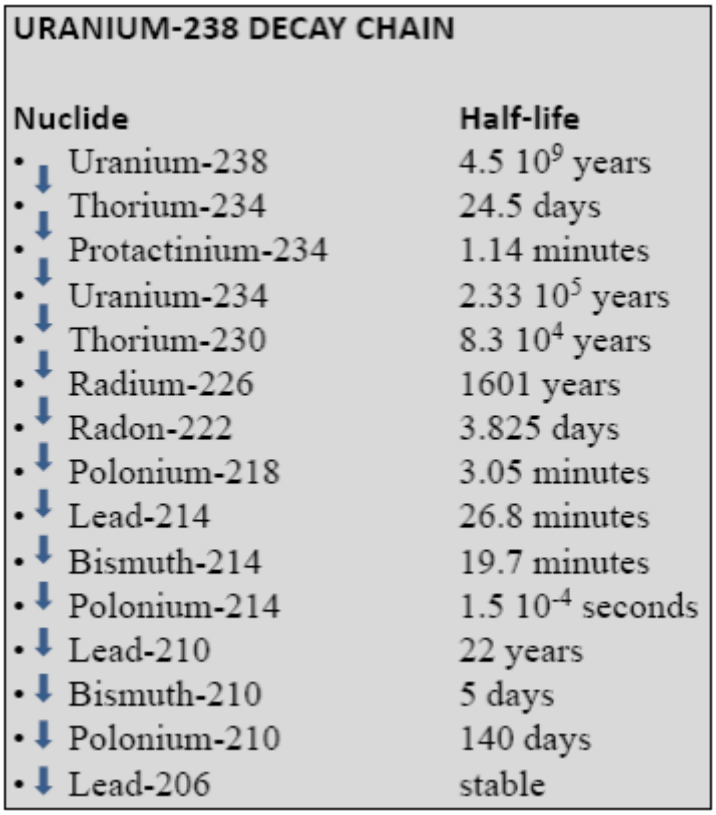

URANIUM-238 DECAY CHAIN

Nuclide	Half-life
Uranium-238	$4.5\ 10^{9}$ years
Thorium-234	24.5 days
Protactinium-234	1.14 minutes
Uranium-234	$2.33\ 10^{5}$ years
Thorium-230	$8.3\ 10^{4}$ years
Radium-226	1601 years
Radon-222	3.825 days
Polonium-218	3.05 minutes
Lead-214	26.8 minutes
Bismuth-214	19.7 minutes
Polonium-214	$1.5\ 10^{-4}$ seconds
Lead-210	22 years
Bismuth-210	5 days
Polonium-210	140 days
Lead-206	stable

Figure 2.10. Daughters in the naturally occurring uranium-238 (^{238}U) decay series (Schøtzig and Schraeder, 1993).

Lead-210 (^{210}Pb), which has a half-life ($t_{½}$) of 22.3 years, is one of the daughters in this series, and is frequently used in dating marine sediments. The age (within the last 120 years) of a sediment sample can be measured based on the content of natural radioactivity; ^{210}Pb and radium-226 (^{226}Ra) (Goldberg, 1963). This is possible when sediments accumulate undisturbed, where the sediment rates also can be measured. The dating can be done by slicing a sediment core from marine sediments into samples representing sediment layers deposited in a certain period. Fresh ^{210}Pb will here deposit on surface sediments together with precipitating material. When buried, the ^{210}Pb decays and its activity concentration in the profile of the core follows the exponential decline with depth.

Two of the sediment cores from the 2012 samples were wrapped in aluminum foil and sealed with aluminum tape in order to prevent escape of radon-222 (^{222}Rn) gas. These samples were stored for at least one month in order to establish the necessary steady-state equilibrium between the radionuclides in the uranium-series (Figure 2.10). The age of a particular layer was found by calculating the amount of ^{210}Pb which had decayed. These calculations have been performed by Ingrid Sværen, where the principle of this procedure is described by (Goldberg, 1963), and all equations used are obtained from Sværen (2010a).

2.2.4. Density correction

Each core layer's porosity was calculated using equation 2.1. Thereafter, the thickness of each layer below 1 cm was corrected for density compression using equation 2.2 (Tadjiki and Erten, 1994). All raw data are presented in Appendix A.

(2.1) $$Porosity\ (\%) = \frac{Sample(g)_{wet\ weight} - Sample(g)_{dry\ weight}}{Sample(g)_{wet\ weight}}$$

(2.2) $$CT_i = NT_i + NT_i \cdot \left[\frac{P_1 - P_i}{100 - P_1}\right]$$

Where

CT_i = the corrected thickness of layer *i*

NT_i = the normal thickness of layer *i*

P_1 = the porosity of the upper layer (1)

P_i = the porosity of layer *i*

The corrected depth of the samples was then estimated by applying these parameters in equation 2.3:

(2.3) $$CD_i = CD_{i-1} + \left[\frac{CT_{i-1}}{2}\right] + \left[\frac{CT_i}{2}\right]$$

Where

CD_i = the corrected depth of layer *i*, in the middle of the layer

2.3. Gamma spectroscopy with an HPGe (high purity Germanium) detector

2.3.1. Instrumentation at IMR

The samples have been measured using two detectors; Rad-11and Rad-12. Rad-11 is an ORTEC GEM-series HPGe Coaxal Detector system, while Rad-12 is an ORTEC GMX-series GAMMMA-X HPGe Coaxal Photon Detector system, where both of them have Pop Top crystal configurations. Resolution (FWHM (Full Width Half Maximum)) at 1.33 MeV (^{60}Co) is 1.95 keV for both the detectors, and the relative efficiency at 1.33 MeV are 58% in Rad-11 and 38% in Rad-12. Rad-11 has a crystal diameter of 68.6 mm, and a length of 76.9 mm,

while the crystal diameter in Rad-12 is 59.0 mm, and the length is 78.3 mm. The detectors are cooled electrically with an Ortec X-Cooler, a mechanical cooler for HPGe detectors, where an Ortec CryoSecure Compressor Power Controller protects the cooler (Quality assurance data sheet Ra11 (2002); Rad12 (2004)).

A circular led shield (Mdl Fabcast 04B1) is used to shield the detector. This is a low background shielding mounted in a frame with 10 cm solid lead with Cu/Cd lining and 25 mm lead under shielding (Sværen, 2010a).

The counting room is surrounded by 195 mm concrete walls with sand having high olivine content. The construction is set up to ensure low background radiation levels, and therefore also a low quantification limit. The program used to collect the gamma spectra is ORTEC GammaVision cooler (Quality assurance data sheet Ra11 (2002); Rad12 (2004)).

2.3.2. The HPGe detector

Gamma-decay is the emission of electromagnetic radiation where the transition occurs between energy levels of the same nucleus (Choppin, 2013):

(2.4) $${}^{A}_{Z}X^{*} \rightarrow {}^{A}_{Z}X + \gamma$$

Each gamma ray emitter emits radiation with one or more unique energies (Schøtzig and Schraeder, 1993), and the intensity of the radiation depends of the amount of the radionuclide.

Gamma-rays do not cause ionization directly, but they do interact with matter. This is what happens in a germanium (Ge) detector, where the gamma-ray will transfer its energy to the detector material by exciting an electron in the Ge crystal to a higher energy state in the conduction band. Ge detectors are semiconductor diodes, where the gap between the valence- and the conduction band is so small that it only needs a tiny amount of excitation energy for an electron to transfer from the valence band to the conduction band. This procedure produces charge carries (electrons and electron holes), and when an external electrical field is applied, the conduction band electrons move towards the positive pole, while the electron holes move towards the negative pole. When the electron returns to its ground state, a photon will be emitted. These photons can be converted to a voltage pulse by integral sensitive preamplifier, proportional to the energy of the detected photon (Debertin and Helmer, 1988).

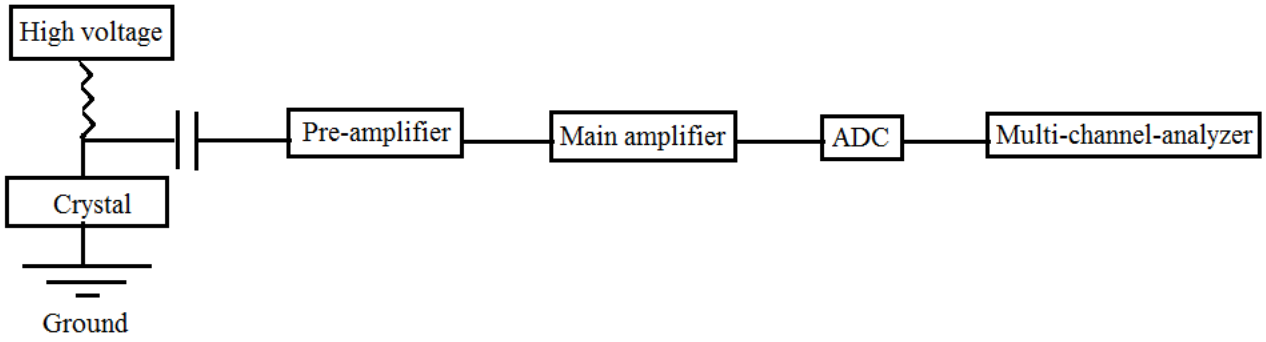

Figure 2.11. Schematic overview of a typical gamma spectrometer (taken from Heldal (2001).

The gamma spectrometer system is shown schematically in Figure 2.11. The preamplifier sends out the produced voltage to the main amplifier, which shapes and amplifies the pulse, preparing it to conversion from an analogue to a digital signal. This is done by an analogue to digital-converter (ADC). Finally, the spectral analyser Multi Channel Analyser (MCA) takes up the energy spectrum.

A peak in the energy spectrum at one or more exact energies enables an identification of the radionuclide, and the area of the peak is proportional to the activity of the radionuclide (Choppin, 2013). Different structures in these spectrums come from the different ways of transferring the gamma energy to the electrons in the detector, and this is done in four different ways; (Coherent Scattering,) photoelectric effect, Compton scattering and pair production (Figure 2.12).

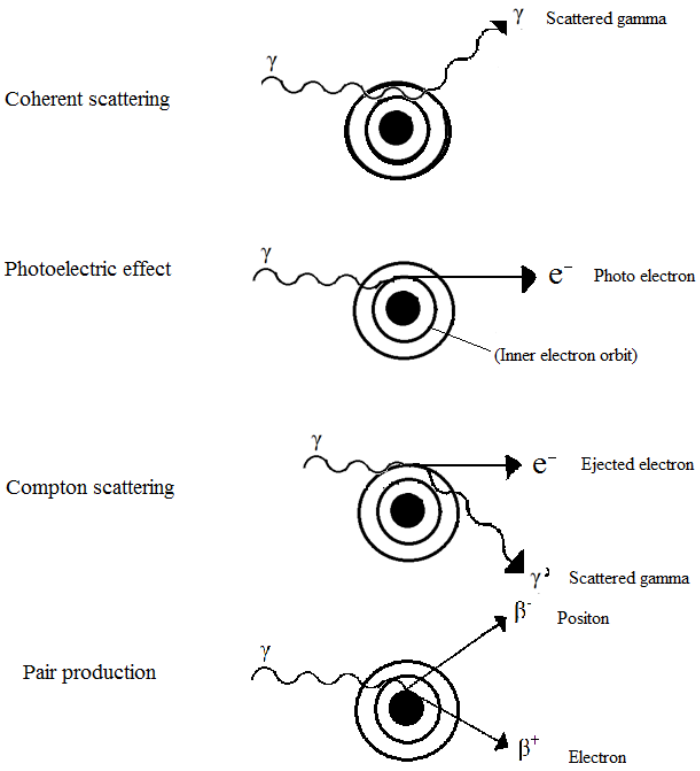

Figure 2.12. Schematic description of the four main processes for gamma-ray interaction and absorption (Choppin, 2013).

In the energy spectrum, the photoelectric effect can be seen by a full energy peak, for example 661.7 kev, which represents the characteristic energy of caesium-137 (^{137}Cs) (Schøtzig and Schraeder, 1993). Here, the total kinetic energy of the gamma ray is transferred to the detector material, and other features in the spectrum represent the spectral internal background. The Compton scattering is an example of where a gamma-ray transfer parts of their energy, where electrons of different energies will be released. When such an electron is absorbed in the detector, it gives rise to the Compton Continue, which can be seen as a continuous distribution of energies in the spectra.

2.4. Measurements

2.4.1. Measuring caesium-137 (^{137}Cs)

The method used at IMR for determination of caesium-137(^{137}Cs) in sediments by gamma spectrometry is accredited by NS-EN ISO/IEC 17025, and is described by Sværen (2010b). Hereafter, all equations are taken from this method.

Measurements of the external background, which come from ^{137}Cs radiation in the environment due to e.g. contamination of the detector, were carried out on an empty detector overnight with a counting time of about 60.000 seconds. The background measurements were used in the calculation of the activity concentrations of ^{137}Cs (and ^{226}Ra and ^{210}Pb) (raw data in Appendix B).

When calibrating the detector, a known quantity of ^{137}Cs is measured in the same geometry as the sample. Here, two ^{137}Cs standards delivered by "Analytics" and "Eckert & Ziegler", with activities of 76.7 ± 4.4% and 2524 ± 1% Bq on the respective reference dates 01.10.2002 and 01.01.2010, were used. The standards are solid matrixes with densities of 1.15 g/cm^3, in 60 mL boxes, which is the specific geometry. After one of the standards was measured, the geometry factor expressing the detector's efficiency was determined (section 2.4.3). Later on, this factor was used in the sample measurements calculations.

The detector is controlled weekly with a ^{137}Cs point source, which is measured for 100 seconds. This is done to ensure that the ^{137}Cs peak is not moving, and that the efficiency of the detector is as expected. A control sample is also measured every second month for at least 60.000 seconds, to check the reproducibility of the measurements. This control sample is an ordinary sediment sample with an activity of (average value of the last five years for both Rad11 and Rad12) 2.8 ± 0.4 Bq/kg ^{137}Cs, which have been measured over several years (Appendix B).

The number of counts in the regions of interest (ROI) (Figure 2.13 (a)) and the counting times were read and recorded in the log book of the respective detector. ROI 1 covers the peak at 661.7 keV, and has a specific width of cannels (varies from detector to detector; 40 channels for Rad11, and 41 for Rad12). ROI 2 and ROI 3 are regions representing the internal background of the measurements, each covering an area of 10 channels, respectively 5 channels to the left and right of the ROI 1 region. In each measurement the gross area, representing the registered counts, in ROI 1, ROI 2 and ROI 3 with corresponding counting time, are manually read. This was done in the same way for background, standard and sample measurements. All calculations were carried out in Microsoft Excel.

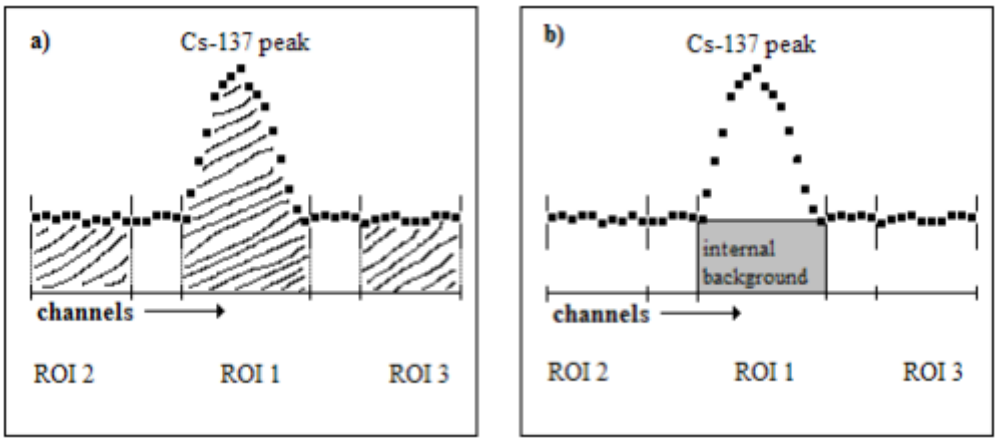

Figure 2.13. (a) An illustration of the region of interest (ROI) in the gamma spectrum of caesium-137 (^{137}Cs), and (b) an illustration of the internal background in the gamma-spectrum for ^{137}Cs (Sværen, 2010b).

All of the 2012 samples were measured for ^{137}Cs, but for the 2013 samples, only the first 10 cm of one core from each station were measured. The selected cores from 2013 were; 194-2, 195-1, 196-1, 197-2 and 199-1 (reference station). Data and results from ^{137}Cs measurements are presented in Appendix C.

2.4.2. Background measurements

The external background (bk) is measured as described in section 2.4.1, where the results are calculated by using equation 2.5:

(2.5) $$bk\ (cps) = \frac{B_1 - \left[\left(\frac{B_2 + B_3}{20}\right) \cdot x\right]}{T}$$

Where

B_1 = gross area (counts) in ROI 1

B_2 = gross area in ROI 2

B_3 = gross area in ROI 3

20 = number of channels in ROI 2 and ROI 3

x = number of channels in ROI 1

T = live counting time (seconds)

Internal background (BK) is related to each measurement and is exemplified in Figure 2.12 (b). Due to e.g. Compton scattering, BK also had to be calculated, which was done by using equation 2.6:

(2.6) $$\text{BK (cps)} = \frac{\left(\frac{N_2 + N_3}{20}\right) \cdot X}{T}$$

Where

N_2 = gross area in ROI 2

N_3 = gross area in ROI 3

x = number of channels in ROI 1

20 = number of channels in ROI 2 and ROI 3

T = live counting time (seconds)

2.4.3. Calibration

In section 2.4.1, the calibration of the detector measuring ^{137}Cs standard, is described. The activity in the standards on the calibration date is calculated by using the decay equation 2.7:

(2.7) $$A_{137-Cs}\,(Bq) = A_0 \cdot e^{-\lambda \cdot t}$$

Where

A_0 = activity on the reference date (Bq)

λ = ln 2/ $t_{½}$, $t_{½}$= half-life of Cs-137 = 11020 days (Schøtzig and Schraeder, 1993)

t = time since reference date (days)

The geometry factor was then calculated by using the results from the standard measuring. Equation 2.8 was used for the calculations:

(2.8) $$G = \frac{A_{127-Cs}}{\frac{N_1}{T} - BK}$$

Where

A_0 = activity on calibration date (eq. 2.6)

N_1 = gross area in ROI 1

T = live counting time (seconds)

Bk = internal background (eq. 2.6)

2.4.4. Sample measurements

After the internal background (BK) for the sample was determined by equation 2.6, the sample activity was found by using equation 2.9:

(2.9) $$a_{137-Cs}\,(Bq) = G \cdot \left(\frac{N_1}{T} - BK\right)$$

Where

G = geometry factor (eq. 2.7)
N_1 = gross area in ROI 1
T = live counting time (seconds)
Bk = internal background (eq. 2.5)

The activity (Bq/kg) in dry weight (d.w.) in each sample could then be calculated by using equation 2.10:

(2.10) $$A_{137-Cs} = \frac{a_{137-Cs}}{w}$$

Where

A_{137-Cs} = activity in sample (eq. 2.9)
w = dry weight of sample (kg)

Finally, by using equation 2.7 the activity A was corrected to activity A_0, for decay since sampling date.

2.4.5. Quantification limit

The quantification level varies for different samples, due to variations in counting time, sample amount and internal background. The quantification limit is based on the minimum net counts in the ^{137}Cs gamma line. Currie (1968) has defined three limiting levels that are shown in Table 2.5.

Table 2.5. Definition of quantification levels (Currie, 1968).

Quantification limit levels	***Definition***
L_c	The net signal level (instrument response) above which an observed signal may be reliably recognized as "detected".
L_d	The "true" net signal level which may be prior expected to lead to detection.
L_q	The level at which the measurement precision will be satisfactory for quantitative determination.

To make sure that low levels of ^{137}Cs are not false identified and quantified, the L_q is consider. The L_q is the conservative way to calculate the lowest measurable level, which is done by equation 2.11:

(2.11) $$L_q = 50 \cdot \left[1 + \sqrt{1 + \frac{B}{25}}\right]$$

Where

B = number of counts

B is found by using equation 2.12:

(2.12) $$B = \frac{N_2 + N_3}{20} \cdot K_1$$

Where

N_2 = gross area in ROI 2

N_3 = gross area in ROI 3

K_1 = number of channels in ROI 1

The L_q is the minimum number of net counts in ROI 1 necessary to reach the quantification limit. The measurement is above this limit when; $N_1 - B > Lq$. If the measurements are below this limit, the results are reported to be less than the quantification limit.

2.4.6. Uncertainty

Every variable in the result calculations has its own uncertainty. The total uncertainty of the activity concentration, s, is composed of the uncertainties from background (sB), calibration

(sG), sample measurements (sa) and sample amount. The uncertainty used is two times the standard deviation (± 2σ). The equation for the uncertainty in measured internal background is showed in equation 2.13 (cps) + 2.14 (counts):

(2.13) $$sBK = \frac{sB}{T}$$

Where

(2.14) $$sB = \sqrt{\left[\frac{x \cdot sN_2}{20}\right]^2 + \left[\frac{x \cdot sN_3}{20}\right]^2}$$

And

sN_2 = $(N_2)^{½}$

N_2 = gross area in ROI 2

SN_3 = $(N_3)^{½}$

N_3 = gross area in ROI 3

T = live counting time (seconds)

x = number of channels in ROI 1

20 = number of channels in ROI 2 and ROI 3

Uncertainty in the geometry factor is calculated by using equation 2.15:

(2.15)

$$sG = \sqrt{\left[\frac{T \cdot sA}{N - BK \cdot T}\right]^2 + \left[\frac{A \cdot N \cdot sT}{(N - BK \cdot T)^2}\right]^2 + \left[\frac{A \cdot T^2}{(N - BK \cdot T)^2} \cdot sBK\right]^2 + \left[\frac{-A \cdot T}{(N - BK \cdot T)^2} \cdot sN\right]^2}$$

Where the following variables from the standard measurement are included:

T = live counting time (seconds)

sT = 1 second

N = gross area in ROI 1

sN = $(N)^{½}$

BK = internal background

sBK = uncertainty in internal background

A = activity from Cs-137

sA = uncertainty in activity from Cs-137

Uncertainty in activity from ^{137}Cs in a sample (Bq) is calculated by using equation 2.16:

$$(2.16) \qquad sa = \sqrt{\left[\left(\frac{N}{T} - BK\right) \cdot sG\right]^2 + \left[\frac{G}{T} \cdot sN\right]^2 + \left[\frac{-G \cdot N}{T^2} \cdot sT\right]^2 + [-G \cdot sBK]^2}$$

Where the following variables from the sample measurements are included:

N = gross area in ROI 1

sN = $(N)^{½}$

T = live counting time (seconds)

sT = 1 second

BK = internal background

sBK = uncertainty in internal background

G = geometry factor

sG = uncertainty in geometry factor

Uncertainty in activity concentration from ^{137}Cs in a sample (Bq/kg) is calculated by using equation 2.17:

$$(2.17) \qquad sA = \sqrt{\left[\frac{1000}{P} \cdot sa\right]^2 + \left[\frac{-a \cdot 1000 \cdot sP}{P^2}\right]^2}$$

Where

a = activity in sample

sa = uncertainty in sample activity

p = sample weight (g)

sP = uncertainty in sample weight

1000 = unit conversion factor

2.4.7. Quality assurance

IMR is participating in international intercomparison exercises to ensure the quality of the measurements taken at the laboratory. These exercises are provided by NPL (National Physical Laboratory), and a part of this programme is to measure a ^{137}Cs sample with an unknown activity concentration, and report the results. The results found at IMR, which participates yearly in such exercises, have been satisfying. The analysis of ^{137}Cs content in sediment samples carried out at IMR are done according to an accredited method, described by (Sværen, 2010b).

Quality assurance is also done by the weekly measuring of the ^{137}Cs point source, and the measuring of the control sample on a regular basis (described in section 2.4.1).

2.5. Analysis of plutonium-238 (^{238}Pu), plutonium-239,240 ($^{239+240}Pu$) and americium-241 (^{241}Am)

The 0-1 and 1-2 cm layers of cores 194-2, 195-1, 196-1, 197-2 and 199-1 (reference station) collected in 2013 were sent to the NRPA for analyse of plutonium-238 (^{238}Pu), plutonium-239,240 ($^{239+240}Pu$) and americium-241 (^{241}Am). They were analysed by alpha spectrometry after radiochemical separation. The radiochemical separation of Pu and Am is described in IAEA (1989).

The sediment samples were initially ashed (550 °C) over night after addition of yield determinants (^{242}Pu and ^{243}Am). The ash was then leached for several hours in *aqua regia* before Pu and Am was co-precipitated with iron (III) hydroxide ($Fe(OH)_3$). Pu was then separated using TBP, ion-exchange (Eichrom anion 1x4 100-200 mesh; 8 M nitric acid (HNO_3) and eluted with 9 M hydrogen chloride (HCl) + 0.1 M ammonium iodide (NH_4I)) and TTA. Am was separated by ion exchange (8 M HNO_3), co-precipitation with calcium oxalate ($Ca(COO)_2$) followed by ion exchange to remove lanthanides, lead-210 (^{210}Pb) and polonium-210 (^{210}Po). The samples were then electrodeposited on stainless steel discs using the method described by (Hallstadius, 1984). Finally the samples were analysed by alpha spectrometry using PIPS detectors (Canberra AlphaAnalyst). The chemical recovery was between 67 and 88 % for Pu and between 36 and 94 % for Am.

2.6. Analyses of uranium-238 (^{238}U), atom ratios of $^{235}U/^{238}U$ and $^{239}Pu/^{240}Pu$ and other elements by the Technical University of Denmark (DTU), RISØ campus

The 0-1 and 1-2 cm layers of cores 194-2, 195-1, 196-1, 197-2 and 199-1 (reference station) collected in 2013 were sent to the Technical University of Denmark (DTU) for analyse of uranium-238 (^{238}U) and the atom ratios of $^{235}U/^{238}U$ and $^{239}Pu/^{240}Pu$. Other elements were also analysed for, which is to be fined in the appendix E. The samples were analysed by mass spectrometry.

10 g of the samples were ashed at 550 C° overnight in glass beakers. Following addition of Hydrogen chloride (HCl) and nitric acid (HNO_3) (*aqua regia*) samples were allowed to digest on a hot plate for 48 hours with gradually increasing heat from room temperature to about 90

C°. Samples were filtered through GF/A filters into pre weighed plastic bottles. A known fraction (about 1%) of the solution was removed for stable elements while ammonia (NH_3) was added to pH 9 to the remaining solution forming iron (III) hydroxide ($Fe(OH)_3$). The samples were stirred for 10 minutes and centrifuged. The precipitate was dissolved in 8 M HNO_3 and passed through a 1 cm diameter and 10 cm long anion exchange column (AG1x4, 100-200 mesh). Matrix elements and uranium were washed out using 100 ml 8 M HNO_3 and Th eluted using 9 M HCl. Finally Pu was eluted by 100 ml 0.5 M HCl and evaporated to dryness. The evaporated samples were dissolved in 3 M HNO_3 and passed through a 1 ml TEVA column to further purify the Pu. Uranium and residual matrix elements were washed out using 30 ml 3 M HNO_3. Finally Pu was eluted using 20 ml 0.1 M HCl, evaporated to dryness, dissolved in 5 ml 3% nitroxyl (HNO) and analysed for Pu-isotopes using an Thermo Scientific X-series II ICP-MS equipped with a CETAC U-5000AT$^+$ ultrasonic nebulizer.

2.7. Grain size analysis

Grain size analyses (Buchanan, 1984) were done on the 0-1 cm layers of cores 194-2, 195-1, 196-1, 197-2 and 199-1 (reference station) collected in 2013. This procedure, described in McCave (2008) and Bianchi et al. (1999), was performed at the Institute of Geology by the author of this thesis with help from the staff of the institute.

The samples were first dissolved in water and then sieved in the fraction of 63µm, where the >63µm residuals (sands and gravels) were dried in an oven at 50°C overnight, before weighting them. The ≤63µm samples (silt and clay) were saved in plastic buckets and left out to dry (approximately one week). The dry ≤63µm samples were then powdered using a mortar (Table 2.4), and 3.8 g were put into plastic shaker cups. These cups were then filled halfway with Calgon (0.05%), and covered with plastic wraps and put on a shaking table for 2 days. The samples were then put into the autosampler, MasterTech 52, which stirred them up again before sending them up to the sedigraph, SediGraph III, for analysis. The performing of the sedigraph grain size analysis is described in (UCL). Later on, the excel program Gradistat, described by Blott and Pye (2001), was used for determining the percentage of different fractions of silt and clay in the ≤63µm samples.

3. Results

3.1. Activity concentrations of caesium-137 (^{137}Cs) in sediment cores

The results of the caesium-137 (^{137}Cs) activity concentrations are presented in section 3.1.1 and 3.1.2, which represent the samples collected in 2012 and 2013, respectively. All raw data are presented in Appendix C.

3.1.1. Samples collected in 2012

The ^{137}Cs activity concentrations range from below the quantification limit to 7.4 ± 0.4 Bq/kg (d.w.) (Table 3.1 and Figure 3.1 to 3.4). The concentrations are typically highest in the 0-1 cm layer and decline further down the core. There is no ^{137}Cs-peak in any of the cores, which can be related to a leakage from *Komsomolets* or other discharge events.

The ^{137}Cs activity concentrations of the samples did not vary much within the station that they were collected from, and showed no evident correlation with the sampling location. Station 122 was the station containing the highest activity concentration. Cores 122-1 and 122-2 had activity concentrations of 4.0 and 7.4 Bq/kg (d.w.) (Table 3.1 and Figure 3.1), respectively in their 0-1 cm layers. This station is, according to the cruise report from 2012 (Appendix F), the station thought to be located farthest from *Komsomolets*. Station 123, which is probably also located at quite a distance from the submarine, was the station containing the lowest activity concentrations (Table 3.1 and Figure 3.2). Here, the 0-1 cm layers of the two cores 123-1 and 123-2, only showed activity concentrations of 0.7 and 1.8 Bq/kg (d.w.), respectively. Station 124, which was the station thought to be located nearest *Komsomolets*, had activity concentrations in the 0-1 cm layers of cores 124-1 to 124-4 ranging from 2.9 to 4.1 Bq/kg (d.w.) (Table 3.1 and Figure 3.3). The last station, station 125, was also thought to be located near the wreck. This station showed activity concentrations of 2.6 and 2.4 Bq/kg (d.w.) in the 0-1 cm layers of cores 125-1 and 125-2, respectively (Table 3.1 and Figure 3.4).

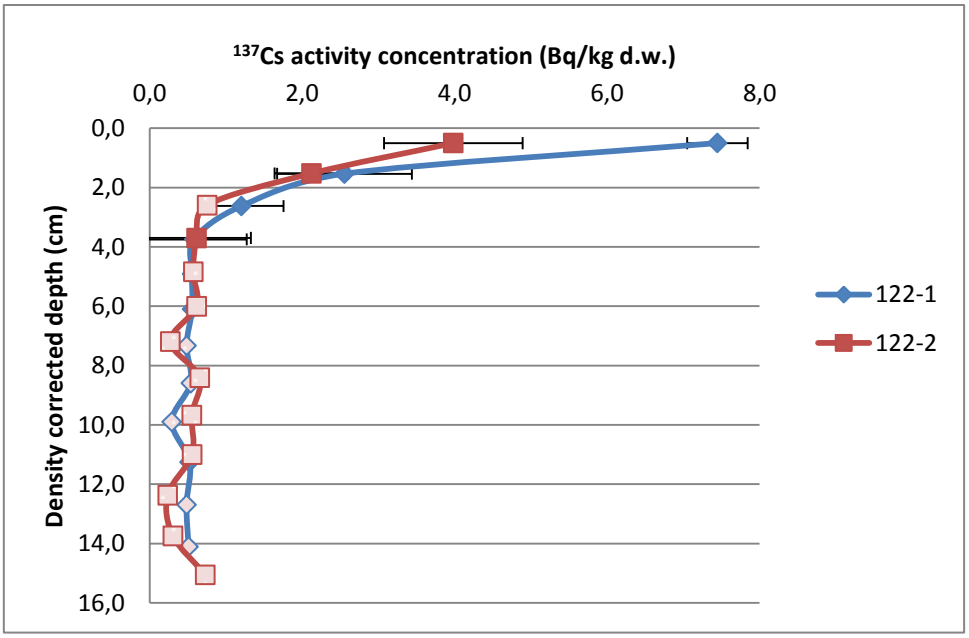

Figure 3.1. Caesium-137 (^{137}Cs) activity concentrations (Bq/kg d.w.) in cores 122-1 and 122-2. Uncertainties (± 2σ) are marked with horizontal error bars. Measurements below the quantification limit are plotted as 0.5-the quantification limit and marked in light pink. Variations in the quantification limit are due to variations in sample sizes and counting time.

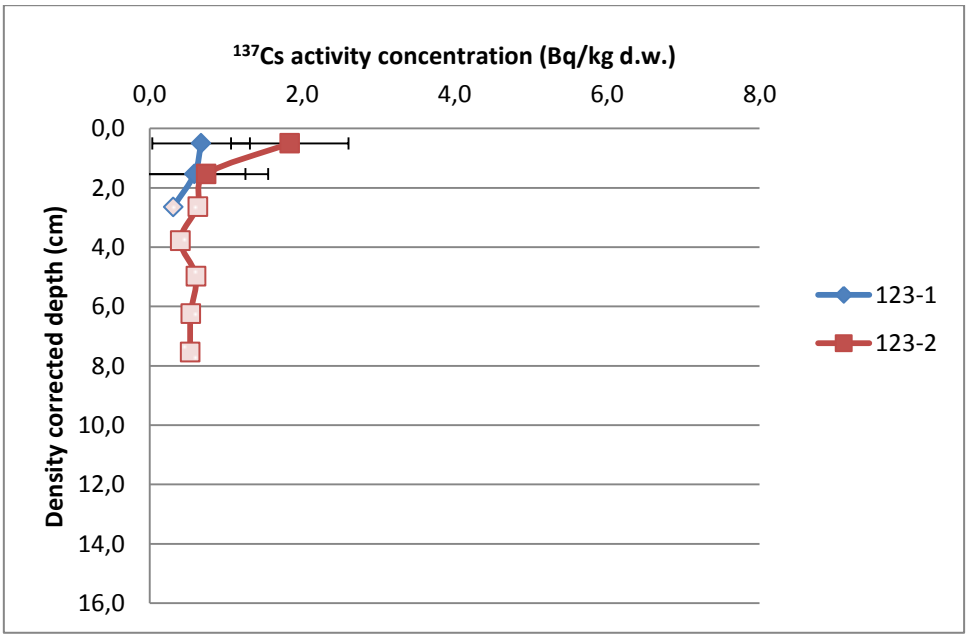

Figure 3.2. Caesium-137 (^{137}Cs) activity concentrations (Bq/kg d.w.) in cores 123-1 and 123-2. Uncertainties (± 2σ) are marked with horizontal error bars. Measurements below the quantification limit are plotted as 0.5-the quantification limit and marked in light pink. Variations in the quantification limit are due to variations in sample sizes and counting time.

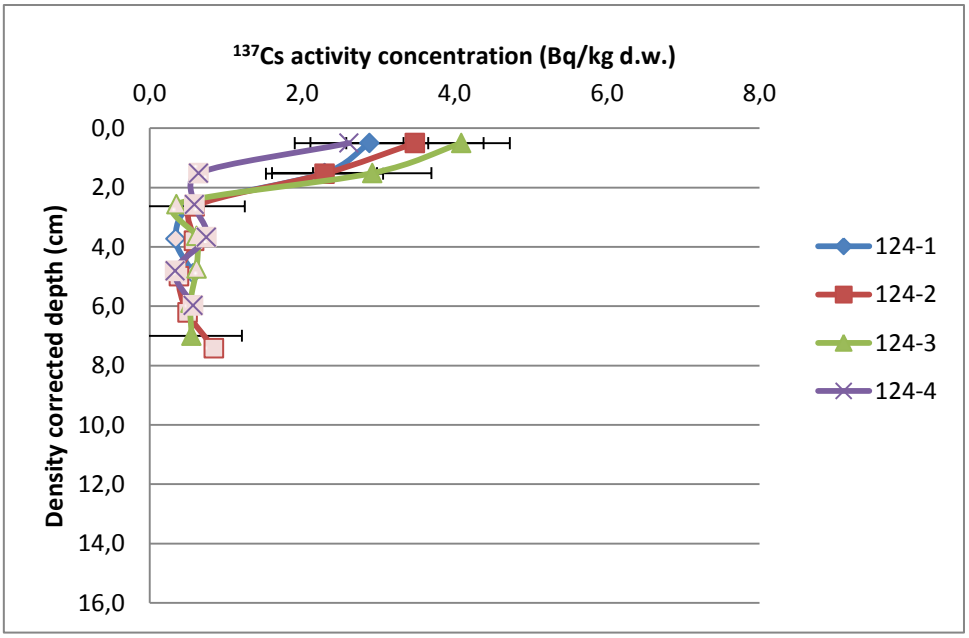

Figure 3.3. Caesium-137 (^{137}Cs) activity concentrations (Bq/kg d.w.) in cores 124-1, 124-2, 124-3 and 124-4. Uncertainties (± 2σ) are marked with horizontal error bars. Measurements below the quantification limit are plotted as 0.5-the quantification limit and marked in light pink. Variations in the quantification limit are due to variations in sample sizes and counting time.

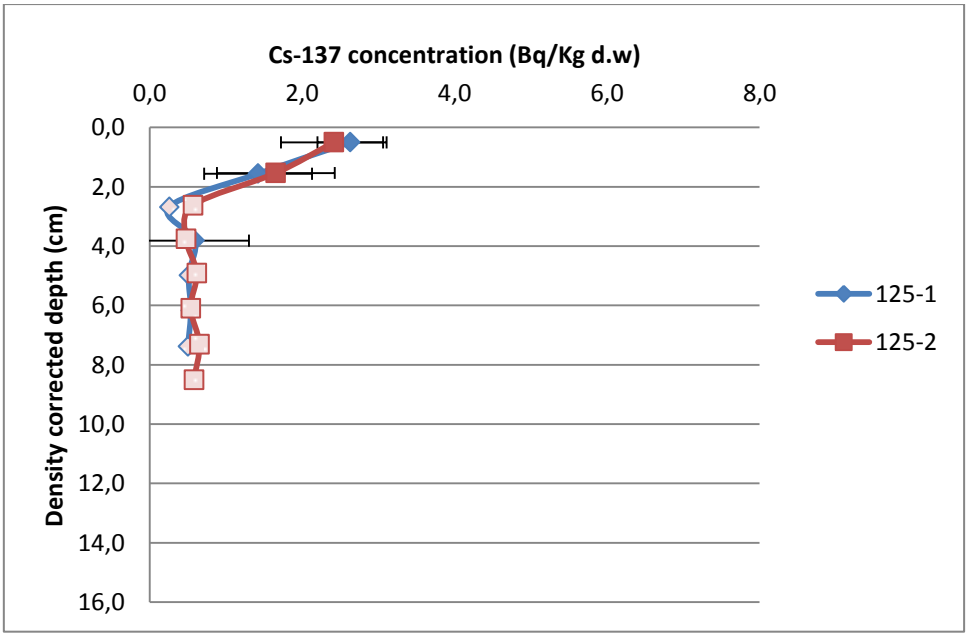

Figure 3.4. Caesium-137 (^{137}Cs) activity concentrations (Bq/kg d.w.) in cores 125-1 and 125-2. Uncertainties (± 2σ) are marked with horizontal error bars. Measurements below the quantification limit are plotted as 0.5-the quantification limit and marked in light pink. Variations in the quantification limit are due to variations in sample sizes and counting time.

Table 3.1. Caesium-137 (^{137}Cs) concentrations and uncertainties for each layer in each core for the sediment samples collected in 2012.

Depth (cm)		0-1	1-2	2-3	3-4	4-5	5-6	6-7	7-8	8-9	9-10	10-11	11-12	12-13
Core 122-1	Cs-137 (Bq/kg) (d.w.)	7.4	2.6	1.2	0.6	< 0.6	< 0.6	< 0.5	< 0.5	< 0.3	< 0.5	< 0.5	< 0.5	
	Uncertainty (Bq/kg) (d.w.)	0.4	0.9	0.6	0.7									
Core 122-2	Cs-137 (Bq/kg) (d.w.)	4.0	2.1	< 0.8	0.6	< 0.6	< 0.6	< 0.3	< 0.7	< 0.6	< 0.6	< 0.2	< 0.3	< 0.7
	Uncertainty (Bq/kg) (d.w.)	0.9	0.5		0.7									
Core 123-1	Cs-137 (Bq/kg) (d.w.)	0.7	0.6	< 0.3										
	Uncertainty (Bq/kg) (d.w.)	0.6	0.7											
Core 123-2	Cs-137 (Bq/kg) (d.w.)	1.8	0.7	< 0.6	< 0.4	< 0.6	< 0.5	< 0.5						
	Uncertainty (Bq/kg) (d.w.)	0.8	0.8											
Core 124-1	Cs-137 (Bq/kg) (d.w.)	2.9	2.3	< 0.6	< 0.3	< 0.6								
	Uncertainty (Bq/kg) (d.w.)	0.8	0.7											
Core 124-2	Cs-137 (Bq/kg) (d.w.)	3.5	2.3	0.6	< 0.6	< 0.4	< 0.5	< 0.8						
	Uncertainty (Bq/kg) (d.w.)	0.9	0.8	0.7										
Core 124-3	Cs-137 (Bq/kg) (d.w.)	4.1	2.9	< 0.4	< 0.6	< 0.6	< 0.8	0.6						
	Uncertainty (Bq/kg) (d.w.)	0.6	0.8					0.7						
Core 124-4	Cs-137 (Bq/kg) (d.w.)	2.6	< 0.6	< 0.6	< 0.7	< 0.3	< 0.6							
	Uncertainty (Bq/kg) (d.w.)	0.7												
Core 125-1	Cs-137 (Bq/kg) (d.w.)	2.6	1.4	< 0.3	0.6	< 0.5	< 0.5	< 0.5						
	Uncertainty (Bq/kg) (d.w.)	0.4	0.7		0.7									
Core 125-2	Cs-137 (Bq/kg) (d.w.)	2.4	1.7	< 0.6	<0.5	< 0.6	< 0.5	< 0.7	< 0.6					
	Uncertainty (Bq/kg) (d.w.)	0.7	0.8											

3.1.2. Samples collected in 2013

The ^{137}Cs activity concentrations in all layers of cores 194-2 and 195-1, respectively located by the front and on the west side of *Komsomolets*, were below the quantification limit. The results are therefore not presented in a figure.

The cores 196-1, 197-2 and 199-1 (reference station) have ^{137}Cs activity concentrations which range from below the quantification limit to 6.4 ± 0.9 Bq/kg (d.w.) (Table 3.2 and Figure 3.5 to 3.7). The cores indicate the same trend as the samples collected in 2012, where the ^{137}Cs activity concentrations are typically highest in the 0-1 cm layer and decline further down the core. Nor in these samples is there any ^{137}Cs-peak in the cores which can be related to a leakage from *Komsomolets* or other discharge events.

The ^{137}Cs activity concentrations of the samples did not vary much within the station that they were collected from, and they showed no evident correlation with the sampling location. Station 196 was the station containing the highest activity concentration (Table 3.2 and Figure 3.5). This station was located by the rear end of the submarine. The second highest concentration was found at reference station 199. Here, the 0-1 cm layer of core 199-1 (reference station) showed an activity concentration of 4.0 Bq/kg (d.w.) (Table 3.2 and Figure 3.7). Station 197, located on the east side of the submarine, had the lowest activity concentration (despite station 194 and 195), where the 0-1 cm layer of core 197-2 had a value of 2.7 Bq/kg (d.w.) (Table 3.2 and Figure 3.6).

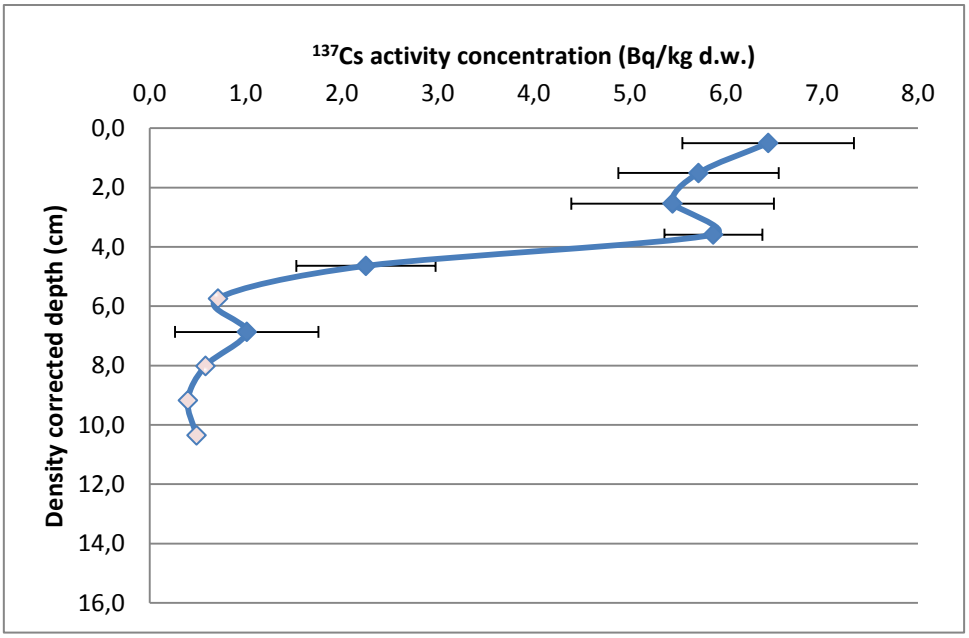

Figure 3.5. Caesium-137 (^{137}Cs) activity concentrations (Bq/kg d.w.) in cores 196-1. Uncertainties (± 2σ) are marked with horizontal error bars. Measurements below the quantification limit are plotted as 0.5-the quantification limit and marked in light pink. Variations in the quantification limit are due to variations in sample sizes and counting time.

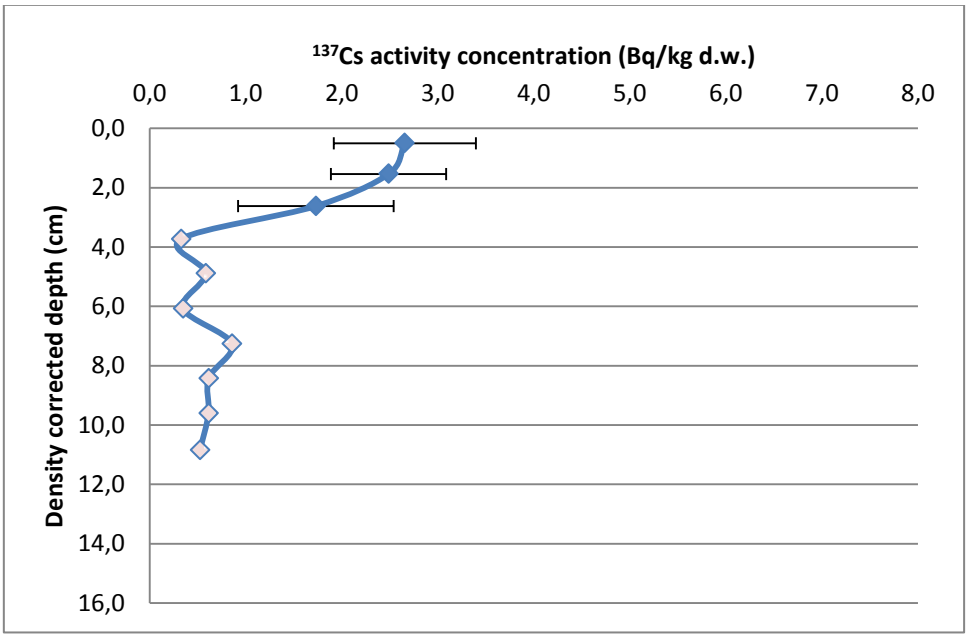

Figure 3.6. Caesium-137 (^{137}Cs) activity concentrations (Bq/kg d.w.) in cores 197-2. Uncertainties (± 2σ) are marked with horizontal error bars. Measurements below the quantification limit are plotted as 0.5-the quantification limit and marked in light pink. Variations in the quantification limit are due to variations in sample sizes and counting time.

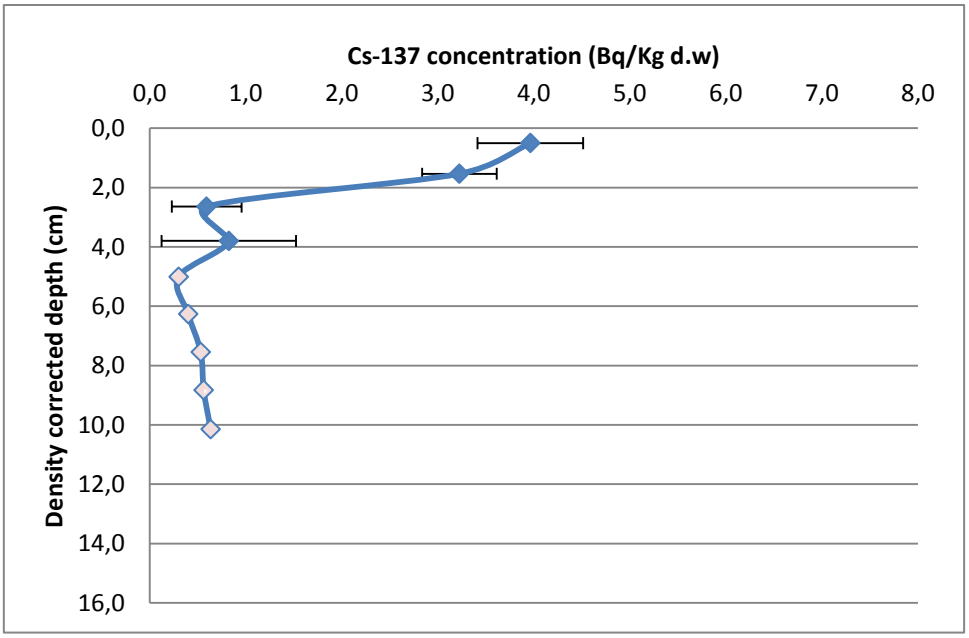

Figure 3.7. Caesium-137 (^{137}Cs) activity concentrations (Bq/kg d.w.) in cores 199-1 (reference station). Uncertainties (± 2σ) are marked with horizontal error bars. Measurements below the quantification limit are plotted as 0.5-the quantification limit and marked in light pink. Variations in the quantification limit are due to variations in sample sizes and counting time.

Table 3.2. Caesium-137 (^{137}Cs) concentrations and uncertainties for each layer in each core for the sediment samples collected in 2013.

Depth (cm)	Core 194-2		Core 195-1		Core 196-1		Core 197-2		Core 199-1	
	Cs-137 (Bq/kg) (d.w.)	Uncertainty (Bq/kg) (d.w.)	Cs-137 (Bq/kg) (d.w.)	Uncertainty (Bq/kg) (d.w.)	Cs-137 (Bq/kg) (d.w.)	Uncertainty (Bq/kg) (d.w.)	Cs-137 (Bq/kg) (d.w.)	Uncertainty (Bq/kg) (d.w.)	Cs-137 (Bq/kg) (d.w.)	Uncertainty (Bq/kg) (d.w.)
0-1	< 0.7		< 0.8		6.4	0.9	2.7	0.7	4.0	0.5
1-2	< 0.3		< 0.9		5.7	0.8	2.5	0.6	3.2	0.4
2-3	< 0.3		< 0.4		5.4	1.1	1.7	0.8	0.6	0.4
3-4	< 0.6		< 0.6		5.9	0.5	< 0.3		0.8	0.7
4-5	< 0.6		< 0.7		2.3	0.7	< 0.6		< 0.3	
5-6	< 0.6		< 0.7		< 0.7		< 0.3		< 0.4	
6-7	< 0.7		< 0.5		1.0	0.7	< 0.7		< 0.5	
7-8	< 0.4		< 0.6		< 0.6		< 0.6		< 0.6	
8-9	< 0.7		< 0.6		< 0.4		< 0.6		< 0.6	
9-10	< 0.6		< 0.6		< 0.5		< 0.5			

3.2. Activity concentrations of plutonium-*238 (^{238}Pu), plutonium-239,240 ($^{239+240}$Pu),* americium-241 (^{241}Am) and uranium-238 (^{238}U) analysis

Activity concentrations of plutonium-238 (^{238}Pu) and plutonium-239,240 ($^{239+240}$Pu) and their plutonium (Pu)-isotope activity ratios (^{238}Pu/$^{239+240}$Pu) in the 0-1 and 1-2 cm layers of the cores 194-2, 195-1, 196-1, 197-2 and 199-1 (reference station) are shown in Table 3.3. The $^{239+240}$Pu activity concentrations range from 0.02-0.94 Bq/kg (d.w.), while the ^{238}Pu activity concentrations range from below the detection limit to 0.05 Bq/kg (d.w.).

The ^{238}Pu activity concentrations of the 0-1 and 1-2 cm layers of core 194-2, and the 0-1 cm layer of core 195-1 were below the detection limit. The ^{238}Pu/$^{239+240}$Pu activity ratios for these layers could therefore not be determined. The other 0-1 and 1-2 cm layers of the sediment samples collected in 2013 had ^{238}Pu/$^{239+240}$Pu isotope activity ratios ranging from 0.03 to 0.06. The lowest and highest value was found in the 0-1 and 1-2 cm layers, respectively in core 196-1.

The activity concentrations of americium-241 (^{241}Am) range from 0.07 to 1.16 Bq/kg (d.w.) in the 0-1 and 1-2 cm layers of the selected cores collected in 2013 (Table 3.4). The lowest and highest activity concentration was found in the 1-2 cm layer of core 194-2 and 0-1 cm layer of core 199-1 (reference station), respectively. The ^{241}Am/$^{239+240}$Pu activity ratios range from 1.03 to 3.28.

Table 3.3. Activity concentrations of $^{239+240}Pu$, ^{238}Pu, and ^{241}Am, and the activity ratios of $^{238}Pu/^{239+240}Pu$ and $^{241}Am/^{239+240}Pu$ for the 0-1 and 1-2 cm layers of cores 194-2, 195-1, 196-1, 197-2 and 199-1 (reference station) collected in 2013.

Core	Depth (cm)	$^{239+240}Pu$, (Bq/kg d.w.)	Uncertainty (± 2σ)	^{238}Pu, (Bq/kg d.w.)	Uncertainty (± 2σ)	^{241}Am, (Bq/kg d.w.)	Uncertainty (± 2σ)	$^{238}Pu/^{239+240}Pu$	Uncertainty (± 2σ)	$^{241}Am/^{239+240}Pu$	Uncertainty (± 2σ)
194-2	0-1	0.03	0.01	< 0.01	-	0.09	0.03	n.d	-	2.64	1.18
194-2	1-2	0.02	0.01	< 0.01	-	0.07	0.02	n.d	-	3.28	1.66
195-1	0-1	0.06	0.02	< 0.01	-	0.10	0.02	n.d	-	1.55	0.47
195-1	1-2	0.16	0.03	0.01	0.01	0.18	0.03	0.04	0.04	1.10	0.28
196-1	0-1	0.84	0.08	0.03	0.01	1.02	0.10	0.03	0.01	1.21	0.16
196-1	1-2	0.90	0.08	0.05	0.01	1.15	0.09	0.06	0.16	1.28	0.15
197-2	0-1	0.67	0.06	0.03	0.01	0.74	0.06	0.04	0.02	1.11	0.14
197-2	1-2	0.57	0.05	0.02	0.01	0.77	0.07	0.04	0.02	1.35	0.17
199-1	0-1	0.94	0.10	0.04	0.02	1.16	0.09	0.04	0.02	1.24	0.17
199-1	1-2	0.73	0.07	0.04	0.01	0.76	0.08	0.05	0.02	1.03	0.15

The activity concentrations of uranium-238 (^{238}U) and the ^{235}U/^{238}U isotope ratios of the 0-1 and 1-2 cm layers for the selected cores collected in 2013 are shown in figure 3.4, where they respectively range from 8.3 to 22.1 Bq/kg (d.w.) and 0.0069 to 0.0073. The isotope ratios of ^{239}Pu/^{240}Pu are also shown in this table including its uncertainty given in percentage standard deviation (stdv). The isotope ratios ranged from 0.152 to 0.194.

Table 3.4. Activity concentrations of ^{238}U and the isotope ratios of ^{235}U/^{238}U and ^{239}Pu/^{240}Pu for the 0-1 and 1-2 cm layers of cores 194-2, 195-1, 196-1, 197-2 and 199-1 (reference station) collected in 2013.

Core	***Depth (cm)***	***^{238}U (mBq/g d.w.) (5% stdv)***	***^{235}U/^{238}U (5% stdv)***	***^{239}Pu/^{240}Pu***	***Uncertainty (% stdv)***
194-2	0-1	15.4	0.0070	0.175	11.4
194-2	1-2	13.7	0.0070	0.169	8.3
195-1	0-1	22.1	0.0070	0.152	6.5
195-1	1-2	14.9	0.0073	0.155	6.5
196-1	0-1	8.3	0.0072	0.175	5.5
196-1	1-2	9.2	0.0071	0.154	6.3
197-2	0-1	10.3	0.0069	0.194	4.0
197-2	1-2	10.2	0.0071	0.164	4.4
199-1	0-1	9.1	0.0069	0.165	4.2
199-1	1-2	9.8	0.0071	0.153	3.9

3.3. Grain size analysis

The result of the grain size distribution of the 0-1 cm layers of the cores 194-2, 195-1, 196-1, 197-2 and 199-1 (reference station) showed somewhat the same result where most of the sample contained silt and clay (see Appendix D). The average percentage of sand and gravel (>63µm) in the samples were approximately 3% (Figure 3.8), where the highest and lowest values were found in the 0-1 cm layers of cores 196-1 and 195-1, respectively. The percentage of silt and clay were also determined (Figure 3.8) after sieving the samples for particles >63µm. The samples mostly contained different fractions of silt, and an average of 20% clay, where clay particles are ≤2µm.

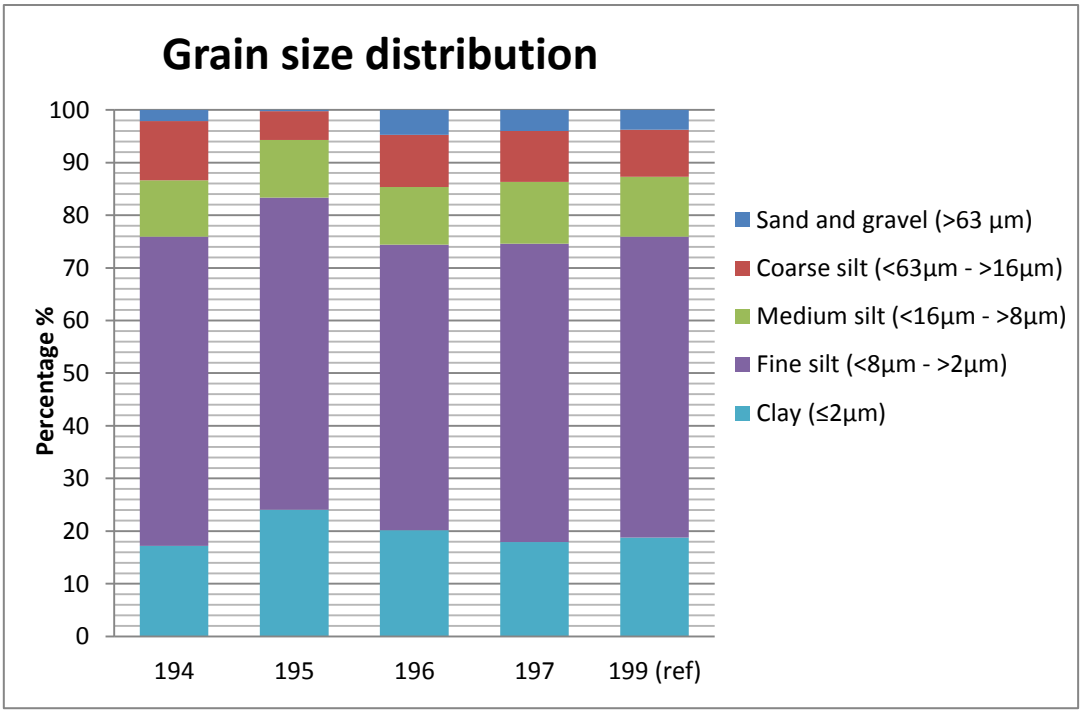

Figure 3.8. Grain size distribution obtained by Gradistat of the 0-1 cm layers of cores 194-2, 195-1, 196-1, 197-2, 199-1 (reference station) collected in 2013.

3.4. Lead-210 (^{210}Pb) dating

3.4.1. Activity concentrations of lead-210 (^{210}Pb) and radium-226 (^{226}Ra) in sediment cores

Lead-210 (^{210}Pb) and radium-226 (^{226}Ra) activity concentrations in cores 122-2 and 123-2 are presented in Tables 3.5 and 3.6 and Figures 3.9 and 3.10, respectively. The activity concentrations are used to calculate the age of each sediment layer (section 3.2.2).

Table 3.5. Lead-210 (^{210}Pb) and radium-226 (^{226}Ra) activity concentrations in core 122-2 (2012).

Depth (cm)	***^{210}Pb (Bq/kg d.w.)***	***Uncertainty (± 2σ)***	***^{226}Ra (Bq/kg d.w.)***	***Uncertainty (± 2σ)***
0-1	262	18	34	4
1-2	166	11	38	4
2-3	123	10	39	4
3-4	74	7	41	4
4-5	71	6	44	4
5-6	67	6	40	4
6-7	62	4	43	4
7-8	47	6	32	4
8-9	37	5	26	3
9-10	34	5	23	3
10-11	30	3	24	2
11-12	34	3	24	3
12-13	35	5	31	5

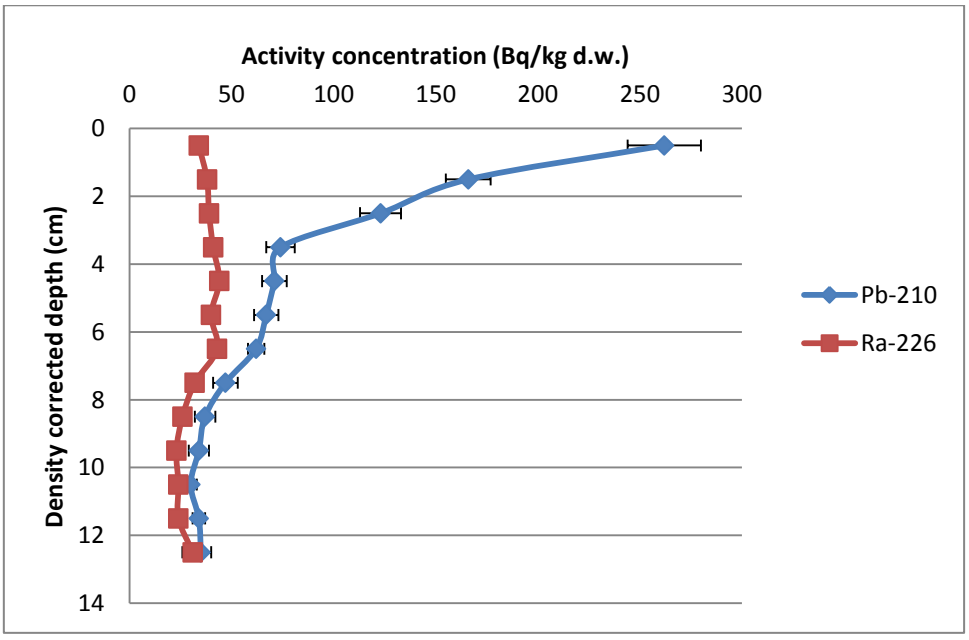

Figure 3.9. Lead-210 (^{210}Pb) activity concentrations (Bq/kg d.w.) (blue line) and radium-226 (^{226}Ra) activity concentrations (Bq/kg d.w.) (red line) in core 122-2. Uncertainties (2σ) are marked with horizontal error bars.

Table 3.6. Lead-210 (^{210}Pb) and radium-226 (^{226}Ra) activity concentrations in core 123-2 (2012).

Depth (cm)	***^{210}Pb (Bq/kg d.w.)***	***Uncertainty (± 2σ)***	***^{226}Ra (Bq/kg d.w.)***	***Uncertainty (± 2σ)***
0-1	151	11	40	4
1-2	100	8	44	5
2-3	82	7	42	4
3-4	70	6	43	4
4-5	52	6	34	4
5-6	39	5	25	3
6-7	27	5	24	3

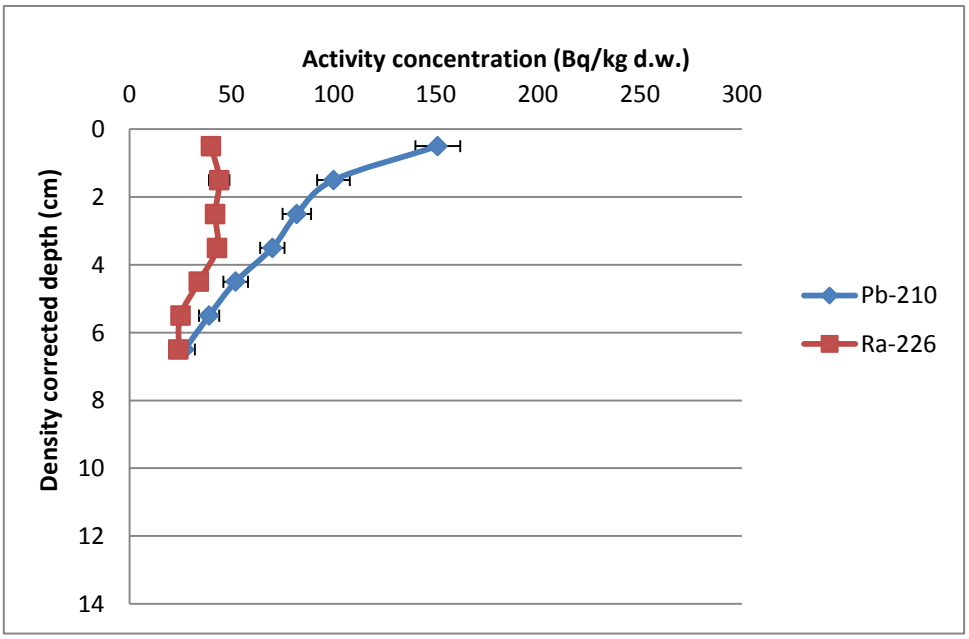

Figure 3.10. Lead-210 (^{210}Pb) activity concentrations (Bq/kg d.w.) (blue line) and radium-226 (^{226}Ra) activity concentrations (Bq/kg d.w.) (red line) in core 123-2. Uncertainties (± 2σ) are marked with horizontal error bars.

3.4.2. Dating results

Dating of the layers in the sediment cores was carried out using the "Constantly Rate of Supply" (CRS) model (Appleby and Oldfield, 1978). The dating results are listed in Tables 3.7 and 3.8. Core 122-2, which is 13 cm long, is somewhat longer than core 123-2, which is only 7 cm. Both cores have sediment layers dated from 2013 and back to the 19th century. There are no ^{137}Cs peaks present in either of the two cores that can verify the dating results.

Table 3.7. Dating results for core 122-2 (2012).

Depth (cm)	***Year; CRS***	***^{137}Cs (Bq/kg d.w.)***	***Uncertainty (± 2σ)***
0-1	2013*	4.0	0.9
1-2	1993	2.1	0.5
2-3	1982	<0,8	-
3-4	1970	0,6	0.7
4-5	1964	<0,6	-
5-6	1957	<0,6	-
6-7	1949	<0,3	-
7-8	1941	<0,7	-
8-9	1932	<0,6	-
9-10	1923	<0,6	-
10-11	1906	<0,2	-
11-12	1891	<0,3	-

**The 0-1 cm layer is reported to be from the year after it was collected because the CRS model gives the result in decimal year (2012.8 ~ 2013).*

The bottom layer (12-13 cm) was not included in the dating calculations being a residual that did not represent a whole cm, where its dry weight was only 22 g (see Appendix A).

Table 3.8. Dating results for core 123-2 (2012).

Depth (cm)	***Year; CRS***	***^{137}Cs (Bq/kg) (d.w.)***	***Uncertainty (± 2σ)***
0-1	2013*	1.8	0.8
1-2	1996	0.7	0.8
2-3	1984	<0.6	-
3-4	1971	<0.4	-
4-5	1955	<0.6	-
5-6	1930	<0.5	-
6-7	1875	<0.5	-

**The 0-1 cm layer is reported to be from the year after it was collected because the CRS model gives the result in decimal year (2012.8 ~ 2013).*

4. Discussion

4.1. Activity concentrations of caesium-137 (^{137}Cs)

4.1.1. *At the site of the* Komsomolets

All the sediment samples collected in 2012 had low caesium-137 (^{137}Cs) activity concentrations. Since the acoustic transponder was not attached to the box-corer during the sampling, there is a possibility that none of the samples were collected close up to the submarine. Here, the given positions of the stations are the positions of the vessel during the sampling. Due to the large depth and strong currents in the area, these positions might differ from the actual positions of where the box-corer hit the seabed.

The 2013 samples were collected with the acoustic transponder attached to the box-corer, and the stations were located as close to the submarine as possible. If there was a leakage from *Komsomolets*, one could expect the stations closest to the wreck to contain the highest activity concentrations. However, these samples do not show any higher ^{137}Cs levels than the samples collected in 2012. There are also no correlations with the positions of the stations and the ^{137}Cs activity concentration detected in the collected samples. One might expect the samples collected at the stations located on the sides of the submarine, the ones closest to the ventilation pipe, to contain the highest ^{137}Cs activity concentrations. But these stations contain even lower activity concentrations than the reference station, where one of them only contains activity concentrations below the quantification limit.

When comparing ^{137}Cs activity concentrations found in sediments in the present study with ^{137}Cs activity concentrations found in sediments in the same area in previous years, the results do not differ that much. As seen from Figure 1.1, the ^{137}Cs activity concentrations found in surface sediments in the area adjacent to *Komsomolets* in the period from 1993 to 2011, varied from below the quantification limit to 6.1 Bq/kg (d.w.). However, note that few sediment cores were analysed for ^{137}Cs in the previous monitoring. But in the study of Heldal et al. (2002), two cores from the same box-corer sample collected in the area adjacent to *Komsomolets* in 1999, were analysed for ^{137}Cs. Both cores only showed results under the detection limit. In 2001, two cores from the same box-corer sample collected in areas adjacent to the wreck, were also analysed for ^{137}Cs, where the 0-1 cm layers showed results of 1.9 and 3.8 Bq/kg (d.w.) (Figure 4.1) (IMR, unpublished data, 2001). The results from both these studies show comparable ^{137}Cs activity concentrations with the result from the 2012 and 2013

samples, where no ^{137}Cs-peaks can be found in their profiles. This strongly indicates that so far, there is little or no leakage from *Komsomolets*. The low levels can also be subscribed to the large depth where the wreck is resting. In addition, its resting place is located far from terrestrial areas and relatively far from any point source.

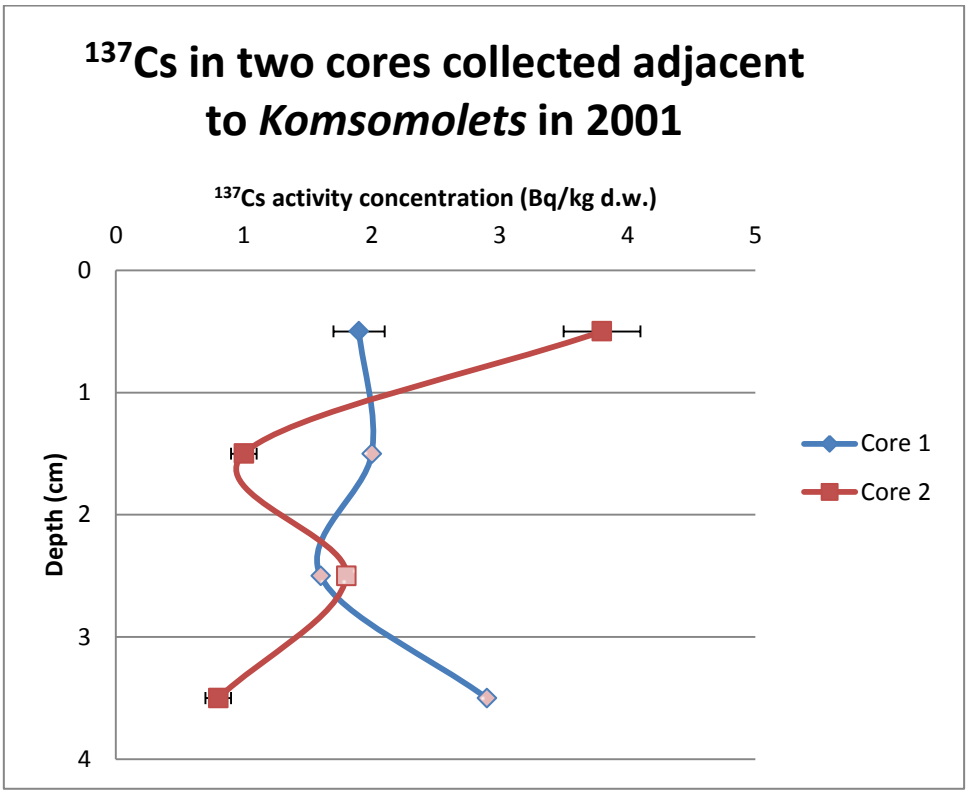

Figure 4.1. Caesium-137 (^{137}Cs) activity concentrations in two cores collected by the IMR in 2001 in the areas adjacent to Komsomolets *(IMR, unpublished data, 2001). The cores were originally ten cm, but only 4 cm (not corrected depth) were determined. Uncertainties are marked with horizontal error bars.*

4.1.2. Comparison with activity concentrations found in the Barents, Norwegian and Greenland Seas.

Figure 4.2 shows average ^{137}Cs activity concentrations in surface sediments in the Barents, Norwegian and Greenland Seas and the area adjacent to *Komsomolets* (the IMR monitoring) in the period of 1993-2011. The average ^{137}Cs activity concentration above the detection limit for each year is plotted.

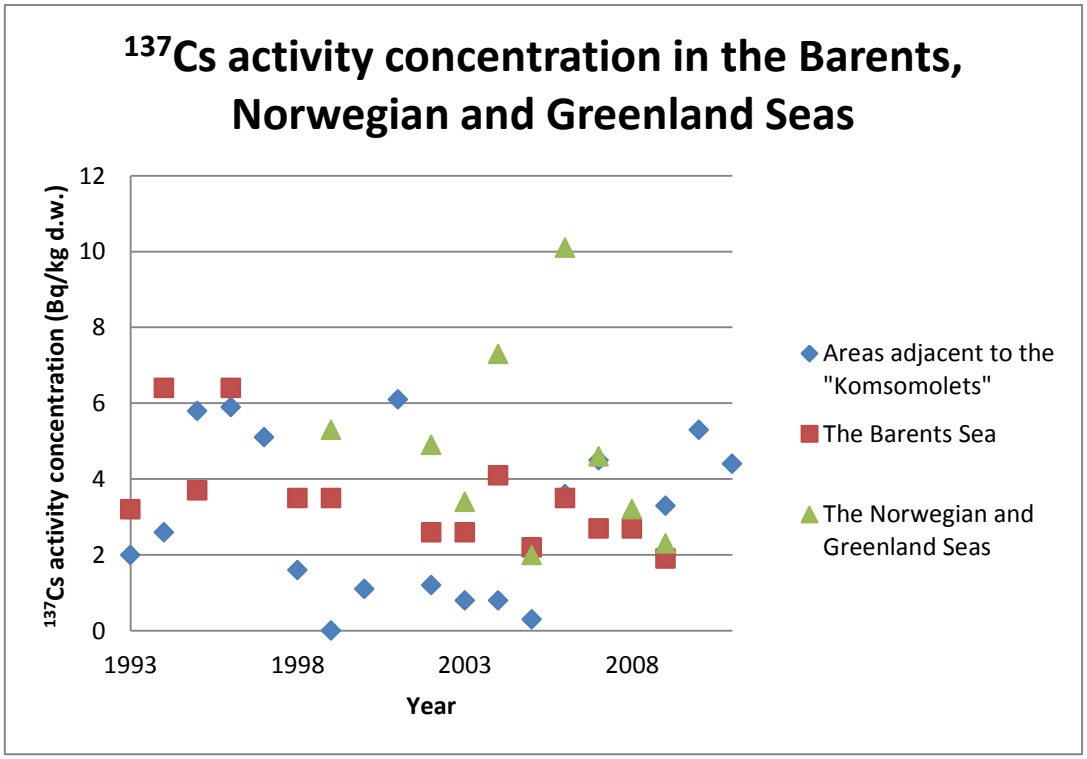

Figure 4.2. Average caesium-137 (^{137}Cs) activity concentrations in surface sediments from the area adjacent to Komsomolets, *the Barents, Norwegian and Greenland Seas in 1993 - 2011 (Føyn and Sværen, 1995, Nies et al., 1999, Heldal et al., 2002, Matishov and Matishov, 2004, Gwynn et al., 2012, NRPA, 2000; 2004; 2005; 2006; 2007; 2008; 2009; 2011). Only activity concentrations above the quantification limit are plotted.*

As seen from Figure 4.2, the ^{137}Cs activity concentrations found in surface sediments collected in the area adjacent to *Komsomolets,* do not vary much from the activity concentrations found in surface sediments elsewhere in the Barents, Norwegian and Greenland Seas. In some years, the ^{137}Cs activity concentrations found in the area close to the wreck, even show the lowest values. The highest activity concentrations are found in the Norwegian Sea in 2004 and 2006, in samples collected near the cost or in the Norwegian Coastal Current (NWCC). Elevated levels of ^{137}Cs are known to be found in these areas, due to contribution of local terrestrial run off from Chernobyl fallout (Gwynn et al., 2012) (Figure 4.3), and transport of discharges in the NWCC, due to the Baltic Sea outflow contaminated by Chernobyl fallout and earlier discharges from European reprocessing plants (Nies et al., 1999).

Many studies have been made in the Barents, Norwegian and Greenland Seas, for example by Føyn and Sværen (1995), Nies et al. (1999) and Heldal et al. (2002), respectively performed in the years 1991- 1993, 1995 and 1998-1999. The ^{137}Cs activity concentrations in the 0-1 cm

layers of the sediment samples collected in 2012 and 2013 are comparable to these studies. E.g. the activity concentrations detected in surface sediment layers in the Barents Sea in the study of Heldal et al. (2002), varied between 0.7 and 6.3 Bq/kg (d.w.). This is almost equal to the activity concentrations found in the Barents Sea by Føyn and Sværen (1995) and Nies et al. (1999), which respectively varied from under the detection limit to 8.6 Bq/kg (d.w.), and from 1.5 to 5.8 Bq/kg (d.w.). On the other hand, the ^{137}Cs activity concentrations detected in surface sediments from the Norwegian Sea by Nies et al. (1999), show a much higher result than for the surface sediment samples collected in the area adjacent to *Komsomolets*. Here, ^{137}Cs activity concentrations up to 48 Bq/kg (d.w.) were detected, but these samples were collected near the Norwegian coast, assumed to be contaminated by earlier Seallafield discharges. The ^{137}Cs activity concentrations found in surface sediment samples in the deep Norwegian and Greenland Seas in the study of Heldal et al. (2002) showed low activity concentrations. The ^{137}Cs activity concentrations found in the deep Norwegian Sea, varied from below the quantification level to 4.8 Bq/kg (d.w.), while ^{137}Cs-activity concentration of 5.4 ± 0.1 Bq/kg (d.w.) was detected in the deep Greenland Sea. These activity concentrations are comparable to the ^{137}Cs activity concentrations in the samples collected near the wreck in the present study.

4.1.3. Comparison with activity concentrations found in other geographical areas

Activity concentrations of ^{137}Cs found in the present work are relatively low compared to activity concentrations found in other geographical areas. The Norwegian Fjords for instance, have ^{137}Cs activity concentrations ranging from under the quantification limit to over 400 Bq/kg (d.w.)(Sværen, 2010a, NRPA 2004; 2007; 2008; 2009; 2011) , and where the highest levels are found in the Sognefjord. One of the main reasons for the high activity concentrations is the Chernobyl accident. As seen from Figure 4.3, mid-Norway was severely affected by this accident, where terrestrial areas were contaminated by precipitation (Sværen, 2010a). Contamination originating from the accident did also reach the Norwegian cost via ocean currents from the Baltic Sea (Loeng, 1991). The Baltic Sea was the marine area most affected by the Chernobyl accident, and shows ^{137}Cs activity concentrations higher than 2000 Bq/kg (d.w.) in sediment samples (Helsinki Commission, 2007).

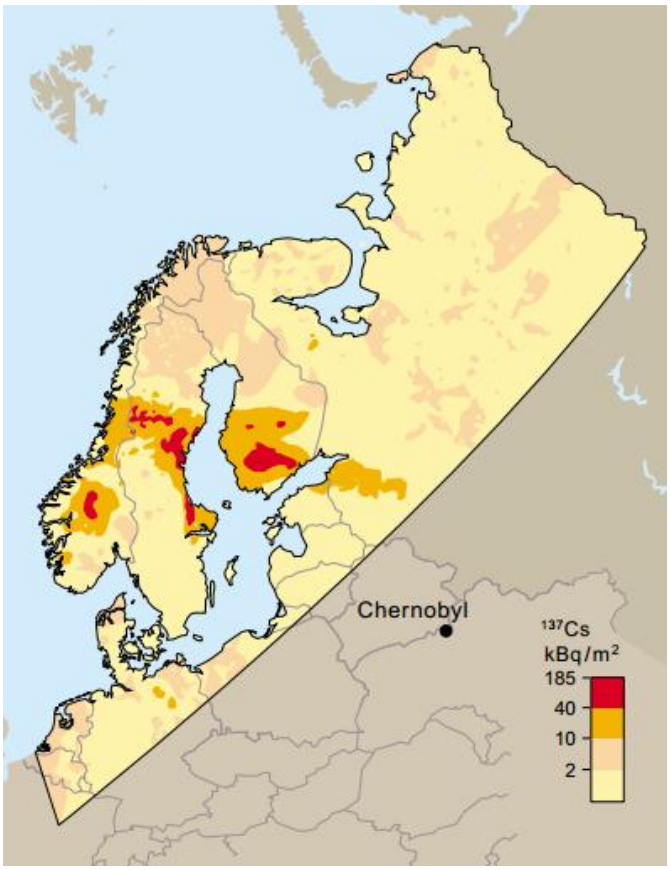

Figure 4.3.Caesium-137 (^{137}Cs) (kBq/m^2) fallout from the Chernobyl accident in terrestrial areas in parts of northern Europe (AMAP, 1997).

The Irish Sea is also one example of a geographical area with surface sediment samples containing different ^{137}Cs activity concentrations than for sediment samples collected in the area adjacent to *Komsomolets*. Here, elevated levels ranging from 60-8000 Bq/kg (d.w.) were found in surface sediment layers collected in 1986 (Jones et al., 2007), which were results of the extensive releases from the nuclear reprocessing plant Sellafield. This area has been monitored since 1960, and the levels have gradually reduced due to steady reductions in releases from Sellafield since the mid-1970's (Hunt et al., 2013). This was consistent with the result of the measurements carried out at the same location in 1999, where the levels were reduced to 70-5000 Bq/kg (d.w.). In 2012, sediment samples collected at Sellafield beach only showed ^{137}Cs activity concentration of 39 Bq/kg (d.w.) (RIFE-18, 2013).

Caesium-137 (^{137}Cs) activity concentrations in sediment samples varying from 2 to 33 Bq/kg (d.w.) in the open Kara Sea was detected in 1992 on the joint Russian-Norwegian Expedition (Salbu et al., 1997). In this area, elevated ^{137}Cs activity concentrations have been found in four overactivity zones (OAZ); the Novozemel'skaya, Vaigach, and the estuaries of Ob and Yenisy (Miroshnikov, 2013). Figure 4.4 gives an overview of these zones, and their ^{137}Cs

activity concentrations found in studies carried out from 1995-2003. Sources of these contaminations mostly originates from global fallout, discharges from reprocessing plants like Sellafield, Mayak, Krasnoyarsk and Tomsk, and leakages from dumped radioactive materials (Miroshnikov, 2013).

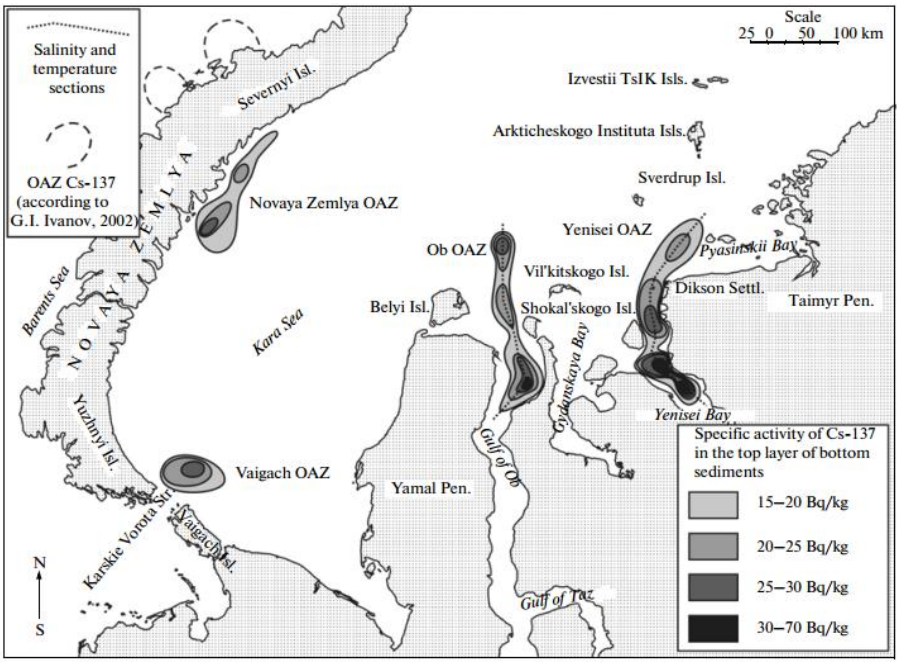

Figure 4.4. Positions of the overactivity zones in the Kara Sea, and their caesium-137 (^{137}Cs) activity concentration (Bq/kg d.w.) distribution in the surface layer of sediments (Miroshnikov, 2013).

4.1.4. Lead-210 dating and vertical distribution of caesium-137 (^{137}Cs) in sediment cores

The dating of the two cores 122-2 and 123-2 collected in 2012 did not have ^{137}Cs-peaks in years/periods clearly indicating a dominating source present. The low levels of ^{137}Cs found are most likely to originate from global fallout. Naturally, no levels of ^{137}Cs activity concentration were detected in sediment layers older than the 1950's and 1960's. If elevated levels were to be found in older sediment layers, a leakage from *Komsomolets* might be expected, as there is a possibility that ^{137}Cs could "wander" downwards in the sediment (AMAP, 1997). The elevated levels in the uppermost layers of these cores can indicate a minor leakage from *Komsomolets*, but because of the low activity concentrations, this is rather unlikely. Since *Komsomolets* rest near the polar front in the Spitsbergen area, which is an ice-melting zone in the Barents Sea, it may also be a result of contamination drifting with ice originating from the Kara Sea (Nurnberg et al., 1994, Pfirman et al., 1995). The peak at the depth of 3-4 cm in core 122-2 can indicate contamination from Sellafield, which had its

largest amount of discharge in the 70's, and where the transient time from Sellafield to the Barents Sea is approximately 6-7 years (Dahlgaard, 1995).

The dating of the two sediment cores starts by showing somewhat similar ages for the same depths of the cores, where 1 cm is approximately ten years in the beginning. But at the depth of 4-5 cm, the cores represent different ages, where this difference increases further down the cores and where both cores ends at the 19th century despite their different length. Since both cores are collected in the same area with most likely the same sedimentation rate, this is probably a result of the total uncertainty in the sampling, slicing and analysing of the cores as well as the uncertainty of the dating, which increases with the depth of the sediment core.

4.2. Activity concentrations of plutonium-238 (^{238}Pu), plutonium-239,240 ($^{239+240}$Pu), americium-241 (^{241}Am) and uranium-238 (^{238}U)

The activity concentrations of plutonium-238 (^{238}Pu) and plutonium-239,240 ($^{239+240}$Pu) found in the 0-1 and 1-2 cm layers of the selected cores in 2013, ranged from under the detection limit to 0.05 Bq/kg (d.w.) and from 0.02 to 0.94 Bq/kg (d.w.) (Tabel 3.3), respectively. There was no correlation between the sampling location and the activity concentrations found in the samples, where the same trends as observed for caesium-137 (^{137}Cs), were also observed for these elements in the respective cores. These activity concentrations show no elevated levels, where they match the activity concentrations found in the deep Norwegian and Greenland Seas in the study of Heldal et al. (2002) in 1999, which ranged from 0.003 to 0.029 Bq/kg (d.w.) and from 0.009 to 0.470 Bq/kg (d.w.), respectively.

The activity concentrations of americium-241 (^{241}Am) found in the present study ranged from 0.07 to 1.16 Bq/kg (d.w.), also showing no correlation between the sampling locations. The levels of this radionuclide and the levels $^{239+240}$Pu have been monitored by the IMR in the area adjacent to the *Komsomolets* in previous years (Figure 1.2), where the result of the monitoring matches the result found in the present study (NRPA, 2000; 2004). However, there are few, available published results on transuranic elements in sediments in this area. When comparing the activity concentrations of these elements with activity concentrations found elsewhere in the Barents and Norwegian Seas, one finds that the levels are somewhat the same, but where some of the samples collected near the coast of Spitsbergen show slightly elevated levels (NRPA, 2004; 2005).

This is also the case for the study Heldal et al. (2002) and the study of Zaborska et al. (2010), where the activity concentrations found near the Spitsbergen area show slightly elevated levels compared to the ^{238}Pu and $^{239+240}$Pu activity concentrations found in the present study. These samples have been collected closer to the shore, where terrestrial run of might have caused these results. Elevated activity concentrations compared to the levels of ^{238}Pu, $^{239+240}$Pu and ^{241}Am found in 2013 are also to be found in sediment samples collected in the Irish Sea (Mitchell et al., 1999) and in the area near the Thule accident (Eriksson et al., 2008). In the western Irish Sea, ^{238}Pu, $^{239+240}$Pu and ^{241}Am activity concentrations were found in surface sediments in period of 1988-1997, where they respectively range from 1.34 to 5.58 Bq/kg (d.w.), 8.0 to 33.3 Bq/kg (d.w.) and 2.1 to 35 Bq/kg (d.w.) (Mitchell et al., 1999). In the study of Dahlgaard et al. (2001), $^{239+240}$Pu activity concentrations found in surface sediments in 1997 in the area affected by the Thule accident, range from 12 to 642 Bq/kg.

The activity concentration of uranium-238 (^{238}U) in the present study, varied from 9.1 to 22.1 mBq/g (d.w.). If a leakage was to happen, one would expect to find the highest activity concentrations in the sediments collected by the front of the submarine, since the warheads are located in the front section of the wreck (Figure 1.4). In the present study, the highest concentration is found on the west side of the submarine, next by the front, and with the lowest values by the rear end of the wreck. Compared to the atom concentrations found in 5 hot particles (50 -100 ng) in the area affected by the Thule accident, these levels are relatively low, where the five particles had atom concentrations ranging from 8.34 to 65.34 ng (Eriksson et al., 2008).

4.3. Using isotope ratios to identify contamination sources

Different sources for radioactive contamination often exhibit characteristic isotope ratios, which can be used to identify the origin of the contamination (Oughton et al., 2004). Isotope ratios (including their references) originating from different sources located at the northern hemisphere are listed in Table 4.1.

Table 4.1. Isotope ratios for various sources (all references in brackets).

Source	***$^{240}Pu/^{239}Pu$ (atom ratio)***	***$^{238}Pu/^{239+240}Pu$ (activity ratio)***	***$^{241}Am/^{239+240}Pu$ (activity ratio)***
Global Fallout	0.175 – 0.190 *(1, 2, 14, 15, 26)*	0.025 – 0.040 *(1, 2, 4, 12, 13, 15, 18, 29)*	0.25 – 0.40* (3[1], 15, 28)
Sellafield	0.18-0.22 *(4, 30, 31, 33)*	0.17 – 0.30 *(4, 10, 11, 12, 29, 31)*	1.5** *(5, 10, 31)*
Cap la Hauge	0.25-0.34 *(8, 32)*	0.36 *(8, 32)*	-
Chernaya Bay	0.03 *(2, 15, 15)*	0.025 *(2, 14)*	0.05*** *(2, 14)*
Riverine discharges (Karsnyarsk, Mayak and Tomsk)	0.05 – 0.30 (*6, 9, 18, 19, 20, 21)*	0,01 ± 0,02 *(9, 20)*	-
Thule	0.03 – 0.06 *(6, 12, 17, 24, 25)*	0.015 – 0.025 *(1, 17)*	0.10* – 0.16 *(3[2], 17, 24)*
Chernobyl –fuel particles	0.40 – 0.52 *(7, 22, 23, 26)*	0.42 – 0.48 *(4, 26, 29)*	0.06 – 0.13*** (3[3], 29)

**Decay corrected to 1995 (originally reference Smith et al. (1987)[1] and Aarkrog et al. (1987)[2])*

***Decay corrected to 1993*

**** Decay corrected to 2000*

*****Decay corrected to 1986 (originally reference Aarkrog et al. (1999)[3])*

Reference: 1.Oughton et al. (2004), 2. Smith et al. (2000), 3. Ikäheimonen (2003), 4. Kershaw et al. (1995), 5. Beks (2000), 6. Lind et al. (2005), 7. Kutkov (1995), 8. Oughton et al. (1999), 9. Oughton et al. (2000), 10. MacKenzie et al. (1998), 11. Vintro et al. (2000), 12. Holme and McIntyre (1984), 13. Ostlund (1990), 14. Kelley et al. (1999), 15. Smith et al. (1995), 16. Beasley et al. (1998), 17.Eriksson et al. (2008), 18. Skipperud et al. (2004), 19.Børretzen et al. (2005), 20. Gauthier-Lafaye et al. (2008), 21. Skipperud et al. (2009), 22. Boulyga and Becker (2002), 23. Muramatsu et al. (2000), 24. Dahlgaard et al. (2001), 25. Mitchell et al. (1997), 26. Varga (2007) 28.UNSCEAR (1982), 29. Holm et al. (1992), 30.Eigl et al. (2013), 31. Povinec et al. (2002), 32.Cundy et al. (2002), 33.McCarthy and Nicholls (1990)

The $^{238}Pu/^{239+240}Pu$ activity ratios found in the 0-1 and 1-2 cm layers of sediment cores collected in 2013 range from 0.03 to 0.06 (Table 3.3). This is comparable to, or slightly higher than the activity resulting from atmospheric weapons tests (Table 2.4). The highest $^{238}Pu/^{239+240}Pu$ activity ratio (0.06) is found in the 1-2 cm layer of core 196-1. This is too low

to match the activity ratio in discharges from European reprocessing industry. This activity ratio has a relative high uncertainty compared to the other samples (Table 3.3), which might have biased this result.

Direct alpha measurements are often associated with considerable uncertainties. The $^{240}Pu/^{239}Pu$ ratio determined by mass spectroscopy is therefore more precise. The $^{240}Pu/^{239}Pu$ mass ratios found in the 0-1 and 1-2 cm layers of sediment cores collected in 2013 varied from 0.152 to 0.194 (Table 3.4). This is comparable to, or slightly lower than the $^{240}Pu/^{239}Pu$ ratios of global fallout (Table 4.1)

Although it appears that global fallout is the main contamination source in the samples analysed in the present study, Sellafield may, however, be a minor contamination source. Liquid waste discharged in the Irish Sea consist of a mixture of Pu from weapons production ($^{240}Pu/^{239}Pu$ = 0.05 – 0.06) and reprocessing of spent nuclear fuel ($^{240}Pu/^{239}Pu$ = 0.2 – 0.4) (Stepanov et al., 1999). This has previously been confirmed by McCarthy and Nicholls (1990), where the average $^{240}Pu/^{239}Pu$ activity ratio found in sediments of the Irish costal zones near the location of emission of waste from Sellafield, was 0.18 in 1977-1986. It is also known that Sellafield is an important source of Pu in the Barents Sea, where 19-27% of the Pu found in sediments in the north-western Barents Sea in the study of Zaborska et al. (2010), was calculated to primarily originate from this reprocessing plant. Also, Herrmann et al. (1998) reported that Pu derived from Sellafield was traced in deep waters of the Norwegian, Greenland and Barents Seas, where the activity concentration of $^{239, 240}Pu$ in the Atlantic current flow, correlate negatively with latitude after passing through the Irish Sea (Zaborska et al., 2010).

The $^{241}Am/^{239+240}Pu$ activity ratios of the samples collected in 2013 range from 1.03 to 3.28 (Figure 3.3). The 0-1 and 1-2 cm layers of core 194-1 had much higher activity ratios then the other samples, but also substantially higher uncertainties. By excluding these samples, the $^{241}Am/^{239+240}Pu$ activity ratios range from 1.03 and 1.54. These activity ratios probably reflect the origin of global fallout in addition to the influence of discharges of ^{241}Am and ^{241}Pu from European reprocessing plants, where most of the samples show activity concentrations between the ratios of these two sources (Table 4.1). The $^{241}Am/^{239+240}Pu$ activity ratio presented for global fallout in Table 4.1 is decay corrected to 1995. This activity ratio will be slightly higher today as plutonium-241 (^{241}Pu) ($t½$ = 14.4 years) decays to ^{241}Am (Mitchell et al., 1999), where the $^{241}Am/^{239+240}Pu$ activity ratio will increase to a maximum of 2.66 in year

2059 (Holm et al., 1992). However, in this study, the build-up of ^{241}Am from ^{241}Pu has not been accounted for, where the amount of sample material in the selected samples collected in 2013 were too small to determine the ^{241}Pu activity. This makes the comparison of ^{241}Am/$^{239+240}$Pu activity ratio with different sources less than a hundred percent reliable.

The Pu isotope ratios found in the present study matches the Pu isotope ratios found in the Barents Sea and the deep Norwegian and Greenland Seas. The ^{240}Pu/^{239}Pu atom ratios correspond to the atom ratios found in the study of Stepanov et al. (1999) in 1991 to 1998, while the ^{238}Pu/$^{239+240}$Pu activity ratios matches or are slightly lower than the activity ratios found in the study of Heldal et al. (2002). The study of Heldal et al. (2002) also show activity concentrations of ^{241}Am and $^{239+240}$Pu, but the combination of these (^{241}Am/$^{239+240}$Pu) show slightly lower values then the ^{241}Am/$^{239+240}$Pu ratios found in the present study, where they range from 0.2 to 1.7. However, the activity concentrations of ^{241}Am and $^{239+240}$Pu in the present study are still too low to indicate other sources than global fallout and the European reprocessing plants.

The ^{235}U/^{238}U atom ratios found in the present study ranged from 0.0069 to 0.0073 (Table 3.4). This match the atom ratios for natural uranium ratios in soil, which is approximately 0.007 (Ranebo et al., 2007). This result indicates that no highly enriched U-isotopes are found in the samples collected close to *Komsomolets* in 2013.

4.4. Grain size distributions

The grain size analyses of the five 0-1 cm layers collected in 2013 were quite similar (see Figure 3.8). This is as expected, as the samples are collected at a relatively large depth and within a small area. Surface sediment samples collected in 1999 in the area adjacent to *Komsomolets* ,were found to contain the minerals illite, kaolite and smectite (Heldal et al., 2002).

The sediment samples collected in this study are likely to have the same mineral content as the sediment samples in the study of Heldal et al. (2002). This indicate that the sediments in the area adjacent to *Komsomolets* may work as a sink for caesium-137 (^{137}Cs), as the clay mineral illite is known to bind irreversible to the ^{137}Cs (Coughtrey and Thorne, 1983). As no ^{137}Cs peaks are found in any layers of the collected sediment cores, this may contribute to confirm that there has been no leakage from the submarine.

4.5. Inaccuracy in sampling and sample preparation

The box-corer might penetrate the seabed with a certain angle (Figure 4.5), depending on the seabed conditions. This differs from the ideal sediment collection described in section 2.1.3, where the result of this inaccuracy will be sediment slices, non-parallel to the sediment surface. The tubes also cause a pressure on the sediment at the seabed. This again causes the sampling material, to a varying extent, to be compressed through the cores. When sub sampling cores in tubes, material will be transported along the walls of the tubes. As a result, the slices of one (or two) centimetres may contain material from adjacent layers.

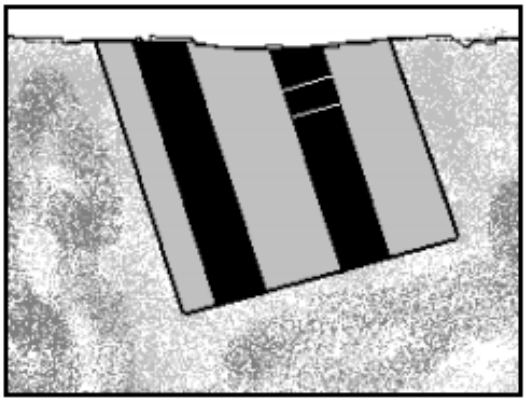

Figure 4.5. Schematic drawing of box-corer sampling, subsampling of cores (in black) and 1 cm slices (white lines) (Sværen, 2010a).

Slicing the cores can also be a source of error, where material might adhere to the tube when rotating the cutting apparatuses in the slicing process. When pressing the sediment core up using the piston, there is some compaction of the sediments due to the friction between the tube and sediments in contact with the tube. The fact that a ruler was used to measure the slices of 1 cm, may also add inaccuracy to the sediment samples, in case of small variation in the size of the slices. Loss of sediment material during the cutting process, may also be a problem, as this is roughly estimated to be 5% in each core (Sværen, 2010a). An evenly distributed loss from each slice will not affect the dating, but if this is not the case, it will cause inaccuracy.

Some of the sediment cores from 2012 got a big residual (see appendix A), which decreased the number of slices in the respective cores. These were the first cores I performed the sample preparation on, so the technique was new to me.

The deviation in measurements between parallel cores from the same box-corer collection, can partly be caused by the sampling and the sample preparation, but chances are that ^{137}Cs is not necessarily homogenous distributed within the sediments.

4.6. The effect and consequences of potential leakages from *Komsomolets*

The results from the present study confirm that no or an insignificant leakage from *Komsomolets* has taken place up until today. Many different estimations and conclusions have, however, been made of the outcome of a potential leakage. For instance, Alexander Kurchatov stated in the Moscow Times in 1994, that the only solution that could solve the problem would be to raise the submarine (Kurchatov, 1994). On the other hand, Høibråten et al. (2003), Føyn (1994b) and Heldal et al. (2013) concluded that *Komsomolets* represents a minor pollution problem, partly because of the great depth at which the wreck is resting.

There are also different estimates of when *Komsomolets* will start leaking. Gladkov et al. (1994) estimated, e.g., that the first step of corrosion of the wreck will take at least 2000 years. If this is correct, *Komsomolets* will in time probably sag into the sediments and after a while be covered by mud, particles and dead plankton (Sivintsev et al., 2005). This will help to reduce the consequence of a potential leakage. Nevertheless, different measures, like covering up the wreck or raising it, have been discussed for preventing a disposal from the submarine (FAS, 2000). This kind of measures are both time consuming and expensive, and may also lead to risk of contamination. For example, an accidental leakage during the rising of *Komsomolets*, would lead to much more harm if it was to happen in the upper mixed layer of the ocean. After all, this is where discharges would contaminate the marine resources directly without being diluted in large water masses in advance (Iosjpe et al., 2011).

The main cause of the Norwegian concern about *Komsomolets* is that its resting place is located close to Norwegian fishing grounds. The fisheries are of major importance of the Norwegian economy, and the Barents Sea is one of the world's richest ocean areas, with yearly catches of 2.0-2.5 million tons of fish (Føyn and Sværen, 1995, Fisheries, 2014). In 2013 a new Norwegian export record was set, with a value of total 61 billion NOK (NSC, 2014). Currently, Norway export seafood to some 140 countries worldwide, with Russia and France being the two most important markets. For both the local consumers and the export industry, it is imminent to document the levels of radioactive contamination in the Barents and Norwegian Seas, including the adjacent area of *Komsomolets*. If a leakage from the wreck should occur, there are reasons to believe it will affect the Norwegian fisheries, regardless of

whether the contamination does or does not, have a direct impact on the fish itself (Føyn and Sværen, 1995).

If future monitoring shows that there has been a leak, certain measures should be considered. First of all, an expanded program of analyses of radioactive contamination in sediments, seawater and marine resources (fish, seaweed, etc.) have to be performed. Furthermore, it is important that good and understandable, scientifically founded information is given to the public. If the Norwegian government manages to communicate this to the public, it may reduce the harm done to the fish industry.

4.7. Suggestion for further work

Most of the latest studies concerning *Komsomolets* rules a leakage from the submarine in the years to come as absolutely unlikely (Gladkov et al., 1994). And if a leakage was to happen, it would not have a significant impact on marine resources (Føyn, 1994b, Høibråten et al., 2003, Heldal et al., 2013). However, it is important that the monitoring of the resting place of the wreck continues. A yearly monitoring is not necessarily required, but the use of the acoustic transponder during sampling, should be a part of the standard procedure every time, as it will reduce the uncertainties related to the sampling position.

Some work in the present study might not need a yearly performance, e.g. the particle size analysis and the dating of the cores. The plutonium (Pu) isotope analysis of the 0-1 cm layers on the other hand, is very much of interest. Here, Pu-isotope activity ratios, obtained from the Pu content in the sediments, may indicate which source a potential elevated activity concentration originates from. This will help to confirm or reject a possible leakage from the submarine if elevated Pu levels were to be found in the sediments from the area adjacent to *Komsomolets*.

Suggestions of further work concerning *Komsomolets* will be;

- Always use the acoustic transponder attached to the box-corer when collecting sediment samples
- Continue monitoring of sediments and seawater at the resting place of the wreck
- Prepare isotope ratios
- Good and understandable, scientifically founded information about the situation of *Komsomolets*, is to be given to the public

5. Conclusion

The present study confirms that an acoustic transponder can be used on sediment sampling equipment on 1700 m depth. This kind of equipment can further be used to sample in the vicinity of any other point target at the seabed, or in the water column. This relatively inexpensive equipment could in some cases replace expensive equipment as Remotely Operated underwater Vehicle (ROV).

IMR has performed yearly monitoring of the levels of radioactive contaminations in sediments and seawater in the area close to *Komsomolets*, since 1993. The first successful sampling with an acoustic transponder attached to the sampling equipment, was performed in 2013. Such sampling will make it easier to detect a possible leak in the future.

The sediment cores collected in 2012 and 2013 did not contain elevated levels of caesium-137 (^{137}Cs). This is consistent with pervious monitoring by IMR in the area adjacent to *Komsomolets*. The ^{137}Cs activity concentrations found in the present study are comparable to ^{137}Cs activity concentrations found in the Barents Sea and the deep areas of the Norwegian and Greenland Seas.

Low levels of plutonium -238 (^{238}Pu), plutonium-239,240 ($^{239+240}$Pu), americium-241 (^{241}Am) and uranium-238 (^{238}U) were found in the 0-1 and 1-2 cm layers of cores collected in 2013. The activity concentrations of ^{238}Pu, $^{239+240}$Pu and ^{241}Am found in the present study are comparable to levels found in previous studies in the deep parts of the Norwegian and Greenland Seas. The isotope ratios of ^{238}Pu/$^{239+240}$Pu, ^{240}Pu/^{239}Pu and ^{241}Am/$^{239+240}$Pu indicate that global fallout is the major source of the activity concentrations found in the present study, followed by the European reprocessing plants, mainly Sellafield. The ^{235}U/^{238}U atom ratio matches with the atom ratio for natural uranium.

The dating of the two sediment cores collected in 2012 had no^{137}Cs-peaks in years/periods clearly indicating a dominating source present. This also points to global fallout as the major source in the area adjacent to *Komsomolets*.

The result of the grain size distribution of the 0-1 cm layers of the selected cores collected in 2013, showed that the sediment samples contained 70 % silt, 20 % clay, and only 3 % sand and gravel. As illite probably is the major mineral in the clay content, the sediments in the area adjacent to *Komsomolets*, may work as a sink for ^{137}Cs where it binds irreversible to this

mineral. As no ^{137}Cs peaks are found in any layers of the collected sediment cores, this may contribute to confirm that there has been no leakage from the submarine.

Public concerns about the condition of *Komsomolets* arose particularly in Norway, since the submarine rests close to the Norwegian fishing grounds. A leak affecting the fish in these areas would have a major effect on the Norwegian export industry and economics. However, the latest studies and modelling have concluded that both a continuous leakages and pulse discharges of ^{137}Cs from the wreck induce negligible activity concentrations of ^{137}Cs in marine resources. It is still reason to believe that a leak from the submarine may affect the Norwegian fish export and economics.

Suggestions for further work concerning *Komsomolets* are to continue the monitoring of sediments and seawater collected at the resting place of the wreck. The acoustic transponder should always be a part of the sampling equipment, to ensure that the samples are collected close to the submarine, so a possible leakage in the future can easily be detected.

References

AARKROG, A. 1994. RADIOACTIVITY IN POLAR-REGIONS - MAIN SOURCES. *Journal of Environmental Radioactivity,* 25**,** 21-35.

AARKROG, A., BOELSKIFTE, S., DAHLGAARD, H., DUNIEC, S., HOLM, E. & SMITH, J. N. 1987. STUDIES OF TRANSURANICS IN AN ARCTIC MARINE-ENVIRONMENT. *Journal of Radioanalytical and Nuclear Chemistry-Articles,* 115**,** 39-50.

AARKROG, A., DAHLGAARD, H. & NIELSEN, S. P. 1999. Marine radioactivity in the Arctic: a retrospect of environmental studies in Greenland waters with emphasis on transport of Sr-90 and Cs-137 With the East Greenland Current. *Science of the Total Environment,* 238**,** 143-151.

AMAP 1997. Arctic Pollution Issues: A state of the Arctic Environment Report Arctic. *Chapter 8. Arctic Monitoring and Assessment Programme (AMAP), Oslo, Norway.*

AMAP 1998. Assessment Report: Arctic Pollution Issues. *Arctic Monitoring and Assessment Programme (AMAP), Oslo, Norway.*

APPLEBY, P. G. & OLDFIELD, F. 1978. The Calculation of lead-210 dates assuming a constant rate of supply of unsupported 210Pb to the sediment. *CATENA,* 5.

BEASLEY, T. M., KELLEY, J. M., ORLANDINI, K. A., BOND, L. A., AARKROG, A., TRAPEZNIKOV, A. P. & POZOLOTINA, V. N. 1998. Isotopic Pu, U, and Np signatures in soils from Semipalatinsk-21, Kazakh Republic and the Southern Urals, Russia. *Journal of Environmental Radioactivity,* 39**,** 215-230.

BEKS, J. P. 2000. Storage and distribution of plutonium, Am-241, Cs-137 and Pb-210(xs) in North Sea sediments. *Continental Shelf Research,* 20**,** 1941-1964.

BIANCHI, G. G., HALL, I. R., MCCAVE, I. N. & JOSEPH, L. 1999. Measurement of the sortable silt current speed proxy using the Sedigraph 5100 and Coulter Multisizer IIe: precision and accuracy. *Department of Earth Sciences, University of Cambridge, Downing Street, Cambridge CB2 3EQ, UK.*

BLINDHEIM, J. 1994. Physical characteristics of the area. *In:* SÆTRE, R. (ed.) *The sunken nuclear submarine in the Norwegian Sea - a potential environmental problem?* Bergen: Institute of Marine research.

BLOTT, S. J. & PYE, K. 2001. GRADISTAT: A GRAIN SIZE DISTRIBUTION AND STATISTICS PACKAGE FOR THE ANALYSIS OF UNCONSOLIDATED SEDIMENTS. *Surface Processes and Modern Environments Research Group, Department of Geology, Royal Holloway University of London, Egham, Surrey, TW20 0EX, UK.*

BOULYGA, S. F. & BECKER, J. S. 2002. Isotopic analysis of uranium and plutonium using ICP-MS and estimation of burn-up of spent uranium in contaminated environmental samples. *Journal of Analytical Atomic Spectrometry,* 17**,** 1143-1147.

BUCHANAN, J. B. 1984. Sediment analysis. *Pp 41-65 in: Holme, N.A., McIntyre, A.D. (Eds.). Methods for the study of marine benthos. Blackwell Scientific Publications, Oxford.*

BØRRETZEN, P., JØLLE, T. & STRAND, P. 2005. *The 6th International Conference on Radioactivity in the Arctic & Antarctic. Proceedings* Østerås, Norway, Norwegian Radiation Protection Authority.

CHAMP, M. A., MAKEYEV, V. V., BROOKS, J. M., DELACA, T. E., VAN DER HORST, K. M. & ENGLE, M. V. 1997. Assessment of the impact of nuclear wastes in the Russian Arctic. *Marine Pollution Bulletin,* 35**,** 203-221.

CHEN, Q. J., DAHLGAARD, H. & NIELSEN, S. P. 1994. DETERMINATION OF TC-99 IN SEA-WATER AT ULTRA-LOW LEVELS. *Analytica Chimica Acta,* 285**,** 177-180.

CHOPPIN, G. 2013. *Radiochemistry and nuclear chemistry,* [S.l.], Academic Press.

COCHRAN, T. B. & NORRIS, R. S. 1993. Russian/Soviet Nuclear Warheads Production. *Working paper NWD 93-1, Natural Resources Defence Concil, Washington, DC, USA.*

COUGHTREY, P. J. 1983. *Radionuclide distribution and transport in terrestrial and aquatic ecosystems. A critical review of data. Volume 1*.

COUGHTREY, P. J. & THORNE, M. C. 1983. *Radionuclide distribution and transport in terrestrial and aquatic ecosystems: A critical review of data, Volume one,* Rotterdam, Balkema.

CUNDY, A. B., CROUDACE, I. W., WARWICK, P. E., OH, J. S. & HASLETT, S. K. 2002. Accumulation of COGEMA-La Hague-derived reprocessing wastes in French salt marsh sediments. *Environmental Science & Technology,* 36**,** 4990-4997.

CURRIE, L. A. 1968. LIMITS FOR QUALITATIVE DETECTION AND QUANTITATIVE DETERMINATION - APPLICATION TO RADIOCHEMISTRY. *Analytical Chemistry,* 40**,** 586-&.

DAHLGAARD, H. 1995. TRANSFER OF EUROPEAN COASTAL POLLUTION TO THE ARCTIC - RADIOACTIVE-TRACERS. *Marine Pollution Bulletin,* 31**,** 3-7.

DAHLGAARD, H., ERIKSSON, M., ILUS, E., RYAN, T., MCMAHON, C. A. & NIELSEN, S. P. 2001. Plutonium in the marine environment at Thule, NW-Greenland after a nuclear weapons accident. *In:* BAXTER, M. S. (ed.) *Radioactivity in the environment.*

DEBERTIN, K. & HELMER, R. G. 1988. *Gamma- and X-ray spectrometry with semiconductor detectors,* Amsterdam, Elsevier.

EGOROV, V. N., POVINEC, P. P., POLIKARPOV, G. G., STOKOZOV, N. A., GULIN, S. B., KULEBAKINA, L. G. & OSVATH, I. 1999. Sr-90 and Cs-137 in the Black Sea after the Chernobyl NPP accident: inventories, balance and tracer applications. *Journal of Environmental Radioactivity,* 43**,** 137-155.

EIGL, R., SRNCIK, M., STEIER, P. & WANNER, G. 2013. U-236/U-238 and Pu-240/Pu-239 isotopic ratios in small (2 L) sea and river water samples. *Journal of Environmental Radioactivity,* 116**,** 54-58.

ENGLAND, M. H. & MAIER-REIMER, E. 2001. Using chemical tracers to assess ocean models. *Reviews of Geophysics,* 39**,** 29-70.

ERIKSEN, V. O. 1990. *Sunken nuclear submarines: a threat to the environment?,* Oslo, Norwegian University Press.

ERIKSSON, M., LINDAHL, P., ROOS, P., DAHLGAARD, H. & HOLM, E. 2008. U, Pu, and Am Nuclear Signatures of the Thule Hydrogen Bomb Debris. *IAEA-MEL, 4 Quai Antonie ler, MC*

98000 Monaco, Monaco, Risoe National Laboratory, P.O Box 49, DK-4000 Roskilde, Denmark, and Department of Radiation Physics, Lund University, SE-221 85 Lund, Sweeden.

FAS. 07.09.2000. *Project 685 Plavnik Mike class [internet]* [Online]. Federation of American Scientists (FAS): http://www.fas.org/man/dod-101/sys/ship/row/rus/685.htm [Read.21.04.2014].

FISHERIES. 2014. *Fisheries* [Online]. http://www.environment.no/Tema/Hav-og-kyst/Fiskeri/#: Directorate of Fisheries and the Norwegian Environment Agency. [Accessed 29.05. 2014].

FØYN, L. 1994a. Introduction. *In:* SÆTRE, R. (ed.) *The sunken nuclear submarine in the Norwegian Sea - a potential environmental problem?* Bergen: Institute of Marine research.

FØYN, L. 1994b. To move or not to move. *In:* SÆTRE, R. (ed.) *The sunken nuclear submarine in the Norwegian Sea - a potential environmental problem?* Bergen: Institute of Marine research.

FØYN, L. & SVÆREN, I. 1995. The Barents sea, its fisheries and the past and present status of radioactive contaminates, and its impact on fisheries. . *The international conference on Environmental Radioactivity in the Arctic* [Online].

GAUTHIER-LAFAYE, F., POURCELOT, L., EIKENBERG, J., BEER, H., LE ROUX, G., RHIKVANOV, L. P., STILLE, P., RENAUD, P. & MEZHIBOR, A. 2008. Radioisotope contaminations from releases of the Tomsk-Seversk nuclear facility (Siberia, Russia). *Journal of Environmental Radioactivity,* 99**,** 680-693.

GLADKOV, G. A., KHLOPKIN, N., S, LYSTSOV, V. N., NEJDANOV, G. A., POLOGIKH, B. G. & SIVINTSEV, Y. V. 1994. Assessment and prognosis of the state of nuclear installation of submarine "Komsomolets". *Working Group under leadership of Academician N. S. Khlopkin, RRC "Kurchatov Institute", Moscow, Russia.*

GOLDBERG, E. D. 1963. Geochronology with Pb-210 in radioactive dating. *International Atomic Energy Agency. Symposium Proceeding, Vienna 1962:121-131.*

GRAY, J., JONES, S. R. & SMITH, A. D. 1995. Discharges to the environment from the Sellafield site, 1951-1992. *Journal of Radiological Protection,* 15**,** 99-131.

GWYNN, J. P., HELDAL, H. E., GAFVERT, T., BLINOVA, O., ERIKSSON, M., SVAEREN, I., BRUNGOT, A. L., STRALBERG, E., MOLLER, B. & RUDJORD, A. L. 2012. Radiological status of the marine environment in the Barents Sea. *Journal of Environmental Radioactivity,* 113**,** 155-162.

GWYNN, J. P., RUDJORD, A. L., LIND, B., HELDAL, H. E., SALBU, B., LIND, O. C., TEIEN, H. C., WENDEL, C., NIKITIN, A. I., SHERSHAKOV, V. M., VALETOVA, N. K., PETRENKO, G. I., KAZENNOV, A. & GRISHIN, D. 2013. Joint Norwegian-Russian Expert Group investigation into the radioecological status of Stepovogo Fjord: The dumping site of the nuclear submarine K-27 and solid radioactive waste. *In:* GWYNN, J. P. & NIKITIN, A. I. (eds.) *Joint Norwegian-Russian Expert Group for investigation of Radioactive Contamination in the Northern Areas.*

HALLSTADIUS, L. 1984. A method for the electrodeposition of actinides. *Nuclear Instruments and Methods In Physics Research, 223 (2-3), 266-267.*

HAYRYNEN, N. 2003. Environmental security: The case of the Kursk. *Environmental Politics,* 12**,** 65-82.

HELDAL, H. E. 2001. *Radioactivity in Norwegian waters: distribution in seawater and sediments, and uptake in marine organisms,* Bergen, Department of Chemistry, University of Bergen.

HELDAL, H. E., VARSKOG, P. & FOYN, L. 2002. Distribution of selected anthropogenic radionuclides (Cs-137, Pu-238, Pu-239,Pu-240 and Am-241) in marine sediments with emphasis on the Spitsbergen-Bear Island area. *Science of the Total Environment,* 293**,** 233-245.

HELDAL, H. E., VIKEBO, F. & JOHANSEN, G. O. 2013. Dispersal of the radionuclide caesium-137 (Cs-137) from point sources in the Barents and Norwegian Seas and its potential contamination of the Arctic marine food chain: Coupling numerical ocean models with geographical fish distribution data. *Environmental Pollution,* 180**,** 190-198.

HELSINKI COMISSION 2007. *long-lived radionuclides in the seabed of the Baltic Sea. Report of the sediment baseline study of HELCOM MORS-PRO in 2000-2005.*

HERRMANN, J., NIES, H. & GORONCY, I. 1998. Plutonium in the deep layers of the Norwegian and Greenland Seas. *Radiation Protection Dosimetry,* 75**,** 237-245.

HOLM, E., RIOSECO, J. & PETTERSSON, H. 1992. FALLOUT OF TRANSURANIUM ELEMENTS FOLLOWING THE CHERNOBYL ACCIDENT. *Journal of Radioanalytical and Nuclear Chemistry-Articles,* 156**,** 183-200.

HOLME, N. A. & MCINTYRE, A. D. 1984. *Methods for the study of marine benthos,* Oxford, Blackwell.

HUNT, J., LEONARD, K. & HUGHES, L. 2013. Artificial radionuclides in the Irish Sea from Sellafield: remobilisation revisited. *Journal of Radiological Protection,* 33**,** 261-279.

HØIBRÅTEN, S., HAUGEN, A. & PER, T. 2003. the environmental impact of the sunken submarine Komsomolets. *FFI report*.

HØIBRÅTEN, S., THORESEN, P. & HAUGAN, A. 1997. The sunken nuclear submarine Komsomolets and its effects on the environment. *Science of The Total Environment*.

IAEA 1989. Measurement of Radionuclides in Food and the Environment. *International Atomic Energy Agency. IAEA, Technical Reports Series No. 295. Vienna, 1989.*

IAEA 2001. Inventory of accidents and losses at sea involving radioactive material. *International Atomic Energy Agency. IAEA, VIENNA, 2001. IAEA-TECDOC-1242*

IAEA 2004. SEDIMENT DISTRIBUTION COEFFICIENTS AND CONCENTRATION FACTORS FOR BIOTA IN THE MARINE ENVIRONMENT. *International Atomic Energy Agency (IAEA). Technical Reports Series No. 422. Vienna, 2004.*

IKÄHEIMONEN, T. K. 2003. DETERMINATION OF TRANSURANIC ELEMENTS, THEIR BEHAVIOUR AND SOURCES IN THE AQUATIC ENVIRONMENT. *Radiation and Nuclear Safety Authority, STUK. University of Helsinki, Faculty of Science. Department of Chemistry, Laboratory of Radiochemistry*.

IMR 2001. Unpublished data. Institute of Marine Research (IMR).

IOSJPE, M., REISTAD, O. & LILAND, A. 2011. Radioecological consequences after a hypothetical accident with release into the marine environment involving a Russian nuclear submarine in the Barents Sea. *Norwegain Radiation Protenction Authority (NRPA). Østerås, 2010.*

JNRE 1996. Dumping of radioactive waste and investigation of radioactive contamination of the Kara Sea. Result from 3 years of investigation (1992-1994) in the Kara Sea. *Joint Norwegian-Russian Expert Group for Investigation of Radioactive Contamination in the Northern Areas. NRPA, Norway, pp.56.*

JONES, D. G., KERSHAW, P. J., MCMAHON, C. A., MILODOWSKI, A. E., MURRAY, M. & HUNT, G. J. 2007. Changing patterns of radionuclide distribution in Irish Sea subtidal sediments. *Journal of Environmental Radioactivity,* 96**,** 63-74.

KAPL 2000. Deep Sea Radiological Environmental Monitoring Performed During September 1998 at the Sites of the Sunken Submarines USS Thresher and USS Scorpion. *KNOLLS ATOMIC POWER LABORATORY. Report KAPL-4842 (July 2000).*

KELLEY, J. M., BOND, L. A. & BEASLEY, T. M. 1999. Global distribution of Pu isotopes and Np-237. *Science of the Total Environment,* 238**,** 483-500.

KERSHAW, P. & BAXTER, A. 1995. The transfer of reprocessing wastes from north-west Europe to the arctic. *Deep-Sea Research Part Ii-Topical Studies in Oceanography,* 42**,** 1413-1448.

KERSHAW, P. J., SAMPSON, K. E., MCCARTHY, W. & SCOTT, R. D. 1995. The measurement of the isotopic composition of plutonium in an Irish Sea sediment by Mass Spectromentry. *J. Radional. Nucl. Chem. 198, 113-124.*

KOLSTAD, A. K. 1995. Tokt til "Kosmolets" i 1993 og 1994. *Strålevernrapport 1995:7. Østerås: Statens strålevern.*

KURCHATOV, A. 05.11.1994. Raise the Komsomolets![internet]. *The Moscow Times*.

KUTKOV, V. A. 1995. Unique from of airborne radioactivity: nuclear fuel 'hot particles' released during the Chernobyl accident. *Environmental Impact of Radioactive Releases. IAEA, Vienna, pp. 625-630.*

LEINEBØ, I. B. 2011. Caesium-137 (137Cs) in sediment cores from the Norwegian Sea -including lead-210 (210Pb) dating and comparsion with organic contamination levels. *Master of Sience Thesis in Environmental Chemistry. Department of Chemistry. University of Bergen*.

LIND, O. C., SALBU, B., JANSSENS, K., PROOST, K. & DAHLGAARD, H. 2005. Characterization of, uranium and plutonium containing particles originating from the nuclear weapons accident in Thule, Greenland, 1968. *Journal of Environmental Radioactivity,* 81**,** 21-32.

LINDAHL, P., LEE, S.-H., WORSFOLD, P. & KEITH-ROACH, M. 2010. Plutonium isotopes as tracers for ocean processes: A review. *Marine Environmental Research,* 69**,** 73-84.

LIVINGSTON, H. D. 2004. *Marine radioactivity,* Amsterdam, Elsevier.

LOENG, H. 1991. FEATURES OF THE PHYSICAL OCEANOGRAPHIC CONDITIONS OF THE BARENTS SEA. *Polar Research,* 10**,** 5-18.

LUKASHIN, V. N. & SHCHERBININ, A. D. 2007. The nepheloid layer and horizontal sedimentary matter fluxes in the Norwegian Sea. *Oceanology,* 47**,** 833-847.

MACKENZIE, A. B., COOK, G. T., MCDONALD, P. & JONES, S. R. 1998. The influence of mixing timescales and re-dissolution processes on the distribution of radionuclides in northeast Irish Sea sediments. *Journal of Environmental Radioactivity,* 39**,** 35-53.

MATISHOV, D. G. & MATISHOV, G. G. 2004. *Radioecology in northern European seas*, Berlin, Springer.

MCCARTHY, W. & NICHOLLS, T. M. 1990. Mass-Spectrometric Analysis of Plutonium in Soils Near Sellafield. *Atomic Weapons Establishment, Aldermaston, Reading, Berkshire RG7 4PR, UK.*

MCCAVE, I. N. 2008. SIZE SORTING DURING TRANSPORT AND DEPOSITION OF FINE SEDIMENTS: SORTABLE SILT AND FLOW SPEED. *In:* ELSEVIER, B. V. (ed.) *Developments in Sedimentology.* Department of Earth Sciences, University of Cambridge, Cambridge, UK.

MIROSHNIKOV, A. Y. 2013. Radiocaesium distribution in the bottom sediments of the Kara Sea. *Water Resources,* 40**,** 723-732.

MITCHELL, P. I., CONDREN, O. M., VINTRO, L. L. & MCMAHON, C. A. 1999. Trends in plutonium, americium and radiocaesium accumulation and long-term bioavailability in the western Irish Sea mud basin. *Journal of Environmental Radioactivity,* 44**,** 223-251.

MITCHELL, P. I., VINTRO, L. L., DAHLGAARD, H., GASCO, C. & SANCHEZCABEZA, J. A. 1997. Perturbation in the Pu-240/Pu-239 global fallout ratio in local sediments following the nuclear accidents at Thule (Greenland) and Palomares (Spain). *Science of the Total Environment,* 202**,** 147-153.

MONTGOMERY, G. 1995. Burial at sea The Komsomolets Disaster. *(CIA) Studies in intelligence,* Volume 38, nuber 5.

MURAMATSU, Y., RUHM, W., YOISHIDA, S., TAGAMI, K., UCHIDA, S. & WIRTH, S. 2000. Concentrations of 239Pu and 240Pu and Their Isotopic Ratios Determined by lCP-MS in Soils Collected from the Chernobyl 30-km zone. *Environmental sience and technology 34, 2913-2917.*

NIES, H., HARMS, I. H., KARCHER, M. J., DETHLEFF, D. & BAHE, C. 1999. Anthropogenic radioactivity in the Arctic Ocean - review of the results from the joint German project. *Science of the Total Environment,* 238**,** 181-191.

NILSEN, T., KUDRIK, I. & NIKITIN, A. 1996. The Russian Northern Fleet. Sources of radioactive contamination. Norway, Oslo: Bellona Foundation.

NRPA 2000. Artificial Radionuclides in the Northern European Marine Environment. Distribution of radiocaesium, plutonium and americium in seawater and sediments in 1995. *Norwegian Radataion Protection Authority 2000:1, (Grøttheim, S).*

NRPA 2003. Radioactivity in the Marine Environment 2000 and 2001. *Result from the Norwegian National Monitoring Programme (RAME). NRPA 2003:8. Østerås: Norwegian Radataion Protection Authority*.

NRPA 2004. Radioactivity in the marine environment 2002. *Result from the Norwegian National Monitoring Programme (RAME). NRPA 2004:10. Østerås: Norwegian Radataion Protection Authority*.

NRPA 2005. Radioactivity in the marine environment 2003. *Result from the Norwegian National Monitoring Programme (RAME). NRPA 2005:20. Østerås: Norwegian Radataion Protection Authority*.

NRPA 2006. Radioactivity in the marine environment 2004. *Result from the Norwegian National Monitoring Programme (RAME). NRPA 2006:14. Østerås: Norwegian Radataion Protection Authority*.

NRPA 2007. Radioactivity in the marine environment 2005. *Result from the Norwegian National Monitoring Programme (RAME). NRPA 2007:10. Østerås: Norwegian Radataion Protection Authority*.

NRPA 2008. Radioactivity in the marine environment 2006. *Result from the Norwegian National Monitoring Programme (RAME). NRPA 2008:14. Østerås: Norwegian Radataion Protection Authority*.

NRPA 2009. Radioactivity in the marine environment 2007. *Result from the Norwegian National Monitoring Programme (RAME). NRPA 2009:15. Østerås: Norwegian Radataion Protection Authority*.

NRPA 2011. Radioactivity in the marine environment 2008 AND 2009. *Result from the Norwegian National Monitoring Programme (RAME). NRPA 2011:4. Østerås: Norwegian Radataion Protection Authority*.

NRPA 2012. Radioactivity in the marine environment 2010. *Result from the Norwegian National Monitoring Programme (RAME). NRPA 2012:10. Østerås: Norwegian Radataion Protection Authority*.

NSC. 06.01.2014. *Strong growth in seafood exports [internet]* [Online]. Norwegian Seafood Council (NSC): http://en.seafood.no/News-and-media/News-archive/Press-releases/Strong-growth-in-seafood-exports2 [Read.21.04.2014].

NURNBERG, D., WOLLENBURG, I., DETHLEFF, D., EICKEN, H., KASSENS, H., LETZIG, T., REIMNITZ, E. & THIEDE, J. 1994. SEDIMENTS IN ARCTIC SEA-ICE - IMPLICATIONS FOR ENTRAINMENT, TRANSPORT AND RELEASE. *Marine Geology,* 119**,** 185-214.

OLGAARD, P. L. 1994. Nuclear Ship Accidents, Description and Analysis. *Department of Electrophysics, Technical University of Denmark, Lyngby, Denmark*.

OSTLUND, P. 1990. Plutonium isotope ratios in baltic sea sediments. *Finnish marine research*.

OUGHTON, D. H., FIFIELD, L. K., DAY, J. P., CRESSWELL, R. C., SALBU, B., SKIPPERUD, L., STRAND, P., DROZHCO, E. & MOKROV, Y. 2000. Plutonium from Mayak: Measurements using accelerator mass spectrometry. *Environmental Sience and technology 34, 1938-1945.*

OUGHTON, D. H., FIFIELD, L. K., DAY, J. P., CRESSWELL, R. C., SKIPPERUD, L. & SALBU, B. 1999. Determination of 240Pu/239Pu isotope ratios in Kara Sea and Novaya Zemlya sediments using accelerator mass spectrometry. *In: symposium on Marine Pollution, IAEA-SM-354, IAEA, Vienna.*

OUGHTON, D. H., SKIPPERUD, L., FIFIELD, L. K., CRESSWELL, R. G., SALBU, B. & DAY, P. 2004. Accelerator mass spectrometry measurement of (240)Pu/(239)Pu isotope ratios in Novaya Zemlya and Kara Sea sediments. *Applied Radiation and Isotopes,* 61**,** 249-253.

PFIRMAN, S. L., EICKEN, H., BAUCH, D. & WEEKS, W. F. 1995. THE POTENTIAL TRANSPORT OF POLLUTANTS BY ARCTIC SEA-ICE. *Science of the Total Environment,* 159**,** 129-146.

POVINEC, P. P., BADIE, C., BAEZA, A., BARCI-FUNEL, G., BERGAN, T. D., BOJANOWSKI, R., BURNETT, W., EIKENBERG, J., FIFIELD, L. K., SERRADELL, V., GASTAUD, J., GORONCY, I., HERRMANN, J., HOTCHKIS, M. A. C., IKAHEIMONEN, T. K., JAKOBSON, E., KALIMBADJAN, J., LA ROSA, J. J., LEE, S. H., KWONG, L. L. W., LUENG, W. M., NIELSEN, S. P., NOUREDDINE, A., PHARM, M. K., ROHOU, J. N., SANCHEZ-CABEZA, J. A., SUOMELA, J., SUPLINSKA, M. & WYSE, E. 2002. Certified reference material for radionuclides in seawater IAEA-381 (Irish Sea Water). *Journal of radioanalytical and nuclear chemistry,* 251**,** 369-374.

POVINEC, P. P., DU BOIS, P. B., KERSHAW, P. J., NIES, H. & SCOTTO, P. 2003. Temporal and spatial trends in the distribution of Cs-137 in surface waters of Northern European Seas - a

record of 40 years of investigations. *Deep-Sea Research Part Ii-Topical Studies in Oceanography,* 50**,** 2785-2801.

QUALITY ASSURANCE DATA SHEET 06.22.04. Rad12. Internal at the IMR.

QUALITY ASSURANCE DATA SHEET 10.30.02. Rad11. Internal at the IMR.

RANEBO, Y., ERIKSSON, M., TAMBORINI, G., NIAGOLOVA, N., BILDSTEIN, O. & BETTI, M. 2007. The use of SIMS and SEM for the characterization of individual particles with a matrix originating from a nuclear weapon. *Microscopy and Microanalysis,* 13**,** 179-190.

RIFE-18 2013. Radioactivity in food and the environment 2012, RIFE18. *Environment agency*.

SAGALEVITCH, A. M. 1995. Results of five years of operation with deep manned submersibles "MIR-1" and "MIR-2" on nuclear submarine "Komsomolets" wreck. *Challenges of Our Changing Global Environment. Conference Proceedings,* Volume1.

SALBU, B., NIKITIN, A. I., STRAND, P., CHRISTENSEN, G. C., CHUMICHEV, V. B., LIND, B., FJELLDAL, H., BERGAN, T. D. S., RUDJORD, A. L., SICKEL, M., VALETOVA, N. K. & FOYN, L. 1997. Radioactive contamination from dumped nuclear waste in the Kara sea - results from the joint Russian-Norwegian expeditions in 1992-1994. *Science of the Total Environment,* 202**,** 185-198.

SARMIENTO, J. L. & GRUBER, N. 2006. *Ocean biogeochemical dynamics,* Princeton, N.J., Princeton University Press.

SCHØTZIG & SCHRAEDER 1993. Halbwertszeiten und Photonen- Emissionswahrscheinlichkeiten von haufig verwendeten Radionukliden. *Physikalish- Technische Bundesanstalt, Braunschweig.*

SFT 2007. Revidering av klassifisering av metaller og organsik miljøgifter i vann og sedimenter.Veileder for klassifisering av miljøkvalitet i fjorder og kystfarevann. *Statens forurensningstilsyn. (TA-2229/2007).*

SIVINTSEV, Y. V., VAKULOVSKY, S. M., VASILIEV, A. P., VYSOTSKY, V. L., GUBIN, A. T., DANILYAN, V. A., KOBZEV, V. I., KRYSHEV, I. I., LAVKOVSKY, S. A., MAZOKIN, V. A., NIKITIN, A. I., PETROV, O. I., POLOGIKH, B. G. & SKORIK, Y. I. 2005. Technogenic radionuclides in the sea surrounding Russia. *Radioecological Consequences of Radioactive Waste Dumping in the Arctic and Far Eastern Seas 'The White Book– 2000', Moscow*.

SKIPPERUD, L., BROWN, J., FIFIELD, L. K., OUGHTON, D. H. & SALBU, B. 2009. Association of plutonium with sediments from the Ob and Yenisey Rivers and Estuaries. *Journal of Environmental Radioactivity,* 100**,** 290-300.

SKIPPERUD, L., OUGHTON, D. H., FIFIELD, L. K., LIND, O. C., TIMS, S., BROWN, J. & SICKEL, M. 2004. Plutonium isotope ratios in the Yenisey and Ob estuaries. *Applied Radiation and Isotopes,* 60**,** 589-593.

SMITH, J. N., ELLIS, K. M., NAES, K., DAHLE, S. & MATISHOV, D. 1995. Sedimentation and mixing rates of radionuclides in Barents Sea sediments off Novaya Zemlya. *Deep-Sea Research Part Ii-Topical Studies in Oceanography,* 42**,** 1471-1493.

SMITH, J. N., ELLIS, K. M. & NELSON, D. M. 1987. TIME-DEPENDENT MODELING OF FALLOUT RADIONUCLIDE TRANSPORT IN A DRAINAGE-BASIN - SIGNIFICANCE OF SLOW EROSIONAL AND FAST HYDROLOGICAL COMPONENTS. *Chemical Geology,* 63**,** 157-180.

SMITH, J. N., ELLIS, K. M., POLYAK, L., IVANOV, G., FORMAN, S. L. & MORAN, S. B. 2000. (PU)-P-239,240 transport into the Arctic Ocean from underwater nuclear tests in Chernaya Bay, Novaya Zemlya. *Continental Shelf Research,* 20**,** 255-279.

STANDRING, W. J. F., STEPANETS, O., BROWN, J. E., DOWDALL, M., BORISOV, A. & NIKITIN, A. 2008. Radionuclide contamination of sediment deposits in the Ob and Yenisey estuaries and areas of the Kara Sea. *Journal of Environmental Radioactivity,* 99**,** 665-679.

STEPANETS, O., BORISOV, A., LIGAEV, A., SOLOVJEVA, G. & TRAVKINA, A. 2007. Radioecological investigations in shallow bays of the Novaya Zemlya Archipelago in 2002-2005. *Journal of Environmental Radioactivity,* 96**,** 130-137.

STEPANOV, A. V., TSVETKOV, O. S., TISHKOV, V. P., BELYAEV, B. N., DOMKIN, V. D., IVANOVA, L. M., OSOKINA, A. A., PLEKHOV, V. S., BOBYLEV, K. L. & JOHANNESSEN, O. 1999. Isotopic composition of plutonium in the bottom deposits of the Norwegian Sea and Greenland Sea and identification of the sources of contaminationheader. *Atomic Energy,* 87**,** 745-752.

STRAND, P., NIKITIN, A., RUDJORD, A. L., SALBU, B., CHRISTENSEN, G., FOYN, L., KRYSHEV, II, CHUMICHEV, V. B., DAHLGAARD, H. & HOLM, E. 1994. SURVEY OF ARTIFICIAL RADIONUCLIDES IN THE BARENTS SEA AND THE KARA SEA. *Journal of Environmental Radioactivity,* 25**,** 99-112.

SVÆREN, I. 2010a. Caesium-137 in sediments from two Norwegian fjords - including dating sediment cores. *Master of Science Thesis in Environmental Chemistry*.

SVÆREN, I. 2010b. Metode R1: Bestemmelse av radioaktivitet cesium i sedimenter og biota, målt med gamma-spektroskopi på HPGe-detektor. *Inter metode, Havforskningsinstituttet.*

TADJIKI, S. & ERTEN, H. N. 1994. Radiochronology of sediemts from the mediterranen sea using natural 210Pb and fallout 137Cs. *Journal of radioanalytical and nuclear chemistry,* Volume.181, No. 2: 447-459.

UCL. *SediGraph particle size analysis.[internet]* [Online]. UCL DEPARTMENT OF GEOGRAPHY. Physical Geography Laboratory http://www.geog.ucl.ac.uk/about-the-department/support-services/laboratory/files/sedigraph_sop.pdf/at_download/file

[Read. 13.05.2014].

UNSCEAR 1982. Ionizing Radiation: Sources and Biological Effects (New York: United Nations). *United Nations Scientific Committee on the Effects of Atomic Radiation, UNSCEAR.*

UNSCEAR 1993. sources and effects of ionizing radiation. *United Nations Scientific Committee on the Effects of Atomic Radiation, UNSCEAR 1993 Report to the General Assembly, with Scientific Annexes, United Nations, New York.*

VARGA, Z. 2007. Origin and release date assessment of environmental plutonium by isotopic composition. *Analytical and Bioanalytical Chemistry,* 389**,** 725-732.

VINTRO, L., SMITH, K. J., LUCEY, J. A. & MITCHELL, P. I. 2000. The environmental impact of the sellafield discharges. *SCOPE-RADSITE Workshop proceedings, Brussels.*

YABLAKOV, A. V., KARASEV, V. K., RUMYANSTSEV, V. M., KOKEEV, M. E., PETROV, O. J., LYSTSOV, V. N., EMEL'YANENKOV, A. F. & RUBSTOV, P. M. 1993. Facts and Problems related to Radioactive Waste Disposal in Seas Adjacent to the Territory of the Russian Fedration, Small World Publishers, Inc., Moscow, Russia.

ZABORSKA, A., MIETELSKI, J. W., CARROLL, J., PAPUCCI, C. & PEMPKOWIAK, J. 2010. Sources and distributions of 137Cs, 238Pu, 239,240Pu radionuclides in the north-western Barents Sea.

Appendices

Appendix A: Sample weights and porosities

Table A1. Sample weights (g) and porosities (%) in the sediment layers of core 122-1

Sampling date			*06.09.12*			
Sample-id			*122-1*			
Layer (cm)	**Empty cups (g)**	**Gross wet weight (g)**	**Gross dry weight (g)**	**Net wet weight (g)**	**Net dry weight (g)**	**Porosity (%)**
0-1	2.5	146.6	66.1	144.1	63.6	55.9
1-2	2.5	120.6	58.1	118.1	55.6	53.0
2-3	2.5	121.9	61.0	119.4	58.5	51.0
3-4	2.6	133.8	68.6	131.2	66.0	49.7
4-5	2.6	134.4	71.1	131.8	68.5	48.0
5-6	2.5	141.0	76.0	138.5	73.5	46.9
6-7	2.5	137.0	76.8	134.5	74.3	44.8
7-8	2.5	135.5	77.6	133.0	75.1	43.5
8-9	2.5	156.6	92.6	154.1	90.1	41.5
9-10	2.5	145.8	91.7	143.3	89.2	37.8
10-11	2.5	179.8	115.7	177.3	113.2	36.2
11-12	8.3	334.3	206.3	326.0	198.0	39.3

Table A2. Sample weights (g) and porosities (%) in the sediment layers of core 122-2

Sampling date			*06.09.12*			
Sample-id			*122-2*			
Layer (cm)	**Empty cups (g)**	**Gross wet weight (g)**	**Gross dry weight (g)**	**Net wet weight (g)**	**Net dry weight (g)**	**Porosity (%)**
0-1	2.6	201.5	91.8	198.9	89.2	55.2
1-2	2.6	125.5	60.1	123.0	57.6	53.2
2-3	2.6	125.8	63.0	123.2	60.4	51.0
3-4	2.6	116.9	60.0	114.4	57.4	49.8
4-5	2.6	142.2	74.7	139.6	72.2	48.3
5-6	2.6	124.3	67.1	121.7	64.5	47.0
6-7	2.6	133.4	72.4	130.8	69.9	46.6
7-8	2.6	134.1	75.7	131.5	73.1	44.4
8-9	2.6	146.2	86.0	143.7	83.5	41.9
9-10	2.6	156.0	96.1	153.5	93.6	39.0
10-11	2.6	156.8	98.1	154.2	95.6	38.0
11-12	2.5	166.7	102.7	164.2	100.2	39.0
12-13	2.5	41.5	24.5	39.0	22.0	43.7

Table A3. Sample weights (g) and porosities (%) in the sediment layers of core 123-1

Sampling date			*06.09.12*			
Sample-id			*123-1*			
Layer (cm)	**Empty cups (g)**	**Gross wet weight (g)**	**Gross dry weight (g)**	**Net wet weight (g)**	**Net dry weight (g)**	**Porosity (%)**
0-1	2.5	187.4	91.1	184.9	88.6	52.1
1-2	2.6	155.8	81.3	153.2	78.7	48.7
2-3	8.3	548.1	303.0	539.8	294.7	45.4

Table A4. Sample weights (g) and porosities (%) in the sediment layers of core 123-2

Sampling date			*06.09.12*			
Sample-id			*123-2*			
Layer	**Empty cups (g)**	**Gross wet weight (g)**	**Gross dry weight (g)**	**Net wet weight (g)**	**Net dry weight (g)**	**Porosity (%)**
0-1	2.5	166.6	77.0	164.1	74.5	54.6
1-2	2.5	136.2	67.3	133.6	64.8	51.5
2-3	2.5	134.4	69.8	131.9	67.3	49.0
3-4	2.5	152.3	82.4	149.8	79.9	46.7
4-5	2.5	174.2	97.6	171.7	95.1	44.6
5-6	2.5	153.7	91.9	151.2	89.4	40.9
6-7	2.5	130.4	77.6	127.9	75.1	41.3

Table A5. Sample weights (g) and porosities (%) in the sediment layers of core 124-1

Sampling date			*06.09.12*			
Sample-id			*124-1*			
Layer (cm)	**Empty cups (g)**	**Gross wet weight (g)**	**Gross dry weight (g)**	**Net wet weight (g)**	**Net dry weight (g)**	**Porosity (%)**
0-1	2.5	159.9	72.5	157.4	70.0	55.5
1-2	2.5	135.2	62.7	132.7	60.2	54.6
2-3	2.5	162.3	81.9	159.8	79.4	50.3
3-4	2.5	149.5	78.4	147.0	75.9	48.4
4-5	8.3	592.4	315.3	584.1	307.0	47.4

Table A6. Sample weights (g) and porosities (%) in the sediment layers of core 124-2

Sampling date			*06.09.12*			
Sample-id			*124-2*			
Layer (cm)	**Empty cups (g)**	**Gross wet weight (g)**	**Gross dry weight (g)**	**Net wet weight (g)**	**Net dry weight (g)**	**Porosity (%)**
0-1	2.5	141.2	62.6	138.7	60.1	56.7
1-2	2.5	151.6	71.4	149.1	68.8	53.8
2-3	2.5	153.7	76.9	151.2	74.3	50.8
3-4	2.5	145.4	75.4	142.8	72.9	49.0
4-5	2.5	154.7	81.7	152.2	79.2	48.0
5-6	2.5	186.2	101.7	183.7	99.2	46.0
6-7	2.5	65.4	34.3	62.9	31.8	49.5

Table A7. Sample weights (g) and porosities (%) in the sediment layers of core 124-3

Sampling date			*06.09.12*			
Sample-id			*124-3*			
Layer (cm)	**Empty cups (g)**	**Gross wet weight (g)**	**Gross dry weight (g)**	**Net wet weight (g)**	**Net dry weight (g)**	**Porosity (%)**
0-1	2.5	185.0	88.9	182.5	86.4	52.7
1-2	2.5	151.8	74.8	149.3	72.3	51.5
2-3	2.5	155.1	78.7	152.6	76.2	50.1
3-4	2.5	137.7	71.5	135.2	69.0	48.9
4-5	2.5	142.4	76.8	139.9	74.3	46.9
5-6	2.5	186.0	105.8	183.4	103.3	43.7
6-7	2.5	117.0	59.2	114.5	56.7	50.5

Table A8. Sample weights (g) and porosities (%) in the sediment layers of core 124-4

Sampling date			*06.09.12*			
Sample-id			*124-4*			
Layer (cm)	**Empty cups (g)**	**Gross wet weight (g)**	**Gross dry weight (g)**	**Net wet weight (g)**	**Net dry weight (g)**	**Porosity (%)**
0-1	2.5	196.9	94.4	194.4	91.8	52.8
1-2	2.5	143.1	70.0	140.5	67.5	52.0
2-3	2.5	175.1	91.4	172.6	88.8	48.5
3-4	2.5	173.8	93.0	171.2	90.4	47.2
4-5	2.5	177.4	98.2	174.9	95.7	45.3
5-6	2.5	202.5	113.3	200.0	110.8	44.6

Table A9. Sample weights (g) and porosities (%) in the sediment layers of core 125-1

Sampling date			*06.09.12*			
Sample-id			*125-1*			
Layer (cm)	**Empty cups (g)**	**Gross wet weight (g)**	**Gross dry weight (g)**	**Net wet weight (g)**	**Net dry weight (g)**	**Porosity (%)**
0-1	2.5	167.4	75.7	164.8	73.1	55.6
1-2	2.5	157.5	79.4	155.0	76.9	50.4
2-3	2.5	138.6	70.1	136.1	67.6	50.3
3-4	2.5	172.5	89.3	170.0	86.8	48.9
4-5	2.5	154.9	82.4	152.4	79.8	47.6
5-6	2.5	149.4	81.7	146.8	79.2	46.1
6-7	2.5	209.8	111.6	207.3	109.1	47.4

Table A10. Sample weights (g) and porosities (%) in the sediment layers of core 125-2

Sampling date			*06.09.12*			
Sample-id			*125-2*			
Layer (cm)	**Empty cups (g)**	**Gross wet weight (g)**	**Gross dry weight (g)**	**Net wet weight (g)**	**Net dry weight (g)**	**Porosity (%)**
0-1	2.5	154.1	71.1	151.6	68.6	54.8
1-2	2.5	157.6	77.4	155.1	74.9	51.7
2-3	2.5	151.7	77.3	149.2	74.8	49.8
3-4	2.5	162.4	85.2	159.9	82.7	48.3
4-5	2.5	153.5	82.5	151.0	80.0	47.0
5-6	2.5	164.8	90.7	162.3	88.2	45.7
6-7	2.5	192.3	108.0	189.8	105.5	44.4
7-8	2.5	105.2	56.8	102.7	54.3	47.2

Table A11. Sample weights (g) and porosities (%) in the sediment layers of core 194-1

Sampling date			*07.04.13*			
Sample-id			*194-1*			
Layer (cm)	**Empty cups (g)**	**Gross wet weight (g)**	**Gross dry weight (g)**	**Net wet weight (g)**	**Net dry weight (g)**	**Porosity (%)**
0-1	2.5	155.0	84.2	152.5	81.7	46.4
1-2	2.5	109.1	57.0	106.6	54.5	48.9
2-3	2.5	126.8	65.9	124.3	63.4	49.0
3-4	2.5	121.5	65.5	119.0	63.0	47.1
4-5	2.5	134.2	75.2	131.7	72.7	44.8
5-6	2.5	121.5	67.6	119.0	65.1	45.3
6-7	2.5	121.6	65.4	119.1	62.9	47.2
7-8	2.5	116.4	63.2	113.9	60.7	46.7
8-9	2.5	118.0	62.1	115.5	59.6	48.4
9-10	2.5	137.5	74.7	135.0	72.2	46.5
10-11	2.5	123.3	70.3	120.8	67.8	43.9
11-12	2.5	136.2	77.0	133.7	74.5	44.3
12-13	2.5	133.5	74.2	131.0	71.7	45.3
13-14	2.5	113.2	63.5	110.7	61.0	44.9
14-15	2.5	155.5	87.6	153.0	85.1	44.4
15-16	2.5	140.2	79.7	137.7	77.2	43.9

Table A12. Sample weights (g) and porosities (%) in the sediment layers of core 194-2

Sampling date			*07.04.13*			
Sample-id			*194-2*			
Layer (cm)	**Empty cups (g)**	**Gross wet weight (g)**	**Gross dry weight (g)**	**Net wet weight (g)**	**Net dry weight (g)**	**Porosity (%)**
0-1	2.5	107.5	53.1	105.0	50.6	51.8
1-2	2.5	153.4	78.3	150.9	75.8	49.8
2-3	2.6	127.8	66.4	125.2	63.8	49.0
3-4	2.5	142.1	74.7	139.6	72.2	48.3
4-5	2.5	139.9	72.5	137.4	70.0	49.1
5-6	2.5	148.1	76.2	145.6	73.7	49.4
6-7	2.6	123.5	65.7	120.9	63.1	47.8
7-8	2.5	127.8	67.2	125.3	64.7	48.4
8-9	2.5	133.9	69.2	131.4	66.7	49.2
9-10	2.5	132.1	68.1	129.6	65.6	49.4
10-11	2.6	140.0	72.4	137.4	69.8	49.2
11-12	2.6	149.4	77.1	146.8	74.5	49.2
12-13	2.5	162.2	86.0	159.7	83.5	47.7
13-14	2.5	145.5	82.4	143.0	79.9	44.1
14-15	2.6	167.3	97.6	164.7	95.0	42.3
15-16	2.5	188.6	110.4	186.1	107.9	42.0
16-17	2.5	177.3	105.1	174.8	102.6	41.3

Table A13. Sample weights (g) and porosities (%) in the sediment layers of core 194-3

Sampling date			*07.04.13*			
Sample-id			*194-3*			
Layer (cm)	**Empty cups (g)**	**Gross wet weight (g)**	**Gross dry weight (g)**	**Net wet weight (g)**	**Net dry weight (g)**	**Porosity (%)**
0-1	2.5	146.5	70.5	144.0	68.0	52.8
1-2	2.5	133.3	66.1	130.8	63.6	51.4
2-3	2.5	162.5	81.5	160.0	79.0	50.6
3-4	2.5	140.5	70.6	138.0	68.1	50.7
4-5	2.5	143.7	71.2	141.2	68.7	51.3
5-6	2.5	160.3	79.6	157.8	77.1	51.1
6-7	2.5	172.2	88.1	169.7	85.6	49.6
7-8	2.5	159.4	86.0	156.9	83.5	46.8
8-9	2.5	153.9	84.3	151.4	81.8	45.9
9-10	2.5	187.5	105.6	185.0	103.1	44.3
10-11	2.5	181.8	104.1	179.3	101.6	43.3
11-12	2.5	167.4	96.3	164.9	93.8	43.1
12-13	2.5	192.5	111.5	190.0	109.0	42.6
13-14	2.5	217.2	126.3	214.7	123.8	42.3
14-15	2.5	157.4	91.1	154.9	88.6	42.8
15-16	2.5	109.1	63.0	106.6	60.5	43.3
16-17	2.5	98.0	55.9	95.5	53.4	44.1

Table A14. Sample weights (g) and porosities (%) in the sediment layers of core 194-4

Sampling date			*07.04.13*			
Sample-id			*194-4*			
Layer (cm)	**Empty cups (g)**	**Gross wet weight (g)**	**Gross dry weight (g)**	**Net wet weight (g)**	**Net dry weight (g)**	**Porosity (%)**
0-1	2.5	175.6	96.0	173.1	93.5	46.0
1-2	2.5	165.3	85.2	162.8	82.7	49.2
2-3	2.5	146.8	76.0	144.3	73.5	49.1
3-4	2.5	173.4	93.1	170.9	90.6	47.0
4-5	2.5	167.8	90.8	165.3	88.3	46.6
5-6	2.5	165.7	88.0	163.2	85.5	47.6
6-7	2.5	142.2	75.3	139.7	72.8	47.9
7-8	2.5	160.5	87.2	158.0	84.7	46.4
8-9	2.5	167.0	95.9	164.5	93.4	43.2
9-10	2.5	173.8	101.8	171.3	99.3	42.0
10-11	2.5	184.5	114.2	182.0	111.7	38.6
11-12	2.5	188.8	120.2	186.3	117.7	36.8
12-13	2.5	191.8	121.1	189.3	118.6	37.4
13-14	2.5	214.7	135.0	212.2	132.5	37.6
14-15	2.5	201.1	123.8	198.6	121.3	38.9

Table A15. Sample weights (g) and porosities (%) in the sediment layers of core 195-1

Sampling date			*07.04.13*			
Sample-id			*195-1*			
Layer (cm)	**Empty cups (g)**	**Gross wet weight (g)**	**Gross dry weight (g)**	**Net wet weight (g)**	**Net dry weight (g)**	**Porosity (%)**
0-1	26.0	84.9	44.8	58.9	18.8	68.1
1-2	26.0	97.7	45.8	71.7	19.8	72.4
2-3	26.0	101.0	46.1	75.0	20.1	73.2
3-4	26.0	118.2	54.0	92.2	28.0	69.6
4-5	26.0	123.2	56.9	97.2	30.9	68.2
5-6	26.0	115.4	54.2	89.4	28.2	68.4
6-7	26.0	129.5	62.3	103.5	36.3	64.9
7-8	26.0	131.7	65.8	105.7	39.8	62.3
8-9	26.0	107.8	54.9	81.8	28.9	64.7
9-10	26.0	124.4	62.4	98.4	36.4	63.0
10-11	26.0	96.7	49.8	70.7	23.8	66.3
11-12	26.0	122.6	62.4	96.6	36.4	62.3
12-13	26.0	137.1	72.0	111.1	46.0	58.6
13-14	26.0	139.2	75.4	113.2	49.4	56.4
14-15	26.0	120.7	63.2	94.7	37.2	60.7
15-16	26.0	120.5	65.3	94.5	39.3	58.4
16-17	26.0	138.2	76.6	112.2	50.6	54.9
17-18	26.0	128.8	72.9	102.8	46.9	54.4
18-19	26.0	190.3	108.7	164.3	82.7	49.7

Table A16. Sample weights (g) and porosities (%) in the sediment layers of core 195-2

Sampling date			*07.04.13*			
Sample-id			*195-2*			
Layer (cm)	**Empty cups (g)**	**Gross wet weight (g)**	**Gross dry weight (g)**	**Net wet weight (g)**	**Net dry weight (g)**	**Porosity (%)**
0-1	2.5	70.5	36.6	68.0	34.1	49.8
1-2	2.5	153.3	78.3	150.8	75.8	49.8
2-3	2.5	114.9	58.2	112.4	55.7	50.4
3-4	2.5	117.6	55.2	115.1	52.7	54.2
4-5	2.5	108.8	48.6	106.3	46.1	56.6
5-6	2.5	111.3	49.3	108.8	46.8	57.0
6-7	2.5	104.8	48.3	102.3	45.8	55.2
7-8	2.5	110.1	51.2	107.6	48.7	54.7
8-9	2.5	118.0	57.5	115.5	55.0	52.4
9-10	2.5	116.1	58.8	113.6	56.3	50.4
10-11	2.5	123.5	63.7	121.0	61.2	49.4
11-12	2.5	123.1	62.7	120.6	60.2	50.1
12-13	2.5	138.9	70.3	136.4	67.8	50.3
13-14	2.5	137.9	74.1	135.4	71.6	47.1
14-15	2.5	109.4	61.5	106.9	59.0	44.8

Table A17. Sample weights (g) and porosities (%) in the sediment layers of core 196-1

Sampling date			*07.04.13*			
Sample-id			*196-1*			
Layer (cm)	**Empty cups (g)**	**Gross wet weight (g)**	**Gross dry weight (g)**	**Net wet weight (g)**	**Net dry weight (g)**	**Porosity (%)**
0-1	2.5	134.2	59.8	131.7	57.3	56.5
1-2	2.5	130.4	59.2	127.9	56.7	55.7
2-3	2.5	137.8	64.0	135.3	61.5	54.6
3-4	2.5	142.0	66.1	139.5	63.6	54.4
4-5	2.5	137.0	64.3	134.5	61.8	54.0
5-6	2.5	143.2	71.8	140.7	69.3	50.8
6-7	2.5	149.6	75.2	147.1	72.7	50.6
7-8	2.5	166.2	84.3	163.7	81.8	50.0
8-9	2.5	146.4	75.7	143.9	73.2	49.1
9-10	2.5	144.8	76.0	142.3	73.5	48.4

Table A18. Sample weights (g) and porosities (%) in the sediment layers of core 196-2

Sampling date			*07.04.13*			
Sample-id			*196-2*			
Layer (cm)	**Empty cups (g)**	**Gross wet weight (g)**	**Gross dry weight (g)**	**Net wet weight (g)**	**Net dry weight (g)**	**Porosity (%)**
0-1	2.5	150.2	62.3	147.7	59.8	59.5
1-2	2.5	136.5	60.5	134.0	58.0	56.7
2-3	2.5	136.4	60.8	133.9	58.3	56.5
3-4	2.5	142.1	64.7	139.6	62.2	55.5
4-5	2.5	155.7	73.0	153.2	70.5	54.0
5-6	2.5	154.1	72.7	151.6	70.2	53.7
6-7	2.5	137.1	66.9	134.6	64.4	52.2
7-8	2.5	167.3	85.5	164.8	83.0	49.6
8-9	2.5	176.7	90.9	174.2	88.4	49.3
9-10	2.5	158.9	83.6	156.4	81.1	48.1

Table A19. Sample weights (g) and porosities (%) in the sediment layers of core 197-1

Sampling date			*07.04.13*			
Sample-id			*197-1*			
Layer (cm)	**Empty cups (g)**	**Gross wet weight (g)**	**Gross dry weight (g)**	**Net wet weight (g)**	**Net dry weight (g)**	**Porosity (%)**
0-1	2.5	166.1	75.9	163.6	73.4	55.1
1-2	2.5	159.5	74.2	157.0	71.7	54.3
2-3	2.5	149.6	73.0	147.1	70.5	52.1
3-4	2.5	151.1	76.0	148.6	73.5	50.5
4-5	2.5	156.7	79.8	154.2	77.3	49.9
5-6	2.5	145.8	74.9	143.3	72.4	49.5
6-7	2.5	160.3	83.3	157.8	80.8	48.8
7-8	2.5	177.7	92.5	175.2	90.0	48.6
8-9	2.5	172.0	88.7	169.5	86.2	49.1
9-10	2.5	181.1	92.8	178.6	90.3	49.4
10-11	2.5	184.4	98.6	181.9	96.1	47.2

Table A20. Sample weights (g) and porosities (%) in the sediment layers of core 197-2

Sampling date			*07.04.13*			
Sample-id			*197-2*			
Layer (cm)	**Empty cups (g)**	**Gross wet weight (g)**	**Gross dry weight (g)**	**Net wet weight (g)**	**Net dry weight (g)**	**Porosity (%)**
0-1	3.9	150.0	64.4	146.1	60.5	58.6
1-2	3.8	162.8	74.5	159.0	70.7	55.5
2-3	3.9	145.6	67.9	141.7	64.0	54.8
3-4	3.9	180.3	86.8	176.4	82.9	53.0
4-5	2.4	162.1	79.8	159.7	77.4	51.6
5-6	2.4	176.7	89.5	174.3	87.1	50.0
6-7	2.4	178.1	87.7	175.7	85.3	51.4
7-8	2.4	160.0	77.8	157.6	75.4	52.1
8-9	2.4	186.5	94.8	184.1	92.4	49.8
9-10	2.4	157.5	83.4	155.1	81.0	47.8
10-11	2.5	152.7	86.5	150.2	84.0	44.1
11-12	2.4	83.8	48.9	81.4	46.5	42.9

Table A21. Sample weights (g) and porosities (%) in the sediment layers of core 199-1 (reference station)

Sampling date			*08.04.13*			
Sample-id			*199-1*			
Layer (cm)	**Empty cups (g)**	**Gross wet weight (g)**	**Gross dry weight (g)**	**Net wet weight (g)**	**Net dry weight (g)**	**Porosity (%)**
0-1	2.4	138.0	56.2	135.6	53.8	60.3
1-2	2.4	145.3	62.9	142.9	60.5	57.7
2-3	2.4	153.7	71.2	151.3	68.8	54.5
3-4	2.4	162.6	76.7	160.2	74.3	53.6
4-5	2.4	155.1	77.2	152.7	74.8	51.0
5-6	2.4	153.9	79.2	151.5	76.8	49.3
6-7	2.4	154.7	79.8	152.3	77.4	49.2
7-8	2.5	183.6	94.6	181.1	92.1	49.1
8-9	2.4	110.0	60.2	107.6	57.8	46.3

Table A22. Sample weights (g) and porosities (%) in the sediment layers of core 199-2 (reference station)

Sampling date			*08.04.13*			
Sample-id			*199-2*			
Layer (cm)	**Empty cups (g)**	**Gross wet weight (g)**	**Gross dry weight (g)**	**Net wet weight (g)**	**Net dry weight (g)**	**Porosity (%)**
0-1	2.5	166.1	72.5	163.6	70.0	57.2
1-2	2.5	185.9	88.5	183.4	86.0	53.1
2-3	2.5	155.9	74.6	153.4	72.1	53.0
3-4	2.5	150.8	73.3	148.3	70.8	52.3
4-5	2.5	158.6	79.8	156.1	77.3	50.5
5-6	2.5	188.1	97.9	185.6	95.4	48.6
6-7	2.5	186.1	97.1	183.6	94.6	48.5
7-8	2.5	207.2	111.7	204.7	109.2	46.7

Appendix B: Data from control, background and calibration measurements

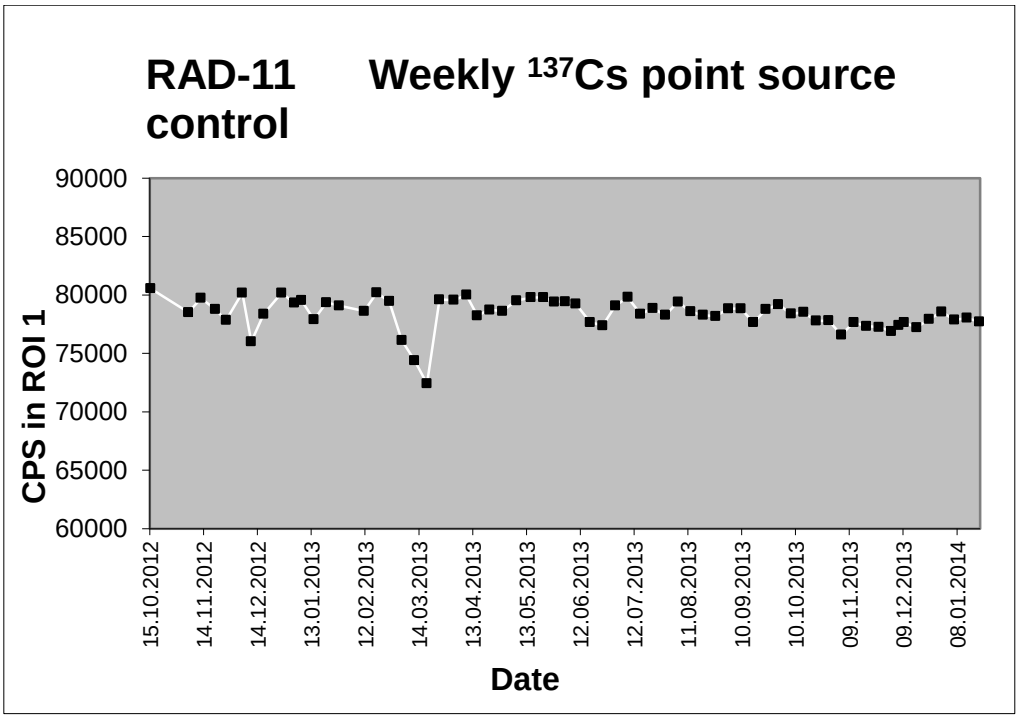

Figure B1: Weekly measurements of caesium-137 (^{137}Cs) in the point source at detector RAD-11.

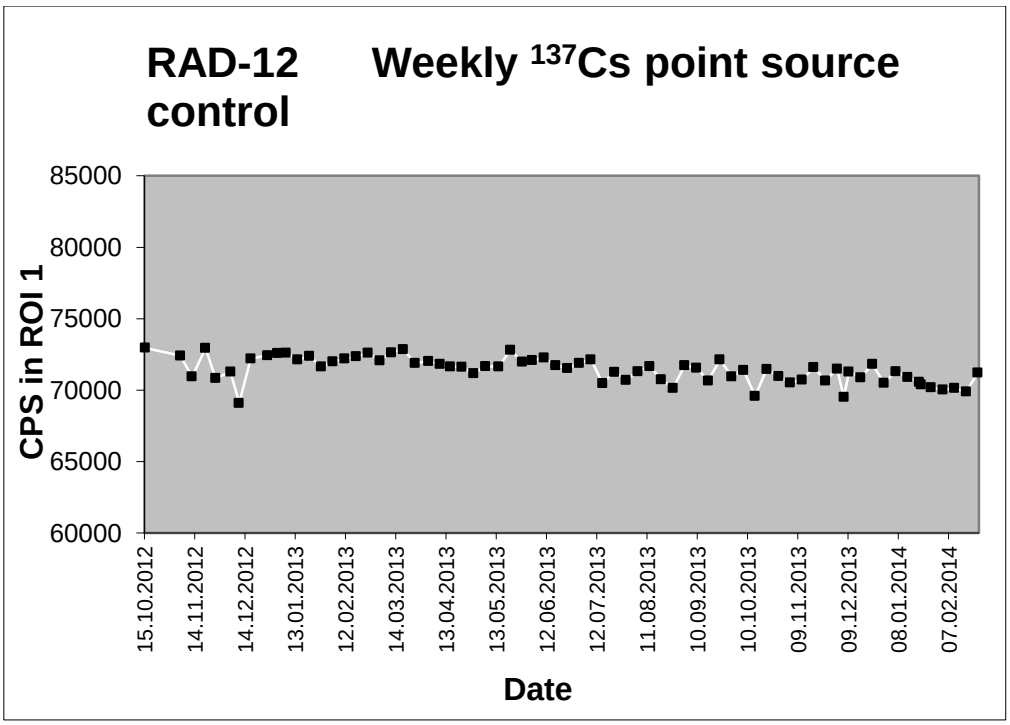

Figure B2: Weekly measurements of caesium-137 (^{137}Cs) in the point source at detector RAD-12

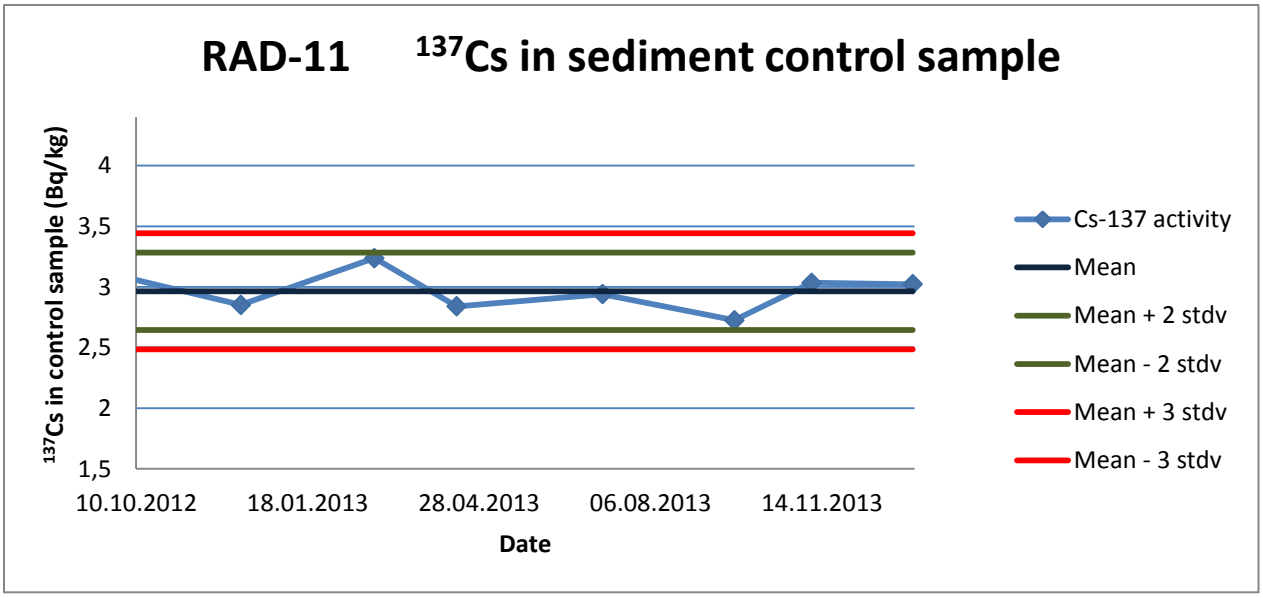

Figure B3: Caesium-137 (^{137}Cs) (Bq/kg d.w.) in a sediment control sample measured at detector RAD-11

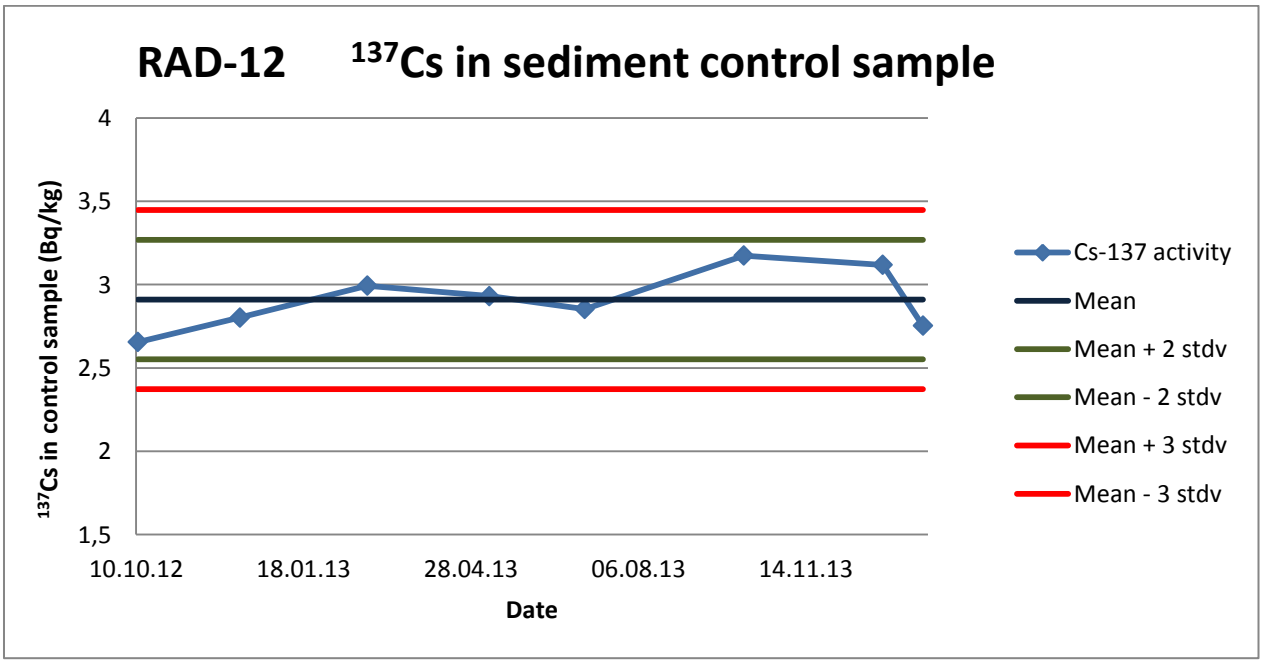

Figure B4: Caesium-137 (^{137}Cs) (Bq/kg d.w.) in a sediment control sample measured at detector RAD-12

Table B1. External Background from caesium-137 (^{137}Cs) in detector RAD-11

Measuring date	Gross area in ROI 1	Gross area in ROI 2	Gross area in ROI 3	Counting time (sec)	Internal background (cps)	External background (cps)
08.10.12	3680	883	961	859737	0.004290	-0.000009
06.12.12	361	72	91	74981	0.004348	0.000467
22.02.13	403	96	98	98788	0.003928	0.000152
14.03.13	295	83	56	73069	0.003805	0.000233
12.04.13	359	97	116	89700	0.004749	-0.000747
08.07.13	951	233	252	251531	0.003856	-0.000076
23.09.13	989	263	264	241641	0.004362	-0.000269
11.11.13	1003	281	260	248595	0.004352	-0.000318
03.01.14	1434	369	379	349794	0.004277	-0.000177
22.01.14	339	71	81	84729	0.003588	0.000413

Table B2. External Background from caesium-137 (^{137}Cs) in detector RAD-12

Measuring date	Gross area in ROI 1	Gross area in ROI 2	Gross area in ROI 3	Counting time (sec)	Internal background (cps)	External background (cps)
08.10.12	3415	837	804	859896	0.00391	0.00006
06.12.12	293	77	89	75121	0.00453	-0.00063
22.02.13	394	104	95	99021	0.00412	-0.00014
08.05.13	238	77	62	65965	0.00432	-0.00071
08.07.13	947	246	227	250936	0.00386	-0.00009
07.10.13	1087	307	274	266197	0.00447	-0.00039
27.12.13	1580	373	368	361785	0.00420	0.00017
22.01.14	342	97	85	85006	0.00439	-0.00037
24.03.14	1021	262	277	251613	0.00439	-0.00033

Table B3. Calibration. Caesium-137 (^{137}Cs) geometry factor measured every second month at detector RAD-11.

Standard no.	Calibration date	Reference date	Activity in the standard (Bq)	Uncertainty in the standard activity (Bq)	Gross area in ROI 1 (counts)	Gross area in ROI 2 (counts)	Gross area in ROI 3 (counts)	Counting time (sec)	Internal background (cps)	G (Bq/cps)	sG (Bq/cps)
26	11.10.12	01.10.02	60.9	0.9	144671	711	496	74897	0.032	32.1	0.5
26	27.02.13	01.10.02	60.4	0.9	170353	902	524	89031	0.032	32.1	0.5
36	14.06.13	01.01.10	2330.8	23.3	6014291	39008	27097	83354	1.586	33.0	0.3
36	30.08.13	01.01.10	2319.5	23.2	1056685	6777	4473	14764	1.523	33.1	0.3
36	09.01.14	01.01.10	2300.3	23.0	6246281	39116	25321	88027	1.464	33.1	0.3

Table B4. Calibration. Caesium-137 (^{137}Cs) geometry factor measured every second month at detector RAD-12.

Standard no.	Calibration date	Reference date	Activity in the standard (Bq)	Uncertainty in the standard activity (Bq)	Gross area in ROI 1 (counts)	Gross area in ROI 2 (counts)	Gross area in ROI 3 (counts)	Counting time (sec)	Internal background (cps)	G (Bq/cps)	sG (Bq/cps)
26	10.10.12	01.10.02	60.9	0.9	127415	576	426	77715	0.026	37.8	0.6
36	15.11.12	01.01.10	2361.9	23.6	9303277	54759	48277	149309	1.380	38.8	0.4
36	07.12.12	01.01.10	2358.6	34.9	4891925	29062	25266	78650	1.382	38.8	0.6
26	28.02.13	01.10.02	60.4	0.9	133730	624	421	81952	0.026	37.6	0.6
36	17.04.13	01.01.10	2339.3	23.4	1066673	6064	5178	17292	1.300	38.8	0.4
36	04.07.13	01.01.10	2327.8	23.3	4874287	27062	23040	79501	1.260	38.8	0.4
36	10.10.13	01.01.10	2313.5	23.1	5530670	30094	25445	90863	1.222	38.8	0.4
36	06.01.14	01.01.10	2300.8	23.0	14004694	75112	62898	231480	1.192	38.8	0.4
36	24.01.14	01.01.10	2298.2	23.0	5660468	30064	25213	93732	1.179	38.8	0.4
36	27.03.14	01.01.10	2289.2	22.9	4281688	22290	18635	71193	1.150	38.8	0.4

Appendix C: Data and results from caesium-137 (^{137}Cs) measurements

Table C1. Data and result from caesium-137 (^{137}Cs) measurements in 1 cm slices from sediment core 122-1

Sample-id/ layer (cm)	Sampling date	Measuring date	Sample mass (g)	Counting time (sec)	Channels in top	Gross area ROI 1 (counts)	Gross area ROI 2 (counts)	Gross area ROI 3 (counts)	Decay corrected activity[a] (Bq/kg d.w.)	Uncertainty (Bq/kg d.w.)
122-1										
0-1	06.09.12	01.11.12	39.20	1000000	41	14193	1404	1752	7.4	0.4
1-2	06.09.12	15.02.13	36.90	93925	40	938	147	184	2.6	0.9
2-3	06.09.12	18.02.13	34.20	234344	40	1779	331	408	1.2	0.6
3-4	06.09.12	19.02.13	49.60	84091	40	720	134	188	0.6	0.7
4-5	06.09.12	20.02.13	48.90	89010	40	652	132	211	*0.6*	-
5-6	06.09.12	21.02.13	49.00	91157	40	656	176	188	*0.6*	-
6-7	06.09.12	28.02.13	55.00	89698	40	637	141	190	*0.5*	-
7-8	06.09.12	01.03.13	55.60	81099	40	614	158	188	*0.5*	-
8-9	06.09.12	04.03.13	55.40	254208	40	1869	494	583	*0.3*	-
9-10	06.09.12	05.03.13	62.30	76332	40	592	167	200	*0.5*	-
10-11	06.09.12	06.03.13	63.40	79945	40	674	148	203	*0.5*	-
11-12	06.09.12	07.03.13	49.10	104878	40	701	182	228	*0.5*	-

[a]*Values in italic; measurements below the quantification limit (0.5*Lq)*

Table C2. Data and result from caesium-137 (^{137}Cs) measurements in 1 cm slices from sediment core 122-2

Sample-id/ layer (cm)	Sampling date	Measuring date	Sample mass (g)	Counting time (sec)	Channels in top	Gross area ROI 1 (counts)	Gross area ROI 2 (counts)	Gross area ROI 3 (counts)	Decay corrected activity[a] (Bq/kg d.w.)	Uncertainty (Bq/kg d.w.)
122-2										
0-1	06.09.12	14.12.12	48.80	80558	41	955	125	144	4.0	0.9
1-2	06.09.12	17.12.12	48.00	259231	41	2395	390	446	2.1	0.5
2-3	06.09.12	18.12.12	46.40	77430	41	557	121	153	*0.8*	-
3-4	06.09.12	19.12.12	50.40	98676	41	737	139	182	0.6	0.7
4-5	06.09.12	20.12.12	51.70	95545	41	659	126	174	*0.6*	-
5-6	06.09.12	21.12.12	54.00	87074	41	561	139	180	*0.6*	-
6-7	06.09.12	27.12.12	48.10	493538	41	3401	814	1001	*0.3*	-
7-8	06.09.12	06.02.13	55.50	77641	41	603	135	167	*0.7*	-
8-9	06.09.12	08.02.13	61.90	81046	41	579	133	156	*0.6*	-
9-10	06.09.12	28.12.12	61.80	88222	41	655	161	192	*0.6*	-
10-11	06.09.12	02.01.13	62.30	435098	41	3306	847	940	*0.2*	-
11-12	06.09.12	11.02.13	65.70	255173	41	1929	539	577	*0.3*	-
12-13	06.09.12	07.01.13	22.20	262135	41	1420	364	376	*0.7*	-

[a]*Values in italic; measurements below the quantification limit (0.5*Lq)*

Table C3. Data and result from caesium-137 (^{137}Cs) measurements in 1 cm slices from sediment cores 123-1 and 123-2

Sample-id/ layer (cm)	Sampling date	Measuring date	Sample mass (g)	Counting time (sec)	Channels in top	Gross area ROI 1 (counts)	Gross area ROI 2 (counts)	Gross area ROI 3 (counts)	Decay corrected activity[a] (Bq/kg d.w.)	Uncertainty (Bq/kg d.w.)
123-1										
0-1	06.09.12	30.01.13	48.90	102972	40	908	180	221	0.7	0.6
1-2	06.09.12	08.03.13	47.10	93816	40	757	146	192	0.6	0.7
2-3	06.09.12	11.03.13	50.20	239944	40	1826	389	496	*0.3*	-
123-2										
0-1	06.09.12	13.02.13	50.20	91808	41	829	143	155	1.8	0.8
1-2	06.09.12	14.02.13	49.10	86222	41	696	119	181	0.7	0.8
2-3	06.09.12	15.02.13	50.00	93244	41	677	154	176	*0.6*	-
3-4	06.09.12	18.02.13	47.60	233461	41	1553	391	440	*0.4*	-
4-5	06.09.12	19.02.13	55.90	83181	41	641	137	164	*0.6*	-
5-6	06.09.12	20.02.13	58.70	94182	41	674	154	184	*0.5*	-
6-7	06.09.12	21.02.13	66.40	82658	41	616	147	175	*0.5*	-

[a]*Values in italic; measurements below the quantification limit (0.5*Lq)*

Table V4. Data and result from caesium-137 (^{137}Cs) measurements in 1 cm slices from sediment cores 124-1 and 124-2

Sample-id/ layer (cm)	Sampling date	Measuring date	Sample mass (g)	Counting time (sec)	Channels in top	Gross area ROI 1 (counts)	Gross area ROI 2 (counts)	Gross area ROI 3 (counts)	Decay corrected activity[a] (Bq/kg d.w.)	Uncertainty (Bq/kg d.w.)
124-1										
0-1	06.09.12	31.01.13	49.30	74554	40	864	124	143	2.9	0.8
1-2	06.09.12	12.03.13	47.60	86972	40	848	121	155	2.3	0.7
2-3	06.09.12	13.03.13	44.80	92550	40	661	148	190	*0.6*	-
3-4	06.09.12	17.06.13	51.60	220382	40	1549	374	530	*0.3*	-
4-5	06.09.12	18.06.13	48.50	96663	40	710	201	200	*0.6*	-
124-2										
0-1	06.09.12	07.02.13	47.10	63850	40	804	108	131	3.5	0.9
1-2	06.09.12	19.06.13	49.00	78072	40	836	127	158	2.3	0.8
2-3	06.09.12	20.06.13	50.40	95535	40	830	160	212	0.6	0.7
3-4	06.09.12	21.06.13	49.90	81965	40	639	129	180	*0.6*	-
4-5	06.09.12	23.06.13	49.20	189320	40	1396	329	432	*0.4*	-
5-6	06.09.12	25.06.13	54.90	99186	40	742	154	257	*0.5*	-
6-7	06.09.12	26.06.13	31.90	81655	40	488	115	142	*0.8*	-

[a]*Values in italic; measurements below the quantification limit (0.5*Lq)*

Table C5. Data and result from caesium-137 (^{137}Cs) measurements in 1 cm slices from sediment cores 124-3 and 124-4

Sample-id/ layer (cm)	Sampling date	Measuring date	Sample mass (g)	Counting time (sec)	Channels in top	Gross area ROI 1 (counts)	Gross area ROI 2 (counts)	Gross area ROI 3 (counts)	Decay corrected activity[a] (Bq/kg d.w.)	Uncertainty (Bq/kg d.w.)
124-3										
0-1	06.09.12	08.02.13	53.90	104987	40	1483	169	212	4.1	0.6
1-2	06.09.12	11.10.13	54.50	83911	41	912	112	165	2.9	0.8
2-3	06.09.12	14.10.13	52.60	243793	41	1804	336	509	*0.4*	-
3-4	06.09.12	15.10.13	54.70	81872	41	597	123	159	*0.6*	-
4-5	06.09.12	16.10.13	54.10	85267	41	580	127	177	*0.6*	-
5-6	06.09.12	17.10.13	59.00	96463	41	612	156	199	*0.8*	-
6-7	06.09.12	18.10.13	57.40	94291	41	704	150	189	*0.6*	0.7
124-4										
0-1	06.09.12	14.02.13	48.80	87502	40	974	124	189	2.6	0.7
1-2	06.09.12	23.10.13	52.20	88455	41	680	120	212	*0.6*	-
2-3	06.09.12	24.10.13	52.60	101032	41	700	144	230	*0.6*	-
3-4	06.09.12	25.10.13	50.20	76153	41	506	120	185	*0.7*	-
4-5	06.09.12	28.10.13	55.80	273019	41	1979	451	642	*0.3*	-
5-6	06.09.12	29.10.13	63.20	83199	41	631	167	174	*0.6*	-

[a]*Values in italic; measurements below the quantification limit (0.5*Lq)*

Table C6. Data and result from caesium-137 (^{137}Cs) measurements in 1 cm slices from sediment cores 125-1 and 125-2

Sample-id/ layer (cm)	Sampling date	Measuring date	Sample mass (g)	Counting time (sec)	Channels in top	Gross area ROI 1 (counts)	Gross area ROI 2 (counts)	Gross area ROI 3 (counts)	Decay corrected activity[a] (Bq/kg d.w.)	Uncertainty (Bq/kg d.w.)
125-1										
0-1	06.09.12	11.02.13	48.60	238690	40	2583	363	453	2.6	0.4
1-2	06.09.12	27.06.13	52.20	72913	40	660	117	131	1.4	0.7
2-3	06.09.12	01.07.13	51.50	354253	40	2725	574	794	*0.3*	-
3-4	06.09.12	02.07.13	50.50	75458	40	585	135	140	0.6	0.7
4-5	06.09.12	03.07.13	52.60	96465	40	665	174	203	*0.5*	-
5-6	06.09.12	04.07.13	54.60	83648	40	598	154	183	*0.5*	-
6-7	06.09.12	05.07.13	58.80	83836	40	602	135	203	*0.5*	-
125-2										
0-1	06.09.12	13.02.13	50.40	91831	40	1049	168	184	2.4	0.7
1-2	06.09.12	31.10.13	50.50	90534	41	810	140	160	1.7	0.8
2-3	06.09.12	02.11.13	51.60	106016	41	752	155	218	*0.6*	-
3-4	06.09.12	04.11.13	54.50	148858	41	1007	265	340	*0.5*	-
4-5	06.09.12	05.11.13	55.90	89159	41	576	147	217	*0.6*	-
5-6	06.09.12	06.11.13	56.10	100182	41	646	157	194	*0.5*	-
6-7	06.09.12	07.11.13	56.20	85332	41	544	175	204	*0.7*	-
7-8	06.09.12	08.11.13	54.50	95141	41	637	151	197	*0.6*	-

[a]*Values in italic; measurements below the quantification limit (0.5*Lq)*

Table C7. Data and result from caesium-137 (^{137}Cs) measurements in 1 cm slices from sediment core 194-2

Sample-id/ layer (cm)	Sampling date	Measuring date	Sample mass (g)	Counting time (sec)	Channels in top	Gross area ROI 1 (counts)	Gross area ROI 2 (counts)	Gross area ROI 3 (counts)	Decay corrected activity[a] (Bq/kg d.w.)	Uncertainty (Bq/kg d.w.)
194-2										
0-1	07.04.13	12.11.13	50.30	84310	41	689	146	170	*0.7*	-
1-2	07.04.13	18.11.13	57.40	261424	41	2218	478	575	*0.3*	-
2-3	07.04.13	25.11.13	54.90	262949	41	2064	448	591	*0.3*	-
3-4	07.04.13	26.11.13	55.80	93181	41	698	186	198	*0.6*	-
4-5	07.04.13	27.11.13	55.90	85393	41	618	145	177	*0.6*	-
5-6	07.04.13	28.11.13	53.70	83478	41	592	133	187	*0.6*	-
6-7	07.04.13	29.11.13	52.10	79235	41	578	121	166	*0.7*	-
7-8	07.04.13	02.12.13	53.60	258160	41	1885	463	640	*0.4*	-
8-9	07.04.13	03.12.13	52.00	82286	41	523	142	161	*0.7*	-
9-10	07.04.13	04.12.13	52.30	100055	41	716	173	182	*0.6*	-

[a]*Values in italic; measurements below the quantification limit (0.5*Lq)*

Table C8. Data and result from caesium-137 (^{137}Cs) measurements in 1 cm slices from sediment core 195-1

Sample-id/ layer (cm)	Sampling date	Measuring date	Sample mass (g)	Counting time (sec)	Channels in top	Gross area ROI 1 (counts)	Gross area ROI 2 (counts)	Gross area ROI 3 (counts)	Decay corrected activity[a] (Bq/kg d.w.)	Uncertainty (Bq/kg d.w.)
195-1										
0-1	07.04.13	13.11.13	42.00	92936	41	668	159	192	*0.8*	-
1-2	07.04.13	05.12.13	43.10	61279	41	413	86	124	*0.9*	-
2-3	07.04.13	09.12.13	43.40	250953	41	1716	379	462	*0.4*	-
3-4	07.04.13	10.12.13	49.90	99425	41	724	162	191	*0.6*	-
4-5	07.04.13	12.12.13	47.60	86057	41	521	128	182	*0.7*	-
5-6	07.04.13	13.12.13	48.60	86641	41	567	126	162	*0.7*	-
6-7	07.04.13	16.12.13	50.10	147784	41	996	248	342	*0.5*	-
7-8	07.04.13	17.12.13	53.10	96826	41	632	132	213	*0.6*	-
8-9	07.04.13	18.12.13	51.90	84750	41	543	135	169	*0.6*	-
9-10	07.04.13	19.12.13	52.90	97639	41	683	166	212	*0.6*	-

[a]*Values in italic; measurements below the quantification limit (0.5*Lq)*

Table C9. Data and result from caesium-137 (^{137}Cs) measurements in 1 cm slices from sediment core 196-1

Sample-id/ layer (cm)	Sampling date	Measuring date	Sample mass (g)	Counting time (sec)	Channels in top	Gross area ROI 1 (counts)	Gross area ROI 2 (counts)	Gross area ROI 3 (counts)	Decay corrected activity[a] (Bq/kg d.w.)	Uncertainty (Bq/kg d.w.)
196-1										
0-1	07.04.13	14.11.13	50.40	82879	41	1208	111	140	6.4	0.9
1-2	07.04.13	04.12.13	48.30	85729	40	1373	138	191	5.7	0.8
2-3	07.04.13	05.12.13	43.70	61480	40	900	98	131	5.4	1.1
3-4	07.04.13	09.12.13	45.00	251011	40	3749	372	501	5.9	0.5
4-5	07.04.13	10.12.13	43.70	99500	40	952	151	177	2.3	0.7
5-6	07.04.13	11.12.13	45.80	62560	40	471	84	133	*0.7*	-
6-7	07.04.13	12.12.13	46.30	86219	40	756	141	176	1.0	0.7
7-8	07.04.13	13.12.13	48.00	86890	40	683	134	186	*0.6*	-
8-9	07.04.13	16.12.13	53.70	148055	40	1095	261	316	*0.4*	-
9-10	07.04.13	17.12.13	55.10	96986	40	712	165	211	*0.5*	-

[a]*Values in italic; measurements below the quantification limit (0.5*Lq)*

Table C10. Data and result from caesium-137 (^{137}Cs) measurements in 1 cm slices from sediment core 197-2

Sample-id/ layer (cm)	Sampling date	Measuring date	Sample mass (g)	Counting time (sec)	Channels in top	Gross area ROI 1 (counts)	Gross area ROI 2 (counts)	Gross area ROI 3 (counts)	Decay corrected activity[a] (Bq/kg d.w.)	Uncertainty (Bq/kg d.w.)
197-2										
0-1	07.04.13	15.11.13	52.70	98190	41	1035	140	192	2.7	0.7
1-2	07.04.13	08.01.14	47.20	193025	41	2011	302	394	2.5	0.6
2-3	07.04.13	09.01.14	48.70	88892	41	798	138	157	1.7	0.8
3-4	07.04.13	13.01.14	49.90	317809	41	2298	511	641	*0.3*	-
4-5	07.04.13	14.01.14	51.10	101377	41	698	149	202	*0.6*	-
5-6	07.04.13	20.01.14	52.20	258583	41	1871	381	543	*0.3*	-
6-7	07.04.13	28.01.14	50.80	84988	41	595	143	179	*0.7*	-
7-8	07.04.13	29.01.14	52.60	92911	41	614	153	193	*0.6*	-
8-9	07.04.13	30.01.14	54.30	91593	41	665	173	184	*0.6*	-
9-10	07.04.13	31.01.14	59.70	102666	41	720	191	211	*0.5*	-

[a]*Values in italic; measurements below the quantification limit (0.5*Lq)*

Table C11. Data and result from caesium-137 (^{137}Cs) measurements in 1 cm slices from sediment core 199-1 (reference station)

Sample-id/ layer (cm)	Sampling date	Measuring date	Sample mass (g)	Counting time (sec)	Channels in top	Gross area ROI 1 (counts)	Gross area ROI 2 (counts)	Gross area ROI 3 (counts)	Decay corrected activity[a] (Bq/kg d.w.)	Uncertainty (Bq/kg d.w.)
199-1										
0-1	08.04.13	11.11.13	46.60	236141	41	2701	332	437	4.0	0.5
1-2	08.04.13	13.01.14	48.50	317611	40	3659	478	601	3.2	0.4
2-3	08.04.13	16.01.14	52.70	285595	40	2440	487	598	0.6	0.4
3-4	08.04.13	17.01.14	50.00	88186	40	744	133	184	0.8	0.7
4-5	08.04.13	20.01.14	52.20	249667	40	1737	432	506	*0.3*	-
5-6	08.04.13	03.02.14	53.80	227725	41	1635	426	444	*0.4*	-
6-7	08.04.13	04.02.14	54.70	108287	41	834	171	213	*0.5*	-
7-8	08.04.13	05.02.14	57.80	83312	41	608	129	145	*0.6*	-
8-9	08.04.13	06.02.14	57.40	85729	41	646	180	197	*0.6*	-

[a]*Values in italic; measurements below the quantification limit (0.5*Lq)*

Appendix D: Data from grain size distribution

Table D1. Result of sieving of the 0-1 layers of selected cores collected in 2013

Sample-id	Sand and gravel (>63 µm)	Coarse silt (<63µm - >16µm)	Medium silt (<16µm - >8µm)	Fine silt (<8µm - >2µm)	Clay (≤2µm)
194-2	2.1	11.3	10.7	58.7	17.2
195-1	0.2	5.5	11.0	59.3	24.0
196-1	4.7	9.9	11.0	54.2	20.2
197-2	4.0	9.7	11.7	56.6	18.0
199-1 (ref)	3.8	8.9	11.4	57.2	18.8

Appendix E: Elements found in sediment samples collected close to *Komsomolets*

Table E1: Elements found by mass spectrometry in the 0-1 and 1-2 cm layers of selected sediment cores collected in 2013

	194-2		195-1		196-1		197-2		199-1 (ref)	
Element	**0-1 cm**	**1-2 cm**	**0-1 cm**	**1-2 cm**	**0-1 cm**	**1-2 cm**	**0-1 cm**	**1-2 cm**	**0-1 cm**	**1-2 cm**
Al /(g/g)	36.1	32.0	39.4	30.4	19.6	22.2	24.6	21.3	20.3	22.0
Ba (mg/g)	0.189	0.156	0.168	0.195	0.223	0.248	0.217	0.214	0.233	0.249
Be (ug/g)	1.006	0.809	1.170	0.824	0.490	0.681	0.672	0.571	0.549	0.591
Ca (mg/g)	32.0	23.7	23.5	52.6	84.8	88.5	69.6	82.9	85.6	78.7
Ce (ug/g)	63.8	55.8	65.9	55.0	35.9	43.4	45.3	36.9	37.8	37.5
Co (ug/g)	18.5	17.0	22.4	17.3	13.0	14.3	14.9	11.7	13.0	14.0
Cr (ug/g)	64.2	56.1	67.3	51.0	33.6	36.1	41.6	32.3	35.1	33.4
Cu (ug/g)	23.4	21.8	26.1	20.9	15.8	16.2	17.7	13.6	15.2	17.1
Fe (mg/g)	36.6	34.0	40.2	32.1	22.4	24.4	26.8	24.2	23.3	22.9
K (mg/g)	11.0	9.5	11.7	8.9	6.2	6.9	7.6	6.0	6.5	7.8
La (ug/g)	30.0	27.0	32.0	25.5	16.9	18.7	20.8	18.3	17.5	17.9
Mg (mg/g)	15.0	13.5	15.7	12.7	8.8	9.5	10.5	9.1	9.3	8.7
Mn (ug/g)	898	736	1108	824	1149	1266	1084	1100	1216	1204
Nd (ug/g)	32	29	36	27	22	25	22	19	19	22
Ni (ug/g)	44	38	51	41	27	29	30	25	27	28
Sr (ug/g)	169	125	117	276	463	491	384	431	475	478
V (ug/g)	98	87	105	87	69	76	77	65	71	74
Y (ug/g)	13.9	12.1	14.6	12.6	10.2	11.2	11.2	10.7	10.6	10.9
Zn (ug/g)	98	89	107	88	61	65	73	55	72	74

Appendix F: Cruise report from monitoring of the area adjacent to *Komsomolets* in 2012

Prøver ved Komsomolets F/F G. O. Sars 2012 (Toktleder: Edda Johannesen)

Tidsbruk

Søk etter ubåten startet ca halv tolv kvelden 5. sept. Etter krysspeiling ble ubåten lokalisert til å ligge innefor området merket av med blått i kart under. Dette området er ca 250-300 x 250-300 meter. Utenfor dette området ble ekkoregistreringene fra ubåten borte. Det ble registrert sterke signaler ved posisjon 73°43.473, 13°15.817 (grønt kryss øverst på kartet) og 73°43.445 og 13°16.007 (nederste grønne kryss). Selve peilearbeidet tok ca 2 timer. Grabbprøver ble tatt ved fire posisjoner (grønne firkanter). Det var vanskelig å få gode prøver, så det ble flere bomskudd, slik at vi totalt på stasjonen brukte 11 timer (ekskludert peiletiden) for å få disse fire prøvene. Hver grabb tar ca 1 time hvis det ikke er noen problemer, men nå tok noen av disse forsøkene 3.5 timer.

Bruk av transponder.

Det ble forsøkt bruk av transponder, men det virket som den hindret grabben i å lukke seg, evt hindret gode prøver, så derfor ble den fjernet etter gjentatte bomskudd.

Gitt presisjonsnivået på ekkomålingene av posisjonen til vraket, så er det muligens ikke nødvendig med en så nøyaktig posisjonering av grabbene som transponderen gir.

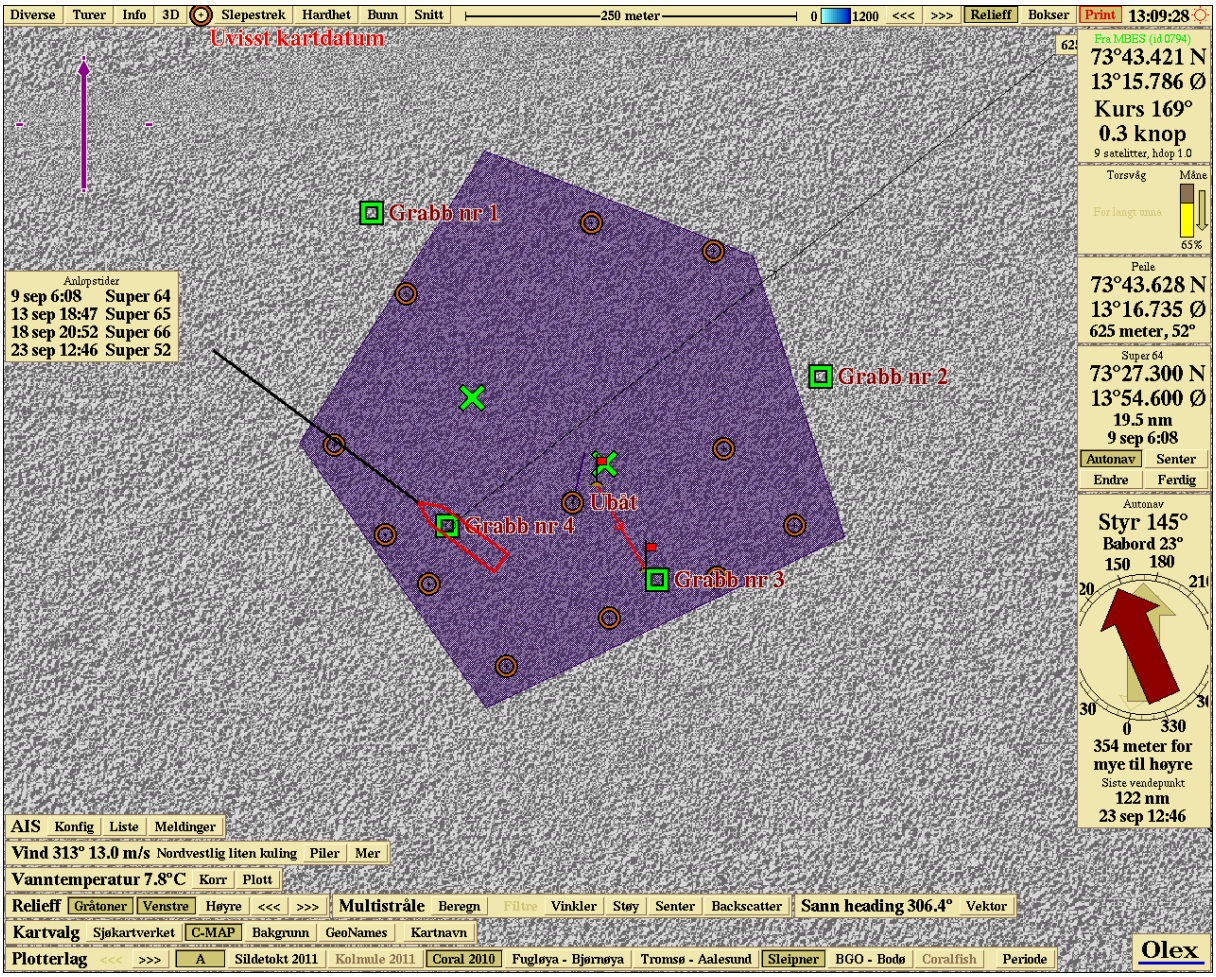

*Skjermbilde med kart fra Olex systemet på GOSars. På kartet vises båtens posisjon ved de fire vellykkede grab-prøvene (grab 1:*73°43.547,13°15.621, *grab 2,* 73°43.482,13°16.318, *grab 3:* 73°43.398,13°16.088, *grab 4:* 73°43.418,13°15.784*)., område med ekkosignaler fra båten (blått) og to kraftige registreringer av ubåten (grønne kryss).*